QUIetening the **E**nvironment for a **S**ustainable **S**urface **T**ransport

QUIESST

TNO innovation for life

FP7-SST-2008-RTD-1
Seventh Framework Programme
Theme 7: Transport

Final report of QUIESST WP 2 – Extrapolation of near field Reflection Index data to far field reflection performance indicators

Deliverables D2.2, D2.3, D2.4, D2.5

Contributor(s)

Main Contributor(s)	Dorien Lutgendorf, TNO
	Foort de Roo, TNO
	Tel.: + 31 88 866 80 43; E-mail: foort.deroo@tno.nl
	Peter Wessels, TNO
Contributor(s) (alphabetical order)	Philippe Jean, CSTB
	Beatriz Bragado Perez, CIDAUT
	Reinhard Wehr, AIT

Review

Reviewer(s)	Jean-Pierre Clairbois, A-tech

Control Sheet

Version History			
Version	Date	Editor	Summary of Modifications
V1.0	2012/10/01	Dorien Lutgendorf	First draft version for comments by WP3 partners
V4.0	2012/12/03	Foort de Roo	Final draft version for approval by co-ordinator
V5.0	2012/12/17	Foort de Roo	Final version

Final Version released by		Circulated to	
Name	Date	Recipient	Date
Foort de Roo	2012/12/17	Coordinator	2012/12/17
		Consortium	2012/12/17
		European Commission	2012/12/17

Table of Contents

Abbreviations

Abbreviation	Meaning
IR	Impulse Response
RI	Reflection Index
RRT	Round Robin test
SPL	Sound Pressure Level
WP	Work Package

Definitions

Term	Definition
$DL_{RI,nf}$	Single Number rating of the near field Reflection Index determined according to the reflection test method developed in WP 3
RI_{ff}	Far field Reflection Index: the ratio between the amount of sound energy that is reflected by the NRD under test and the energy reflected by a reference NRD per 1/3-octave band
$DL_{RI,ff,xm}$	Single Number rating of the Sound Reflection Indices in the far field determined for a receiving position at 100 m distance from the reflecting NRD and at a height of x m above the ground,
$DL_{RI,ff,LR}$	Average Single Number rating for the three lower receiving positions, representative for Low-rise buildings
$DL_{RI,ff,HR}$	the average Single Number rating for the two higher receiving positions, representative for High-rise buildings
Gain	Specific contribution to the far field Single Number rating due to either the shape or the absorptive material effect.

List of Figures

List of Tables

1   Introduction

1.1   Objective of Work Package 2 of the QUIESST project

Sound reflectivity is one of the intrinsic acoustical characteristics of noise barriers. It describes which percentage of an incident sound field is reflected back towards the opposite side of the road. The reflectivity is determined by the absorption properties of the material of the barrier as well as by the geometrical shape of the barrier, which may enhance or diminish sound reflections in certain directions. The reflectivity effect in the far field is thus not only related to the barrier and its design, but also to the receiving position in the far field.

Until now the reflectivity of noise barrier elements is primarily treated as the inverse of the intrinsic sound absorption of noise barriers. This last quantity is tested in the reverberation chamber of an acoustic laboratory according to the European standard EN 1793-1 [1]. The basic test methodology is derived from the international standard ISO 354. This methodology implies that the noise barrier elements are tested in a diffuse sound field, which occurs in enclosed reverberant spaces. Diffuse means that the sound field contains sound waves of all angles of incidence on the test sample and that the sound energy in the test room is distributed evenly over the room. This method of testing gives relevant test conditions for applications where the barrier elements are used in diffuse or semi-diffuse sound field conditions, like tunnels and deep trenches. As the incident sound field is omnidirectional the possible influences of the geometrical barrier shape on the reflectivity characteristics are disregarded.

If however the barrier elements are used in the most common outdoor applications, being placed along motorways and railways, the incident sound field cannot be considered as diffuse, but more as a combination of directional sound waves under varying angles of incidence. In such an incident sound field, the directional influences of the barrier shape may be used to control the reflection contributions to the far field. The effect of tilted noise barriers on the far field reflected sound is well known, but also other barrier shapes may be used to achieve a reduction of the reflected sound in the far field.

Therefore, in order to test the sound absorptive performance of noise barrier elements in a way that is fully relevant for the most common type of application, the tests should be performed with directional incident sound waves. Measuring the reflectivity, including sound absorption and shape effects, would require testing in the far field, at a considerable distance (greater than 20 to 30 m) from the reflecting noise barrier. This way of testing is very difficult because the reflected sound is normally less powerful than the direct sound and will be completely mixed with it. Also, ambient noise and contributions of reflections from the ground and other obstacles are likely to disturb far field reflection measurements.

These problems can be controlled by measuring the reflected sound in the near field (at 0,25 m from the barrier surface). Already in the EU Adrienne project (1995 – 1997) a near field reflection test method was developed. The method was based on in situ testing along a road or in an outdoor test arrangement where no disturbing sound reflections from other objects or walls occur. Testing of the sound reflection properties of noise barriers in the near field, however, is not as easy as it may seem, because also in the near field the incident and the reflected sound field in front of a barrier are completely mixed, if a continuously operating sound source is used. Therefore measuring the contribution of the reflected sound separately requires special measures. These are: using an impulsive sound source signal and separating the incident and the reflected sound in the time domain by time windowing.

If the receiving position is very close to the reflecting surface also other disturbing sound contributions, caused by ground reflections and edge diffractions, can be excluded from the measured signal by time windowing. This measurement methodology was implemented in

the CEN Technical Specification 1793-5 [2], which until now has been used mostly for investigation purposes and not for basic noise barrier performance testing.

In WP 3 of the QUIESST project an improved version of the near field reflection test method was developed. One of the major improvements is the use of 9 receiving positions on a 2-dimensional grid instead of 9 positions on a 1-dimensional arc shaped array. By using these revised measurement positions the averaging of the reflected sound field is improved compared to the first version of the method. Nevertheless the specified measuring distance of 0,25 m from the reflecting surface implies that any surface unevenness has a direct effect on the measured sound. If the reflecting surface is completely flat, one mirror-like reflection of the sound wave will occur. If, however, the surface has irregularities, like corrugations or staggered parts of the surface, the reflected sound field will be scattered, creating several reflections with different directions and intensities. This effect occurs mostly at medium-high frequencies (for which the wavelengths are smaller than the dimensions of the surface irregularities). This results in a very complex sound field in front of a non-flat reflecting surface. For this reason the measurements of the reflected sound at such a short distance from the test sample (in the near field) will only give a measure of the total reflected sound energy if the surface is fully flat or has only minor irregularities that are small compared to the wave lengths of the sound. For many noise barrier designs these conditions are not fulfilled. This means that results of reflection tests for non-flat barriers cannot be used to compute the contribution of reflected sound at a larger distance (in the far field).

Moreover, at the close-by receiving position the effects of the geometrical shape on the far field reflection performance cannot be derived directly from the test results. As, however, the geometrical shape of barrier elements can significantly influence the reflection contributions in the far field it is relevant to take these geometrical parameters into account for the assessment of the intrinsic performance of noise barrier elements.

In order to characterise the barrier reflectivity also in the far field the basic approach of Work Package 2 of the QUIESST project is to use the test data obtained with the improved near field reflection test method delivered by WP 3 as a starting point and to develop a computation method to derive the far field reflection effects from these near field test data.

The final result of this development is an engineering computation method that gives the far field performance indicator for a specific barrier type. This engineering method is a simplified method that is developed using databases of near field and far field computation results obtained with advanced numerical simulation methods. Due to this approach an easy to handle, fast computation method can be delivered that approximates the accuracy of more complex and computation time intensive numerical models.

1.2 Overview of previous work

The first task of WP 2 was to investigate the available numerical simulation methods for accurate simulation of the near field test arrangement and test signals [x]. This investigation was based on the original near field test method as described in CEN/TS 1793-5 [2]. As the separation between the incident and the reflected sound in the near field test method is performed in the time domain also the simulation of this process had to be performed in the time domain.

Three simulation models were identified that could achieve the necessary simulation accuracy in the time domain. Two of these models were finite difference time domain (FDTD) models and the third model was the Boundary Element frequency domain model (BEM), the results of which were transformed to the time domain with an inverse Fourier transformation. This latter method proved to be the most robust and the least computation time requiring. Therefore this method was chosen to generate a database of near field simulation results for a variety of barrier designs and materials.

Based on the findings of task 2.1 recommendations were formulated for the choice of microphone positions for the improved near field test method in WP 3 [3].

The development of an improved near field test method introduced many changes of the test set-up and the data-processing compared to the original method according to CEN/TS 1793-5 [2]. Moreover the final decisions about the details of the near field test method were only made in spring 2012. When this information became available considerable changes of the simulations were necessary to adapt to the newly developed test method (see Section XXX).

The further steps of the development of the engineering far field computation method are described and discussed in the present report.

1.3 Approach and lay-out of this report

The development of a simplified method to estimate the values of the far field performance indicator can be subdivided in several essential steps which are illustrated in Figure 1 and listed below:

1. Simulation of the reflected sound field in the near field in order to be able to match simulation results with the measured results. Part of this work is presented in [4].
2. Matching simulations with measurement data to determine the general level of absorption;
3. Simulation of the reflected sound field in the far field in order to create a database of far field results.
4. Development of a simplified engineering method to obtain far field effects with the information from the database and material properties extracted from the near field measurement.
5. Defining a performance indicator for the noise barrier's reflectivity in the far field.
6. Validation of the (numerical) methods applied to compute the near and far field reflection indices.
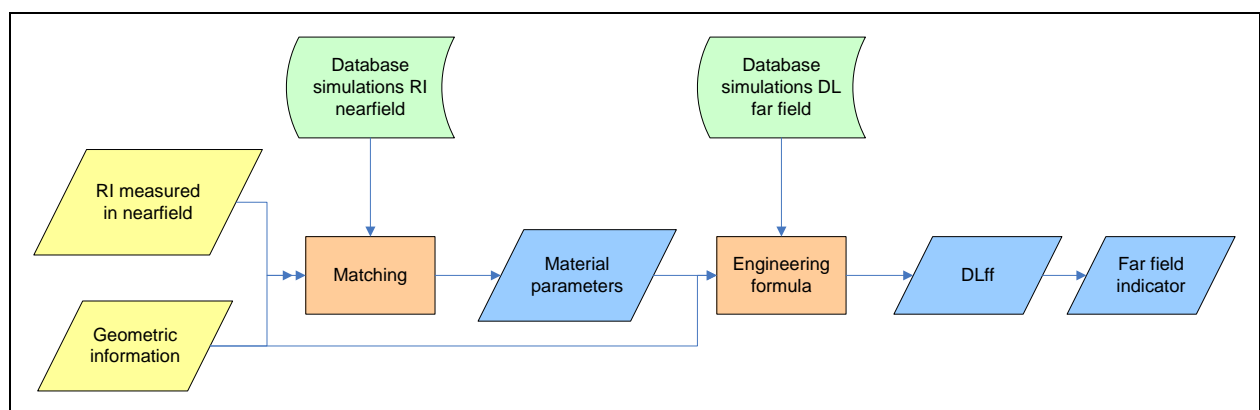
Figure 1 - Overview of the development process for the engineering method to estimate the far field indicator values.

Each of these steps is dealt with in different sections of this report. In chapter 2 of this report the numerical simulations, mentioned under step 1 and 3, are described. Chapter 3 deals with step 5, the description of the Far field indicator. Together chapters 2 & 3 constitutes the deliverables D2.2 and D2.3.

In chapter 4 the analysis leading to the engineering method is reported. This is the content of the original deliverable D2.4. The validation in the far field is collaboration with WP2 partners CIDAUT and AIT and is described in chapter 5 (= deliverable D2.5).

2 Numerical simulations for near- and far-field database

In order to create an engineering method a data set is created by performing numerical simulations. In previous work [5], [6] several methods and issues of the methods have already been discussed and the insights obtained are used in this study. This chapter describes the material and barrier categories which are defined, the effect of focusing on 2D simulations and describes the set-up of the near and far field simulations. The position of this section within the total research is shown in Figure 2.
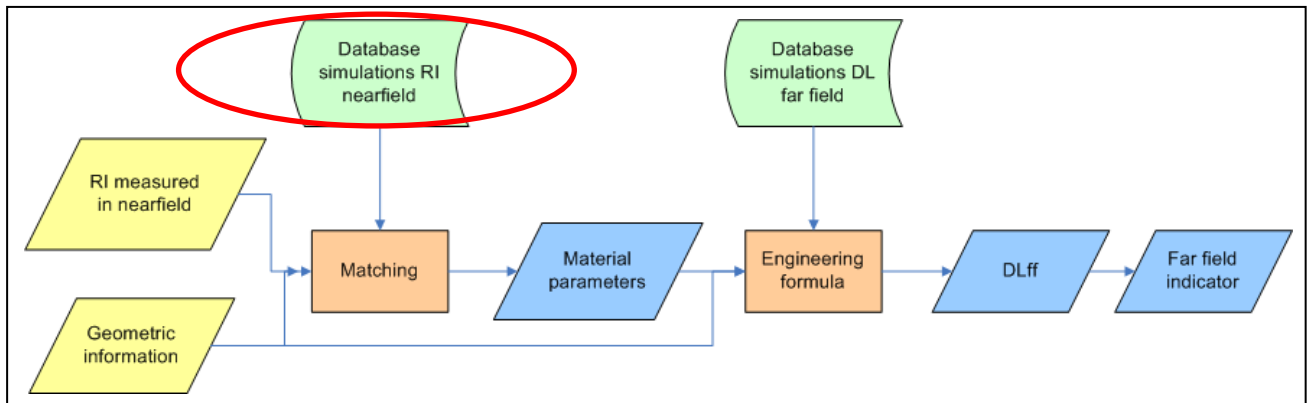
Figure 2 - Overview of approach – step 1&3

2.1 Effect of simulation dimensionality (2D versus 3D)

As the numerical simulation method used is two-dimensional (2D), a short study about the effects of this choice was performed by WP2 partner CSTB [7]. Several different barrier geometries are simulated in 2D, 2.5D and 3D to evaluate the effect of the dimensionality of the simulation method on the obtained results. Here we define 2.5D as the case of a 2D geometry with a point or incoherent line source.

Barriers used in this sub study are assumed 3.5m by 3.5m and are rigid, absorptive, or a combination of both. The surface of the barrier is flat, non-flat or alternating flat and non-flat, some examples are shown in Figure 3.

A source is placed either 1.25 m or 5 m away from the barrier at different lateral positions. The acoustic pressure is computed around the barrier at different distances R from its centre: R=5,10,20,30,40 m.

Computations are made for a relevant series of frequencies of 100, 500, 1000 and 2000 Hz.
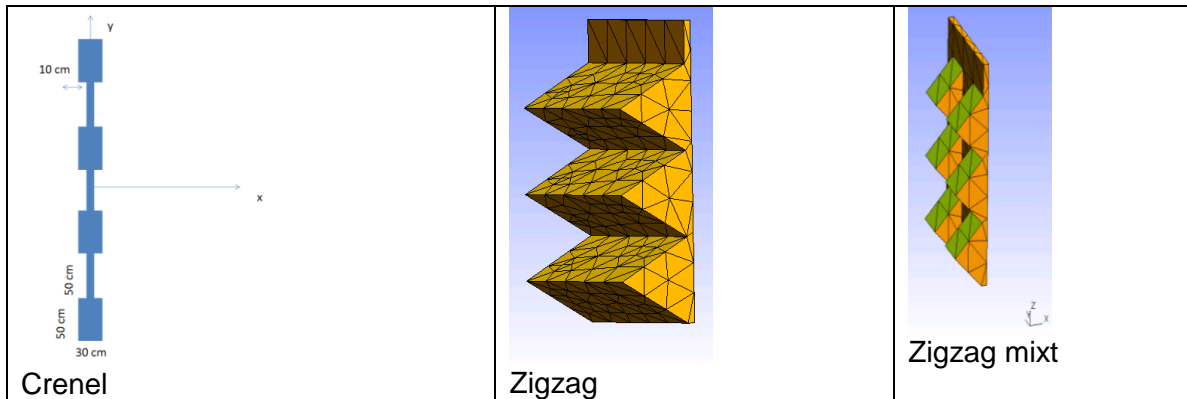
Figure 3 - Sketch of surface configurations of 2-3D effect

In order to restrict the total length of this report not the complete study [7] is described here but only the main observations and conclusions. As an illustration of the results the radiated pressure is plotted in Figure 4 as a function of the angle of incidence for the three different types of simulations (2D, 2,5D and 3D). The three show very similar effects.
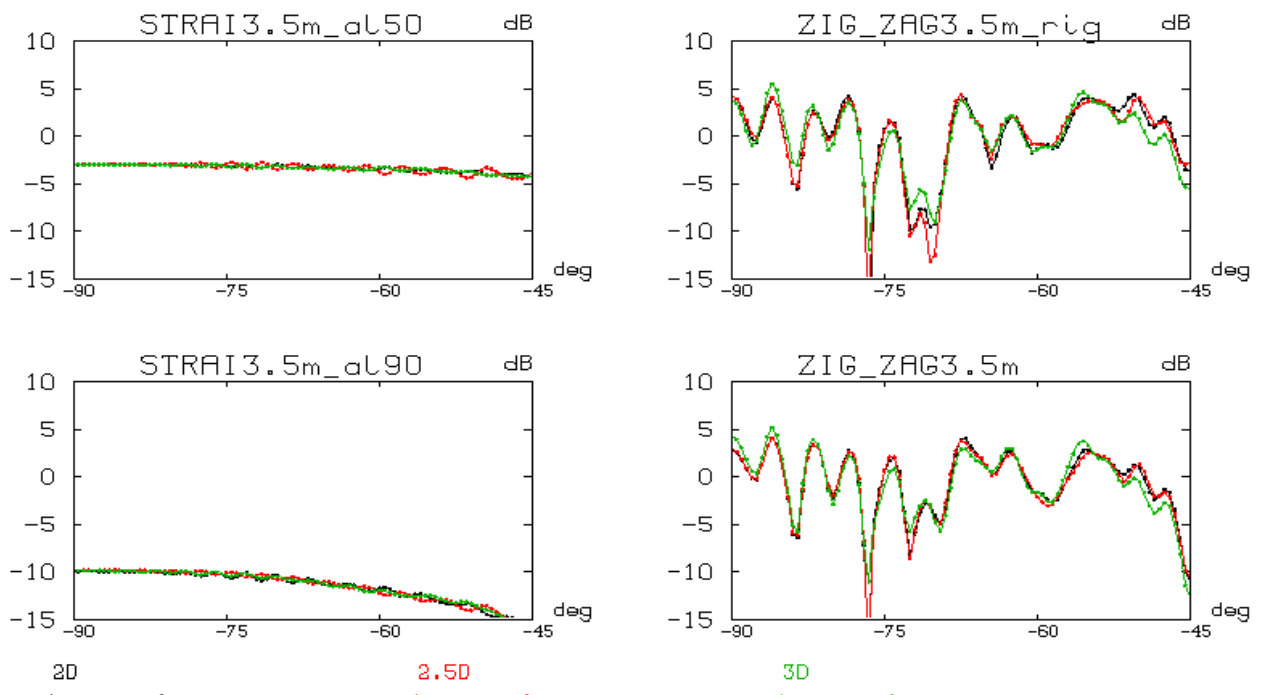
Figure 4 - Comparison of 2D, 2.5D and 3D results at 2000Hz with the source at 1.5m in front of the barrier. Two left figures are results for a straight barrier at two different levels of absorption (50 and 90 %), two figures at the right are a rigid and absorptive zigzag barrier.

Several conclusions are drawn:
- The difference between 2D and 3D results is small, between 2D and 2.5D even very small for barriers which are invariant in the horizontal direction (at 50m distance). So

2D simulations would give an acceptable representation of the real situation for these barriers.

- At distances of 20 meters from the barrier and further the reflected sound field shows a monopole-like behaviour (source at 1.25 or 5m distance). From this distance the complex sound field has formed a more general 'far field'. So far field validation measurements can be executed at a distance of 20 m or more.
- With a 2.5D type barrier (invariant in horizontal direction) only the end/side diffraction has an effect when the source is shifted in horizontal direction (0.5 and 1m). This 2.5D effect can be neglected and a 2D simulation is sufficiently accurate.
- The horizontal shift of the source (0.5 and 1m) shows a significant effect in the 3D simulation.
- However, this effect also occurs for flat barriers and is probably caused by end diffractions of the samples (3,5 m wide)
- There are no indications that the 2D simulation approach would not be appropriate for barriers with homogeneous surface structures.

2.2 Estimate of minimum distance to exclude complex near field sound

Before choosing a representative far field situation the distance at which the global sound source starts to behave as a point source must be checked. This is done by comparing the sound field of a complex barrier with the sound field of a flat reference barrier and with a normal geometrical attenuation. An extremely non-flat barrier with a rigid ground is used as a test case.

Flat barrier with ground	Complex barrier with ground
10.3 ms	
20.6ms	
36.1ms	
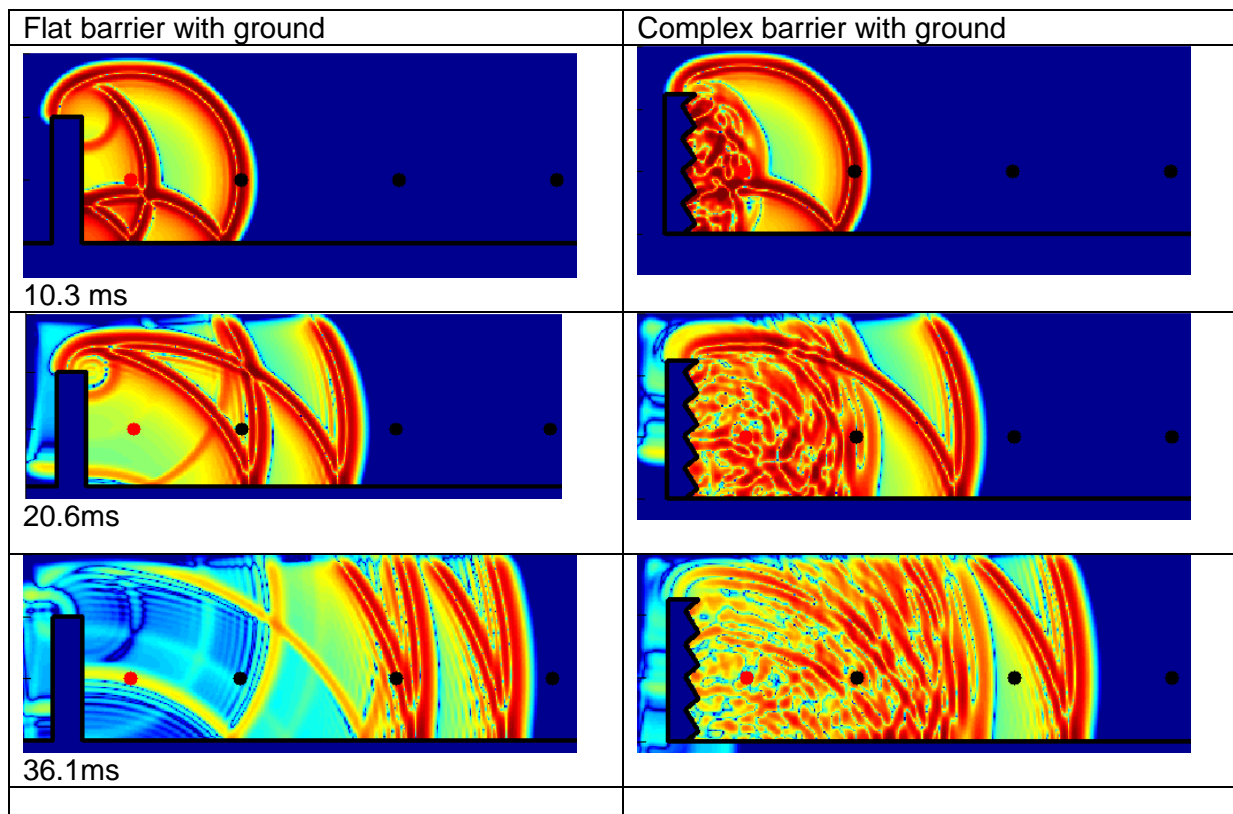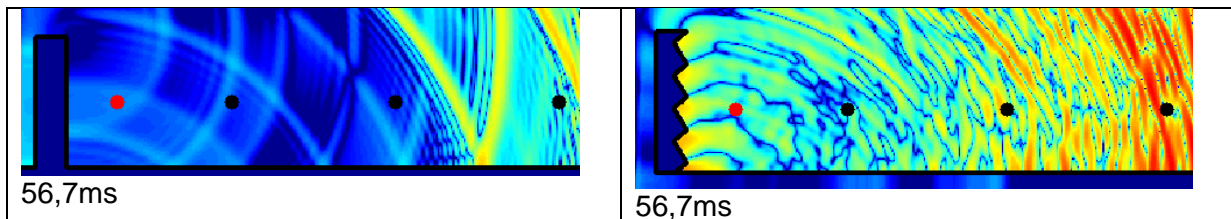
Figure 5 - **Three time domain snapshots of SPL. The shown range is 15m from barrier.**

The main reflections can be clearly distinguished in the snapshots in Figure 5, In case of the complex barrier these main propagation waves are built up and followed by multiple smaller reflections.

Beside a time domain simulation also a frequency domain simulation is done. The different interference patterns between the sound fields of the flat and complex barrier can be seen in Figure 6. The figure shows two results for the complex barrier; one where a rigid ground is modelled and one without.

No ground modelled

Rigid ground modelled
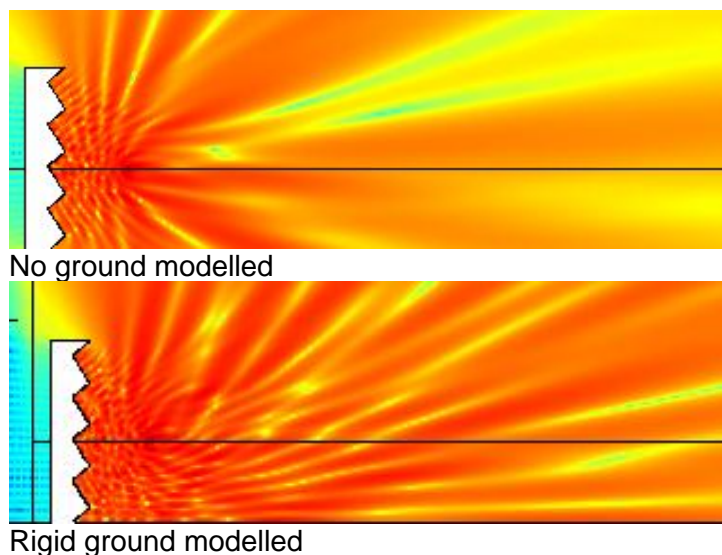
Figure 6 - **Frequency results for 860Hz. Range shown is 15 m from the front of the barrier**

At 15 meter distance from the barrier the sound field shows significantly less local disturbances when compared to the near field (0 – 5 m from the barrier). From the sub study described in the previous section a range of 20m is a safe distance to exclude the complex pressure field very close to the barrier and is a distance were the source behaves like a point source. For far field simulations or validation measurements a distance larger than 20m is sufficiently accurate.

2.3 Materials categories

The materials used in the numerical near field and far field simulations are chosen such that a data base of simulation results can be generated that covers the vast majority of barrier types and variations. There are several common type of materials used in noise barriers. They may be subdivided in the following material categories:

A.   Rigid: All materials with a hard (non-porous) surface and reflective surface characteristics;
B.   Porous concrete;

C.   Perforated metallic or plastic cassettes or sheets with a mineral or glass wool slab inside or underneath.

In the simulations only uniform absorption characteristics over the complete barrier will be applied. In the approximate engineering model barrier designs with mixed absorption characteristics may be represented by an equivalent homogenous variant in order to predict the far field reflectivity performance.

Also absorption materials that do not comply with one of the above mentioned material categories may be represented with an equivalent variant from the data base.

2.3.1 Material category A: Rigid surfaces

These are the acoustically hard (fully reflective) surfaces. The specific acoustical impedance Z is supposed to be infinite. There is only 1 material variant within this material category.

2.3.2 Material category B: Porous concrete

In the simulations porous concrete is modelled with the impedance model for porous materials with a rigid skeleton according to Hamet et al. [8] In order to cover the range of variations that may occur in porous concrete barrier samples the following input parameter settings are used in de simulations, giving a total of 6 variations of porous concrete. Their theoretical absorption curves are shown in Figure 7

Table 1 - Properties material category B

Material	impedance model	flow resistivity [kPa s m-2]	Layer thickness d. [m]	structure factor [-]	porosity [-]
Porous concrete	Hamet et.al	10, 20	0.5, 0.1, 0.15	4	0,25
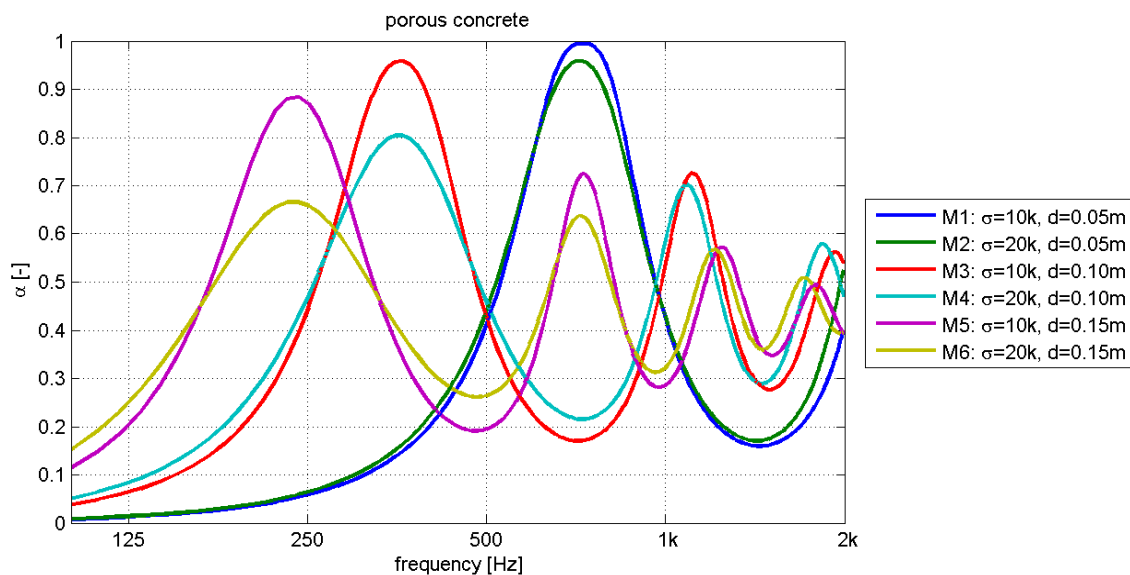
Figure 7 - Absorption curves of the 6 variations of porous concrete

2.3.3 Material category C: Mineral wool in Cassette

As mineral wool cannot be applied outdoors in an unprotected form this type of material is supposed to be contained in perforated metal or plastic cassettes or covered with a perforated metal or plastic sheet or a partly open framework of wooden laths. These materials are modelled by a hybrid impedance model (combination of Delany and Bazley [9]

with Hamet [8]) with a perforated plate covering the absorptive material. A porosity of 0.9 is common for mineral wool type materials.

Table 2 - Properties material category C

Absorptive Material	impedance model	flow resistivity [kPa s m-2]	Layer thickness d. [m]	structure factor [-]	porosity [-]
Mineral wool	D&B + Hamet	10 30 50	0.05 0.10	3	0.9
Perforated plate		Percentage holes pp [%]	Thickness plate dp [mm]	Diameter holes dh [mm]	
Aluminium		35	2	5	

This results in the following absorption curves for material category C, see Figure 8:
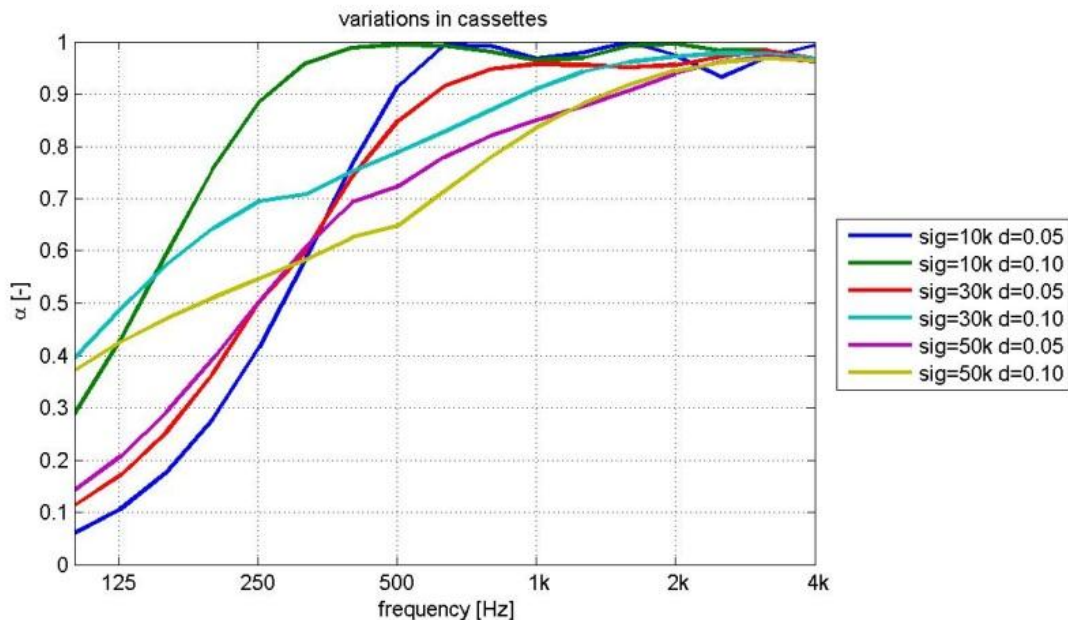
Figure 8 - Absorption curves cassette with mineral wool

2.4 Barrier geometry categories

Also for the geometrical shape of the barriers to be simulated the intention is to cover a large proportion of the total range of variations. Six different basic barrier categories are defined. All geometric variation settings used in this study are summarised in Table 3, a complete overview in pictures of all barrier variants is given in appendix 8.1.
All simulated barriers have a height of 4m. The thickness of the main structure of the barrier is 0.10m.

Table 3 - Barrier variations

Barrier category	Flat - tilted	Panes	Sawtooth	Zigzag	Steps
Geometrical variations	**Angle** of $$\theta_{min} = 70°$$ $$\theta_{max} = 90°$$ **inclination** $d\theta = 5°$	**Profile depth** $B_{min} = 0.05m$ $B_{max} = 0.15m$ $dB = 0.05m$ **Profile height** $H = 0.1m, 0.25m,$ $0.5m, 1.0m$ **Ration in/outward** R=20%, 50%, 80%	**Profile depth** $B_{min} = 0.10m$ $B_{max} = 0.30m$ **Profile height** $H_{min} = 0.33m$ $(=12 elements)$ $H_{max} = 0.80m$ $(=5 elements)$	**Profile depth** $B_{min} = 0.10m$ $B_{max} = 0.30m$ **Profile height** $H_{min} = 0.33m$ $(=12 elements)$ $H_{max} = 0.80m$ $(=5 elements)$	**Tilt:** $$\theta_{min} = 0°$$ $$\theta_{max} = 15°$$ $d\theta = 5°$ **Profile height** $H_{min} = 0.33m$ $(=12 elements)$ $H_{max} = 1.0m$ $(=4 elements)$
Total number	**5**	**30**	**24**	**24**	**9**

2.5 Overview material and geometrical shape combinations

In the simulations the combinations of material type with geometrical barrier design given in Table 4 were included.

Table 4 - Overview barrier shape – material combinations

Material categories		A Rigid	B Porous concrete	C Min. wool cassette
Barrier shape categories	# variations	1	6	6
Flat	5	5	30	30
Saw tooth	24	24	144	144
Zigzag	24	24	144	144
Panes	30	30	180	180
Steps	9	9	54	54

A total of 1196 combinations are modelled in the simulations.

2.6 Near field simulations

The near-field simulations were performed by CSTB with their BEM code Micado (see also the description in Appendix B of D2.1 [4] and in D5.1 [5]). The set-up of the near field simulations follows the final version of the new measurement description [3], see Figure 9. Instead of the original array of 9 microphones on a vertical rotational arc according CEN TS 1793-5 [2] the revised method [3] specifies a two-dimensional array of a 3 x 3 microphone grid. As the chosen near field simulation method is two-dimensional only the 3 microphones in the vertical plane through the source position can be included in the simulations. These microphones are located at heights 1.6m, 2.0 and 2.4 meter. The source height h_s is 2 meters as the barrier is 4 meters high.
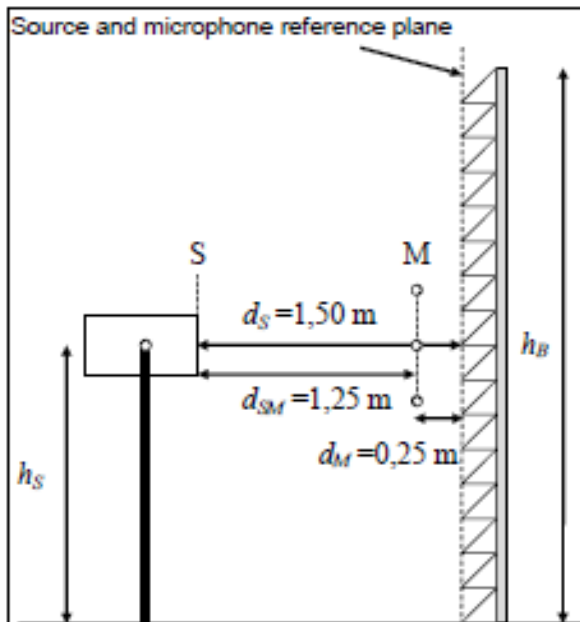
Figure 9 - Near field measurement set-up

2.6.1 Determination of the Near Field sound Reflection Index RI_{nf}

From the results of the simulation the near field sound reflection index RI_{nf} can be calculated, in a similar way as the 'old' RI calculation: by time windowing the contribution of the reflection and the contribution of the direct sound are determined. The ratio between the energy content of both gives the reflection index of the barrier. In the simulations the processing of the data is executed in exactly the same way as in the measurements. The detailed description of the new data processing method is given in formula (1) in section 5.2. of D3.3 [3]. The main differences with respect to the previous version of the method [2] are listed below:

- Instead of the rotational set-up, the rectangular nine microphone grid, previously used for insulation, is now also used for the reflection test method;
- The approach for positioning the window for the reflected component has changed;
- Adrienne windows with different lengths are used for the different microphones positions;
- Averaging the results of the nine microphones is done in a different way;

- A method for aligning the free field impulse response with the barrier impulse response in the time domain has been added;
- A correction term for the source directivity is introduced;
- A correction term for possible changes of the sound source gain is introduced;
- A test signal is provided to be able to check the post-processing software.

As far as possible these new details of the RI_{nf} determination were followed in the simulations. The positioning of the time window was adapted so that reflections which arrive after the ground reflection were cut off by time-windowing and were not taken into account. For the signal subtraction a precise alignment of the free field impulse response and the barrier impulse response is required, which makes a high time resolution necessary. Also the positioning of the time windows in accordance with the measurement data processing requires a high time resolution. As the time domain data are derived by Fourier transform from frequency domain simulation results, these should therefore have a high frequency resolution.

Due to computation time limitations the maximum simulation frequency is 10kHz and frequency resolution is 10Hz. This means that the obtained impulse response has a time resolution of 0.1ms, which is much less than the measured impulse response (sample frequency = 44kHz gives dt = 0.02ms). The issues which arise when performing the post processing on simulated (BEM) data of a lower resolution then the measurement data are described in more detail in the previous WP2 report D1.2 [4].
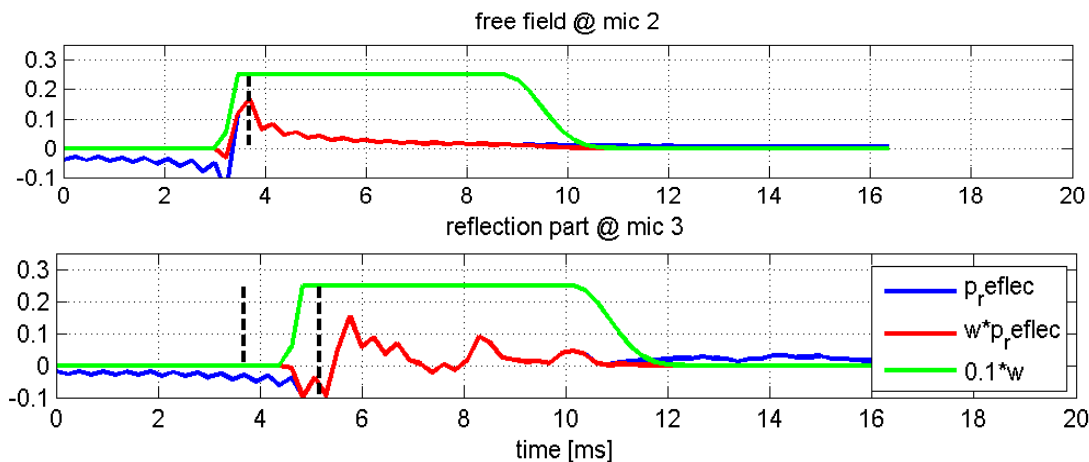
Figure 10 - Example of windowing impulse responses from BEM simulation

2.6.2 Results

Each barrier geometry with a specific material gives an average (over three microphones since simulations are 2D) spectrum of RI_{nf} and one single number rating $DL_{RI\ nf}$. In total there will be 1196 spectra and single number results in the near field database.

Single number results:
Results of DL_{ri} for all barrier types (rows) and all materials (colums) is shown in Figure 11. The different colors represent the different submaterials within each material category. On the x-as the index of the geometric variations is plotted.
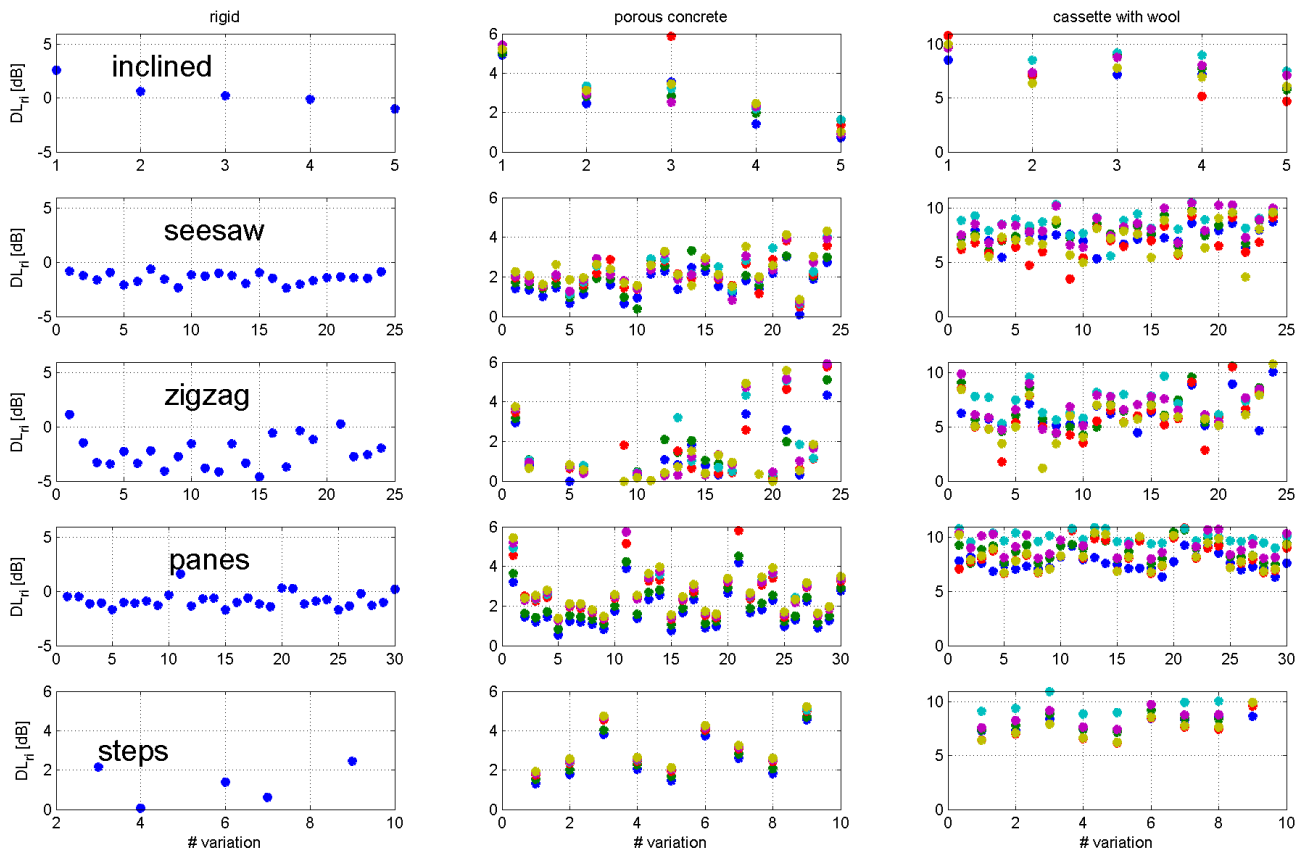
Figure 11 - All DLnf results (Color legenda: see Figure 7 for porous concrete and Figure 8 for mineral wool cassettes)

Obviously the rigid material shows relatively low DL_{RI} in comparison with both the porous concrete and the cassettes with mineral wool due the higher sound absorption of these materials.

2.7 Far field simulations

In line with the choice of the Far Field performance indicators (see chapter 30 the far field simulations are performed for a source at 5 meter from the barrier $(y_s, z_s) = (5,0)$ and receivers at 100 meter distance from the reference plane of the barrier, see also Figure 12. The source is placed on the rigid ground to decrease the variation of the effect of reflections via the ground. Receiver heights are 1.5, 5, 10, 20, 40 meter. The barrier has a height of 4 meter.
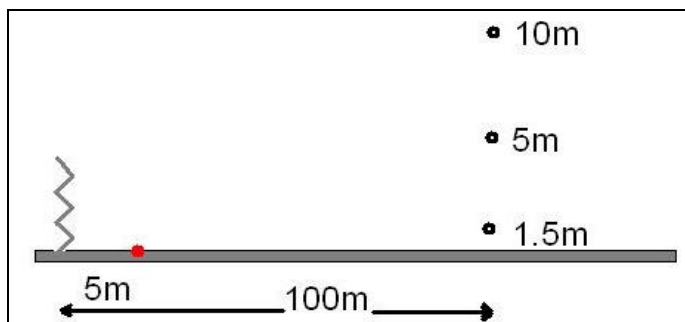
Figure 12 - Geometry far-field simulations

2.7.1 Determination of Far Field sound Reflection Index

By post processing the simulation results the Far Field Reflection Index RI_{ff} can be obtained. The RI_{ff} is defined as the ratio between the amount of energy which is reflected by the complex shaped barrier and the energy reflected by a reference barrier. As a reference a flat rigid vertical barrier of the same height is chosen. From this RI_{ff} the equivalent absorption can be derived, which should be assigned to a flat barrier (with the same height) in order to obtain the same reflection pattern:

$$RI_{ff} = 1 - \alpha_{eq} = \frac{\left(\left|P_{data}(f)\right| - \left|P_{free}(f)\right|\right)^2}{\left(\left|P_{ref}(f)\right| - \left|P_{free}(f)\right|\right)^2}$$

(1)

In formula (1) is:
P_{data} the complex pressure from the barrier under test;
P_{ref} the complex pressure from the reference barrier;
P_{free} the complex pressure in a free field originating from the same source position without reflection contributions.

In both contributions the free field P_{free} is subtracted to obtain only the contribution of the reflected sound. Similar to the single number rating of the near field test method a far field single number is calculated by weighting the third-octave band values of the RI_{ff} spectrum with the A-weighted traffic noise spectrum (L_i):

$$DL_{RI,ff} = -10 \log\left(\frac{\sum\limits_f RI_{ff} \cdot 10^{0.1L_i}}{\sum\limits_f 10^{0.1L_i}}\right)$$

(2)

2.7.2 Results

An overview of single number results for all barrier- material combinations for the receiver at 1.5m is given below in Figure 13. The different colours correspond to the different sub-materials within that material category.
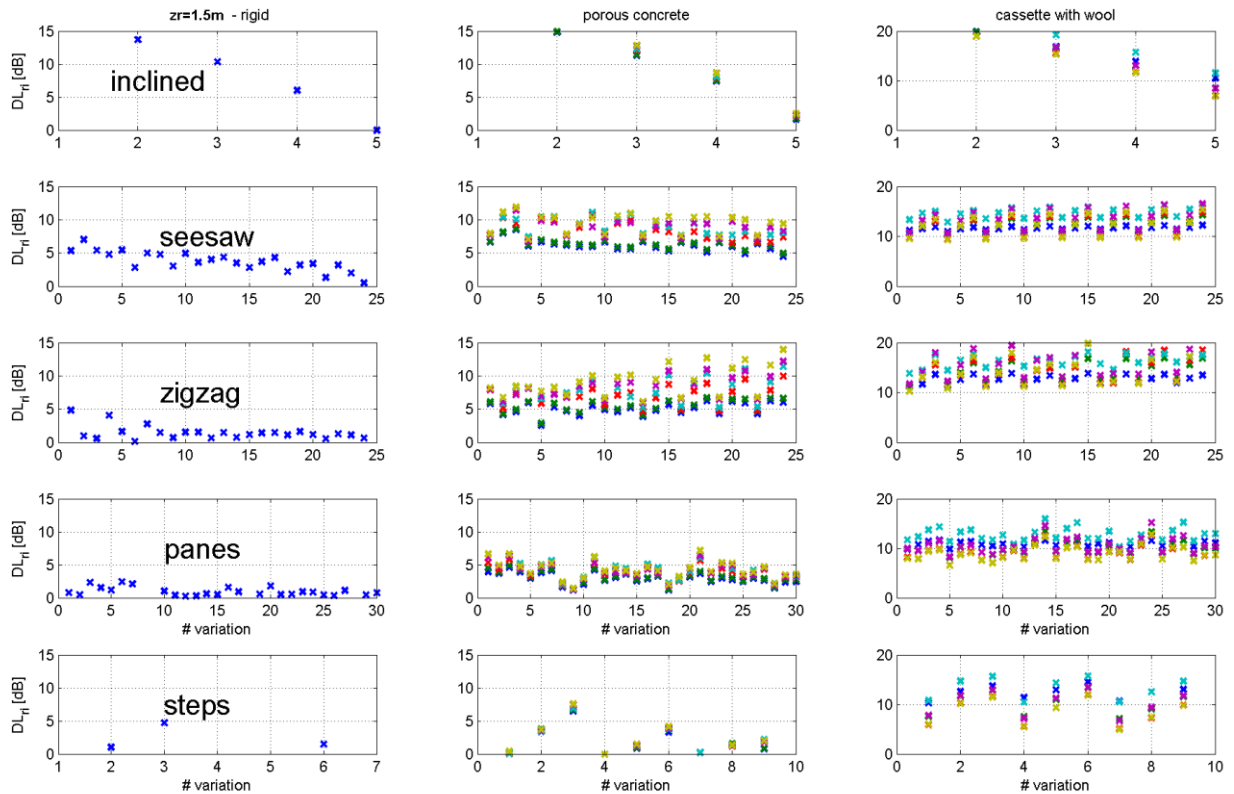
Figure 13 - All DL$_{ff}$ results for the receiver position at 1.5m height and 100 m distance from the barrier.

In the figure the DL$_{ff}$ values are shown as a function of the geometric variation (variations of depth and height of the surface irregularities). In these results a repetitive behaviour can be distinguished, showing a correlation between geometric variation and the DL$_{ri}$. In the next section the separate effects of shape and material properties are explored in order to investigate the possible bases for a far field extrapolation formula.

2.8 Shape versus material effect

When the reflection result of a barrier is compared to three different references, the separate effects of the shape and of the material properties can be visualized. It gives an insight in how much the material and shape separately contribute to the total reflective effect of the barrier.

The first reference is a flat rigid vertical barrier, giving the total reflection effect of the barrier considered. The second reference is a barrier with the same shape as the barrier of interest but rigid, giving the effect of the material. Third, the contribution (indicated as "gain") of shape can be found when comparing the result of a barrier with a flat vertical barrier with the same material. The different comparisons are depicted in Table 5.
The results of these analyses for a receiver position of 5 m height are presented in appendix 8.3.

Table 5 - Overview of splitting shape and material effect (Gain = partial effect in the far field resulting from either shape, material of both)

Type of effect	Barrier	Reference
Shape and material effect $Gain_{shapematerial} = DL_{barrier} - DL_{flat,rigid}$		
Material effect $Gain_{material} = DL_{barrier} - DL_{barrier,rigid}$		
Shape effect $Gain_{shape} = DL_{barrier} - DL_{flat,nonrigid}$		
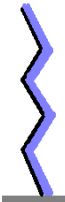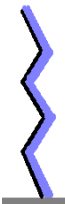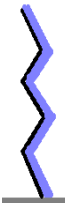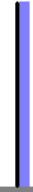
The results in appendix 8.3 lead to a number of observations:

- With no absorption on the barrier all effect originates from the complex shape of the barrier. Typically an effect between 0 and 4 dB can be achieved. Only the inclined barrier can exceed this value due to its tilt angle. As the data are based on a receiver height of 1,5 m the tilt angle directs the reflected sound to higher areas, so only a small amount of reflected sound energy reaches this receiving point.
- With a high amount of absorption like mineral wool the effect of shape is much lower than the effect achieved by the absorptive material. Only for the inclined barrier the shape effects remain significant. In case porous concrete is used the effect of shape and the effect of the material are similar. This dominance of the material effect by high absorption is probably due to the occurrence of multiple reflections against the material caused by complex shapes. In such cases the complex shape increases the effective absorption of the material.
- There seems to be a correlation between material effect and shape effect, such that if the shape effect is high, also the material effect will be high. This again may be due to the multiple reflections that cause a high shape effect which in turn increases the material effect as a result of repetitive reflections against the material.

Most barriers show a shape effect which still depends on the absorption type. Therefore the contributions of shape and material are correlated and cannot be fully separated. Only for the inclined and the steps barrier shapes a more effective separation is possible.

This correlation between the shape and the material effects has consequences for the development of an engineering extrapolation method for prediction of the far field reflectivity. Separation of the factors of influence is not generally possible, so therefore the interactions between these factors have to be taken into account. See section 4.3.

3 Far field indicator

In the previous chapter a set of far field results is created, giving reflection indices for each barrier at several receiver points in the far field. In this chapter the choice of these far field receiver points is motivated and a far field performance indicator is proposed, which is suitable to express a rating of the characteristic reflectivity of noise barriers and which will be easy to use by noise barrier producers and product end users like road authorities. The position of this section within the total research scheme is shown in Figure 14.
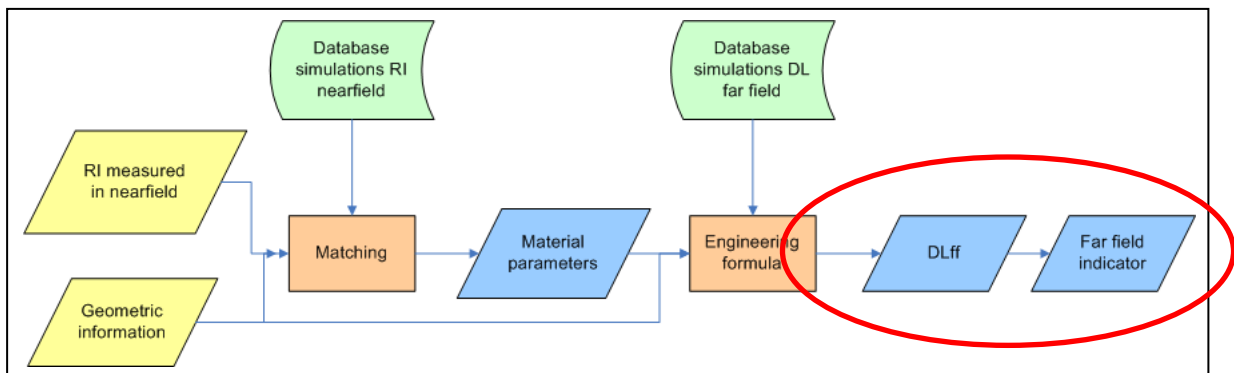
Figure 14 - Overview of approach – step 5

3.1 Motivation for the choice of far field receiver positions

It is obvious that the actual contribution of sound reflections against the barrier may vary strongly with the height of the receiver positions above the ground and with the distance between the receiver positions and the barrier. In a sub-study (see section 2.2 and [7]) it was demonstrated that for distances larger than 20 m from the barrier the reflected sound behaves like a monopole. Therefore the relative influence of reflections to the total sound field will vary only slightly with distance, depending on the relative positions of the sound source and the mirror source representing the reflected sound.
This implies that it is not necessary to assess the contribution of the reflected sound at many distances in order to get representative information on the reflectivity performance of a barrier design.

In order to define a rather simple and yet representative performance criterion for the far field reflectivity a relatively small number of far field receiver positions was chosen.
The minimum distance of dwellings adjacent to a highway from a reflecting barrier at the opposite side of the road may be approximately 30 m, while a maximum distance is hard to define. Therefore only one distance of 100 m was chosen, which is believed to be characteristic for many common noise barrier applications.
For the receiver heights the values of 1,5, 5, 10, 20 and 40 m were chosen, which are supposed to be representative for the majority of practical cases.

3.2 Considerations and choice of a far field indicator

As described in chapter 4 the far field simulations have resulted in a set of Reflection Indexes at five different receiver heights (1.5, 5, 10, 20, 40m) at 100m distance from the barrier. The rating of barriers should be easy to interpret and should be useful to distinguish between the performances for higher and for lower building heights. Therefore the results at the five receiver positions in the far field are grouped and averaged to get two performance indicators

in decibels; one for Low-rise buildings and one for High-rise buildings according to equations (3) and (4). This is illustrated in Figure 15.

$$DL_{RI,ff,LR} = \frac{DL_{RI,ff,1.5m} + DL_{R,Iff,5m} + DL_{RI,ff,10m}}{3} \qquad (3)$$

$$DL_{RI,ff,HR} = \frac{DL_{RI,ff,20m} + DL_{RI,ff,40m}}{2} \qquad (4)$$

Figure 15 - High rise and low rise buildings, with receivers at 1.5, 5, 10, 20, 40m height.

Depending on the set of requirements a barrier can be selected by its performance in an environment with High-rise buildings or with Low-rise buildings. An example of how the performance may vary for different barrier types is shown in Figure 16.
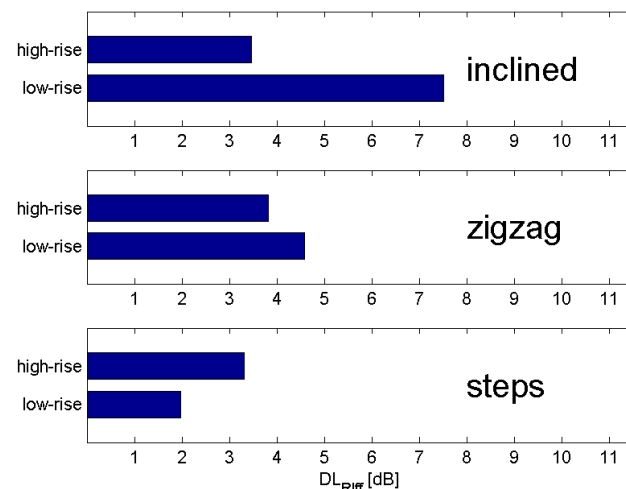
Figure 16 - Example of differences in far field indicators for different barrier types

3.3 Results expressed in Performance Indicator

For all barrier-material configurations in the far field simulation results data-base the High and Low-rise performance indicators are determined from the results at the five receivers heights. The complete set is shown in Figure 17 where each row corresponds to a type of barrier and each column corresponds to a type of material. The dashed line represents the

high-rise indicator and the solid line the low-rise indicator. The different colours represent the different sub-materials within each material category. (The lines in these graphs are drawn to visualise the effects of the different sub-materials, but do not have a physical meaning, as there are no intermediate values between the different geometric variants)
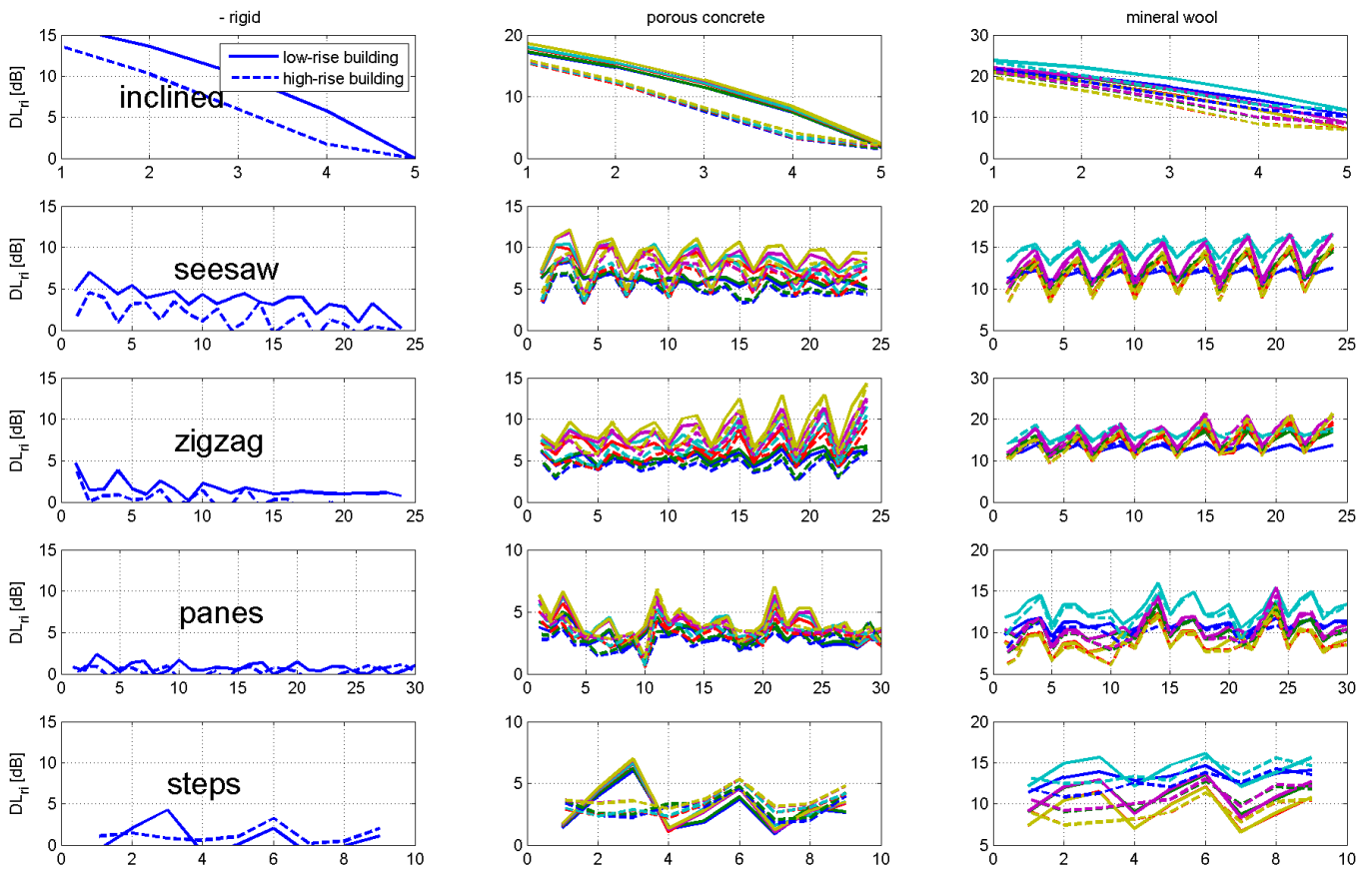
Figure 17 - Values of the Far Field Performance indicators as a function of geometric variations and variations in material properties.

4 Approximate engineering method

The final aim of this research is that reflection measurement results can be translated into a rating of the reflectivity of the barrier in the far field. This translation is split in two separate steps. First the level of material absorption of the barrier is extracted from the near field reflection test data. This process is based on finding the best match between simulated and measured results and is described in section 4.2 and depicted in Figure 18 with the red circle. The second step, described in section 4.3, involves determining the DL_{RI} in the far field with an approximation function which will lead to the far field performance indicator (see chapter 3). This step is depicted in Figure 18 with the orange circle.
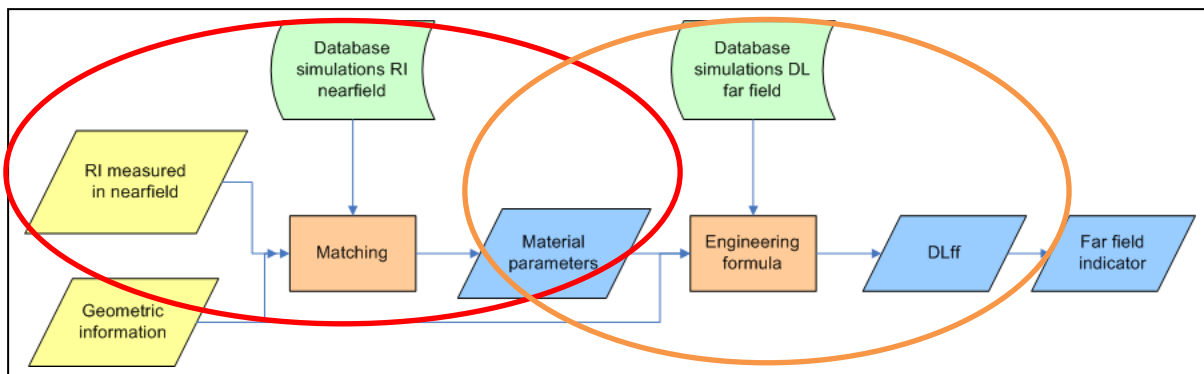
Figure 18 - Overview of approach – step 2 & 4

4.1 Near field measurement results from WP3 Round Robin tests

For the development of a method for extraction of the material absorption characteristics it was necessary to use near field test data from tests with the revised near field reflection test method developed in WP 3.

Therefore the data from the Round Robin test (RRT) executed in WP 3 of the Quiesst Project on 13 barrier samples by 8 laboratories were used. The detailed report with results of this RRT can be found in [11]. An overview of all the measured barrier samples in this RRT is given in Figure 22. In this Round Robin test the average RI spectra of each barrier are determined by all laboratories, see for example the test results of the absorbing timber barrier sample in Figure 19.
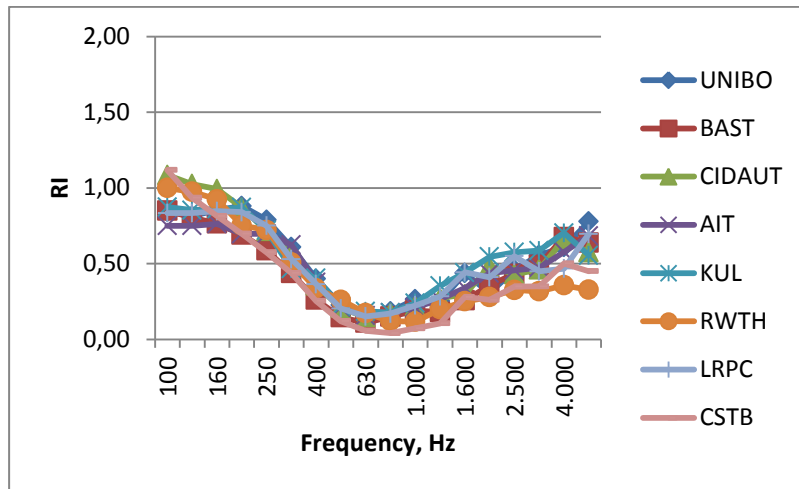
Figure 19 - Example of measurement results RRT - Absorbing Timber barrier sample in Valladolid

The spread of the results of the eight laboratories appears to depend on the barrier sample under test. In order to avoid specific deviations produced by one laboratory the extraction of the level of absorption of a tested sample is carried out for the measured average RI curve, in which the results of the eight laboratories are averaged. Due to this averaging the resulting curve is smoothened and the specific frequency dependent absorption characteristics that are predicted by the theories for porous materials with a rigid structure cannot be observed in the measurement results. The measured RI spectra of the barrier samples averaged over all laboratories are shown in Figure 20.
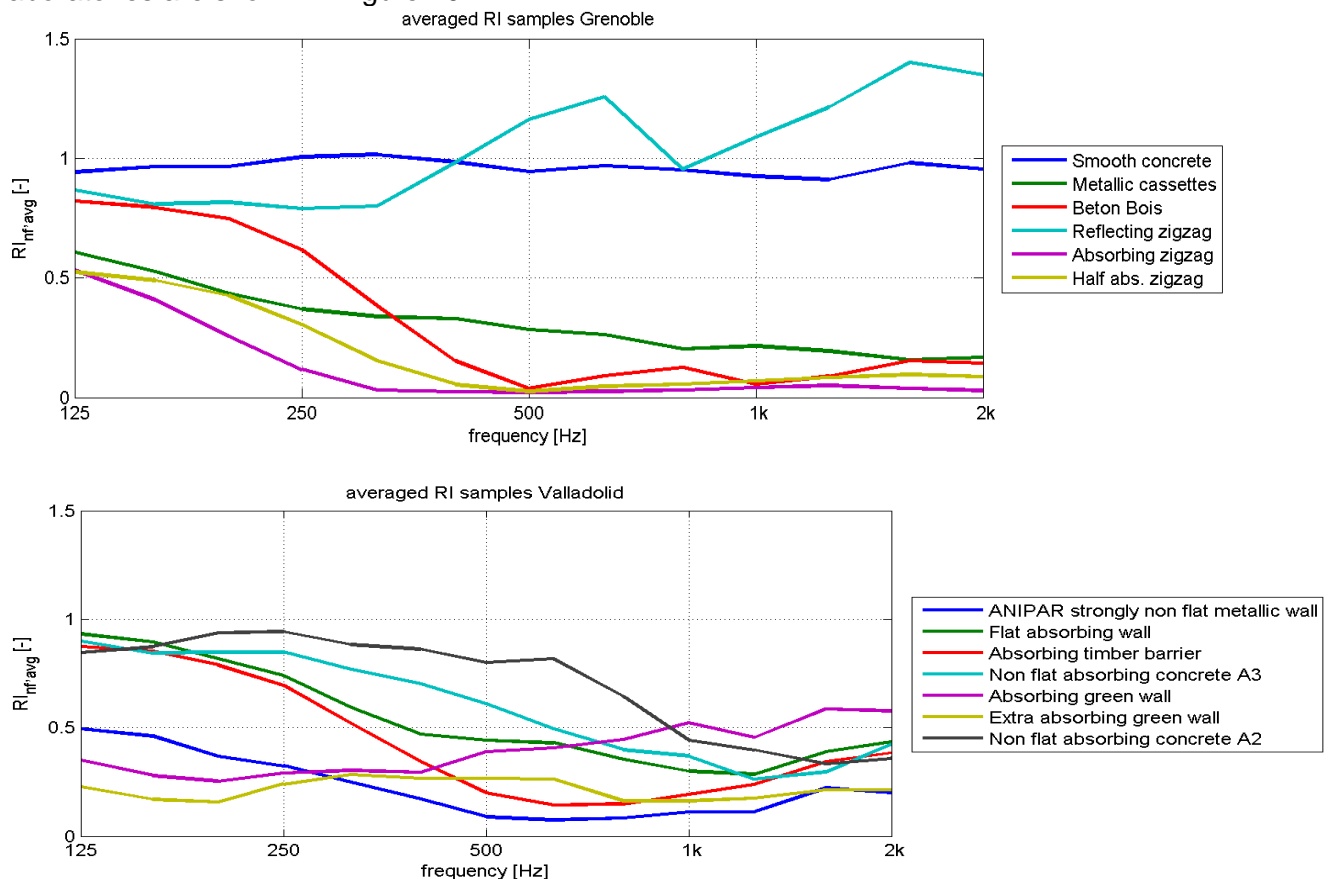
Figure 20 - Average Reflection Index frequency characteristics for Round Robin test barriers

All laboratories also delivered the single number rating $DL_{RI,nf}$ for each of the barriers. The averages over the eight laboratories plus the minimum and maximum measured values are shown in Figure 21.
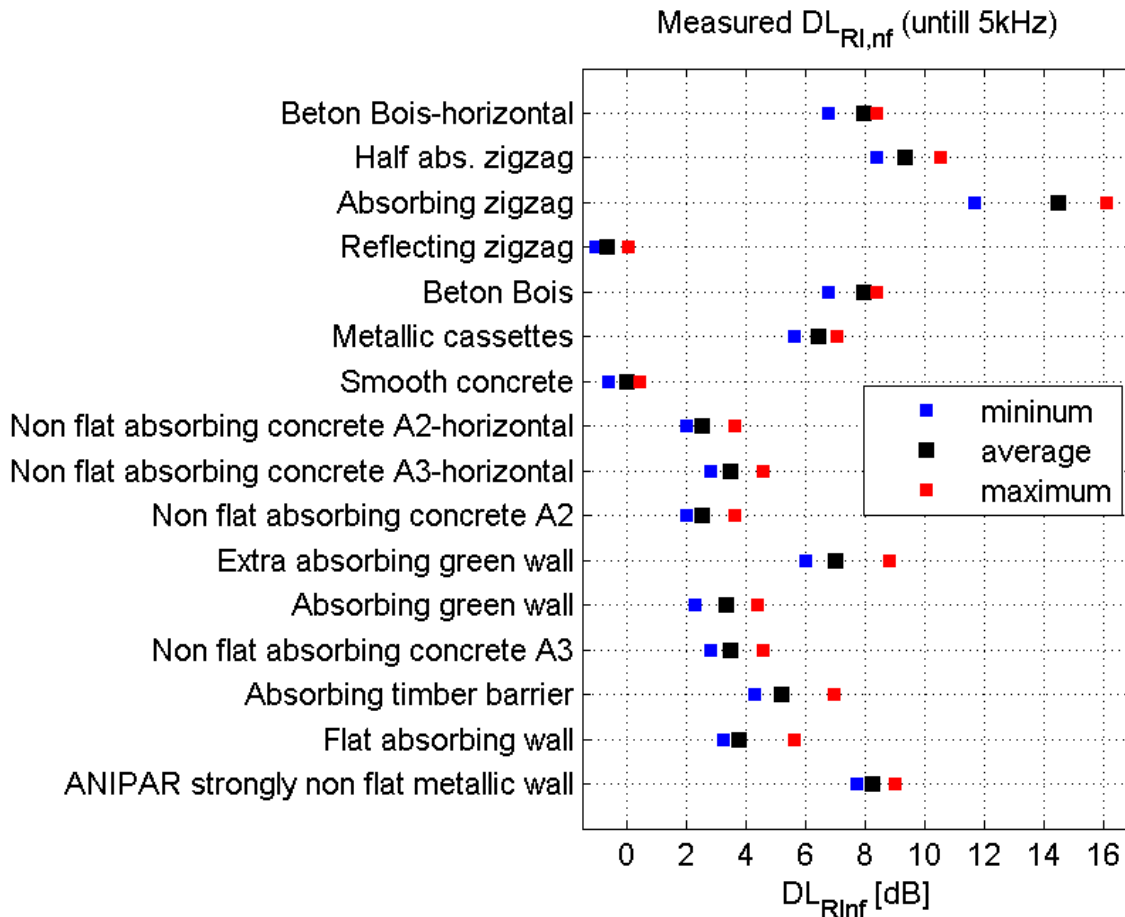
Figure 21 - Measured single number values for all barriers in the RRT

For each of the tested barriers the barrier category and material category is identified as well as the relevant geometric information, see Table 6 and Figure 22

The absorbing concrete samples A2 and A3 in Vallodolid and the beton-bois sample in Grenoble have vertical corrugations. As the simulations are made with a 2-dimensional modelling in the vertical plane through the sound source and the 3 middle receiver positions of the microphone grid, the vertical corrugations cannot be included in the model and the samples appear as flat samples, which may lead to a mismatch between simulation and measurement. Therefore also an alternative modelling is applied in which the vertical corrugations are assumed to be placed horizontally. The alternative descriptions of these samples are indicated with numbers 8, 9 and 16.

Table 6 - Overview of Round Robin test barriers (numbers of the test samples correspond to the pictures in Figure 22)

	Valladolid	Type	Mattype	H	B	theta
1	'ANIPAR strongly non flat metallic wall'	zigzag	C	1	0,36	0
2	'Flat absorbing wall (concrete+rockwool+perforated metallic plate)'	inclined	C	0	0	0
3	'Absorbing timber barrier'	inclined	C	0	0	0
4	'Non flat absorbing concrete A3'	inclined	B	0	0	0
5	'Absorbing green wall'	zigzag	B	1,06	0,475	0
6	'Extra absorbing green wall'	zigzag	B	1,06	0,475	0
7	'Non flat absorbing concrete A2'	inclined	B	0	0	0
8	'Non flat absorbing concrete A3' - horizontal	zigzag	B	0,12	0,14	0
9	'Non flat absorbing concrete A2 - horizontal	zigzag	B	0,09	0,065	0
	Grenoble					
10	'Smooth concrete'	inclined	A	0	0	0
11	'Metallic cassettes'	inclined	C	0	0	0
12	'Beton Bois'	inclined	B	0	0	0
13	'Reflecting zigzag'	zigzag	A	0,57	0,57	0
14	'Absorbing zigzag'	zigzag	C	0,57	0,4	0
15	'Half abs. zigzag'	zigzag	C	0,57	0,285	0
16	'Beton Bois - horizontal	zigzag	B	0,10	0,080	0

	5 **6**	
	7/9 **10**	
	11 **12/16**	
	13-15	

Figure 22 - Pictures of Round Robin test barrier samples

4.2 Extraction of effective absorption from near field measurement

4.2.1 Investigation of different procedures for matching simulations with measurements

The near field measurement data contain information about the general level of absorption of the material of the barriers. This information is needed to evaluate the performance of the barrier in the far field (see section 4.3). The extrapolation method described in 4.3 uses as input data the geometrical shape factors, the type of material and the material parameters flow resistivity and porous layer thickness. This section describes how the best fitting values of flow resistivity and layer thickness can be extracted from the near field test data by comparing the test data with simulated data from the database.

Ideally the simulated and measured results would be rather similar if the correct input data were used for the simulations. It was hoped that by comparing the actually measured data with the simulated data from the data base the best matching variant in the data base could be found without serious difficulties. The search would have to be focussed on barrier variants with a similar geometrical shape as the tested barrier. The material parameters of the best matching simulated variant would then be used as input data for the extrapolation method.

However, due to a number of reasons it proved to be much more difficult to find simulated variants that showed a satisfactory similarity with the measured results. In many cases the basic output of the simulations did not resemble the measured results in terms of frequency characteristics of the near field Reflection Indices (RI). The reasons for these differences are manifold:

- The time and frequency resolution of the simulations are far less than those of the measurements, due to limitations of computer capacity and computation time. Therefore the window placement in the simulations could not be done as accurately as in the measurement post processing. This resulted in possibly large deviations between simulation and measurement for the frequency range above 1 kHz;

- The measurement results for each microphone of the receiver grid could not be made available in a uniform format without a serious additional effort. Therefore the average results over 9 microphone positions were used. In the simulations the averaging was applied for the results of 3 receiving positions on the vertical centre line of the grid. Furthermore the results were averaged over 8 laboratories in order to avoid measurement deviations of individual laboratories. This two-step averaging resulted in very smooth frequency characteristics of the measured results, also for porous materials with a rigid structure. For these materials this did not correspond to the simulated results, where the smoothing of the frequency curves due to averaging did not occur to the same extent. In fact the measured results of the rigid structured porous materials did not at all show the rather peaky frequency characteristics that would be expected according to the theoretical models, but resembled more the theoretically expected smooth frequency characteristics of fibrous porous materials;

- For a very accurate simulation of the intricate sound field close to an uneven barrier surface the exact receiving positions relative to the tops and valleys of the surface profile should be known. However, such detailed information was not recorded during the measurements and could therefore not be used as input for the simulations. Moreover, the total amount of possibilities to position the microphone grid in front of the barrier under test is so large that it would be impossible to carry out simulation for each of the receiving positions that might be used during the measurements;

- The measured absorption values of the porous concrete test samples A2 and A3 in Valladolid are far less than might be expected according to the apparent thickness of the porous layers. This may indicate that the material properties of these samples are not equivalent to those of products of usual quality. Only by assuming much thinner porous layers than the visual assessment indicated a reasonable correspondence between simulated and measured results could be found.

The simulations of the near field RI values were executed in a systematic way for a large number of variations in barrier type, barrier shape, material type and material properties (see section 2.6). The results were stored in a database and these data were used to find a match for each of the Round Robin test results.

Several possible procedures of matching were considered. In total the database with near field simulation results consist of 1196 different barriers variants (combinations of materials and barrier geometries, see section 2.5) and the measured data can be compared with all of these data or with a selection from this dataset.

The least restrictive matching procedure would be to make no selection in advance of the barrier type, geometry and material for the data in the database. In that case the measured result would be compared to all 1196 simulation results. This procedure would neglect the available information about the barrier type, geometry and material and may therefore lead to an unrealistic match.

If, on the other hand, all available information concerning barrier type, geometry and material type would be used, each barrier would only be compared to the number of material variants within the chosen material type. For both porous concrete and mineral wool material the number of variants is six, for rigid materials it is only one. In this most restrictive matching procedure the choice of simulation results would be rather small and may not lead to a sufficiently accurate match between simulation and measurement results. If the actual acoustical behavior of the material deviates from theoretically assumed behavior of such a material a large discrepancy may occur. This could be overcome by including also other material types in the selected data set and enlarging the possibilities for a suitable match. Also because there is hardly any difference between the measured frequency characteristics of rigid structured porous materials and fibrous porous materials merging the different material types would make sense.

Based on these considerations the choice was made for a matching procedure in which the near field measurement data are compared with the simulation results in the data base for a selection of 13 variants of different materials. The selection of barrier type and geometry is limited to one variant that has the closest resemblance to the actually tested type and geometry.

The last question with respect to the matching procedure was how to deal with the differences between the frequency characteristics of the measured and simulated results. In most cases the form of the frequency characteristics of simulation and measurement did not agree very well, so some method of evening out the differences per frequency band would be necessary.

In a first approach the differences were evaluated per frequency band and then the absolute values of the differences were summed. The best fit between simulation and measurement was considered the case with the smallest sum of differences. In this approach all frequency bands are summed with equal weight, without taking account of A-weighting or traffic noise spectrum. When using this procedure of matching it appeared that it did not result in the smallest possible differences between the single number ratings $DL_{RI\,nf}$ of the simulated and measured data.

Therefore it was decided to minimize the differences between the $DL_{RI\ nf}$ values of the simulated and measured results. In that approach the A-weighting and traffic noise spectral weighting are taken into account and the matching procedure is simpler that in the first approach. However, because the simulated results are not reliable in the frequency range above 1 kHz, special values of $DL_{RI\ nf}$ are used, based only on the frequency range below 1 kHz, for the simulated as well as the measured data.

4.2.2 Results of matching for the Round Robin Test data

For each barrier from the RRT the measured single number rating was matched according to the procedures described in the previous section and the matching error was determined.
Error! Not a valid bookmark self-reference. gives an overview of the simulation results that are available (in blue) for matching for each of the RRT test results, with the selected matching case (in green).
Figure 24 shows, in order of measured absorption, the results of the matching procedure, followed in Figure 25 by the corresponding difference between the measured and the fitted simulation values.
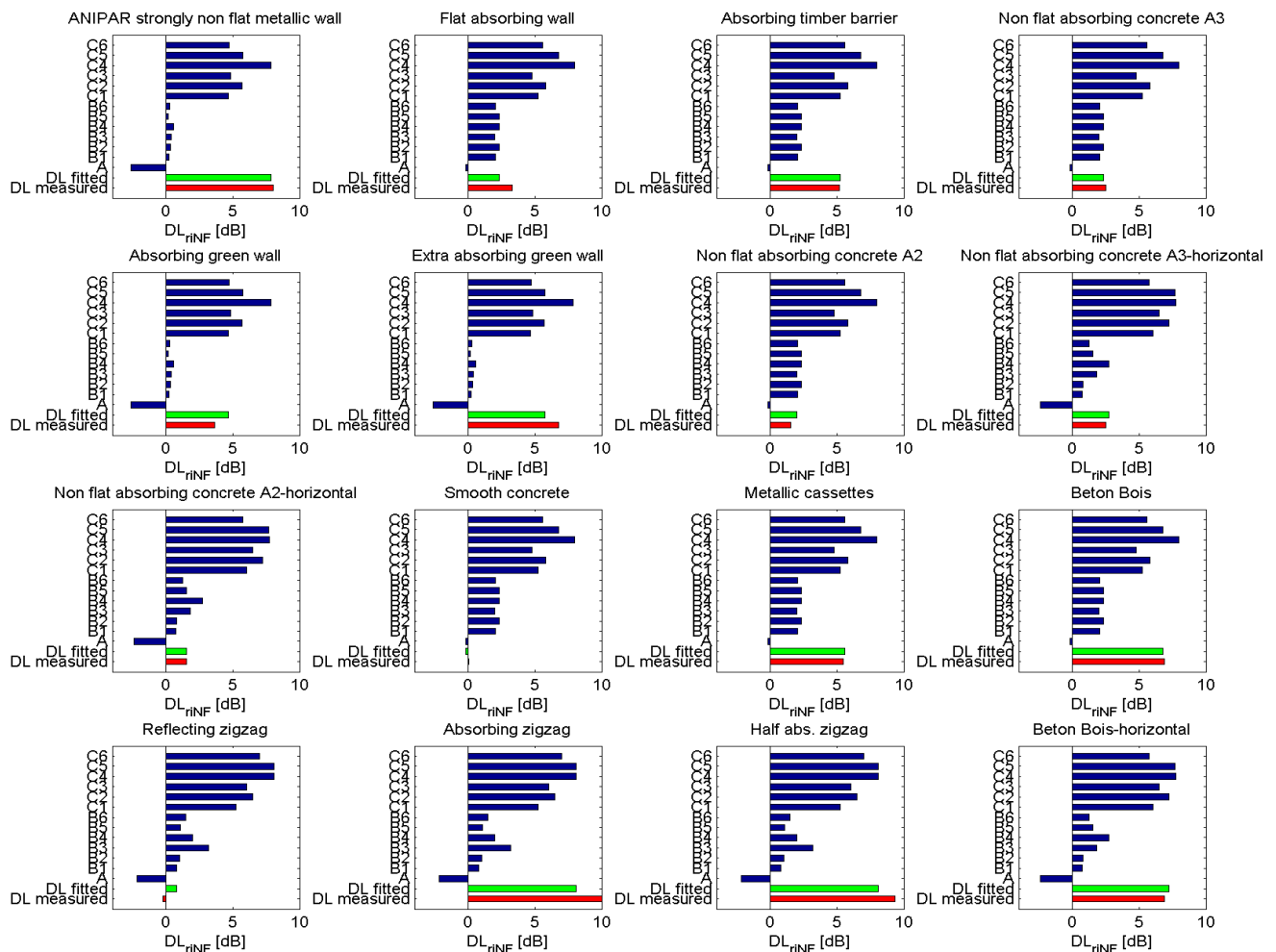
Figure 23 - Overview of $DL_{RI\ nf}$ values (range < 1kHz) of available simulation results per tested barrier sample with the finally selected matching case and the $DL_{RI\ nf}$ value of the measurement result
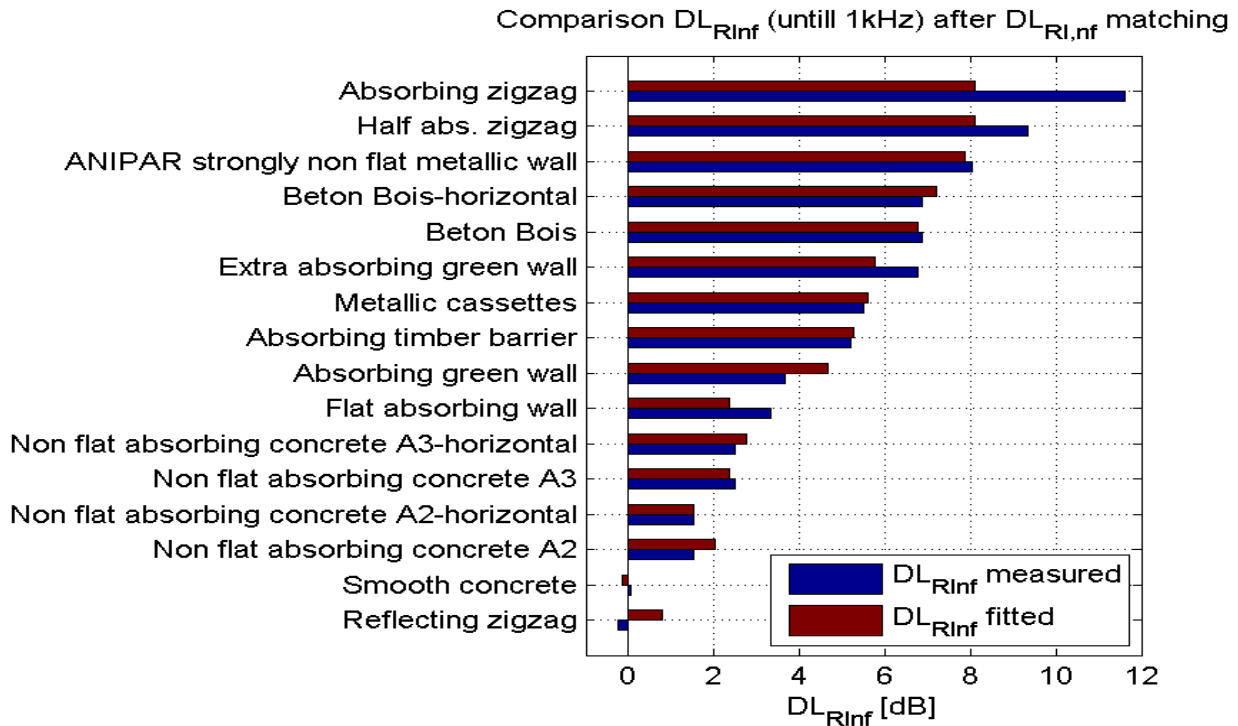
Figure 24 - Comparison between Round Robin Test results and best fitting simulated variants (based on near field single number rating $DL_{RI,nf}$ in the frequency range 125 - 1000 Hz)
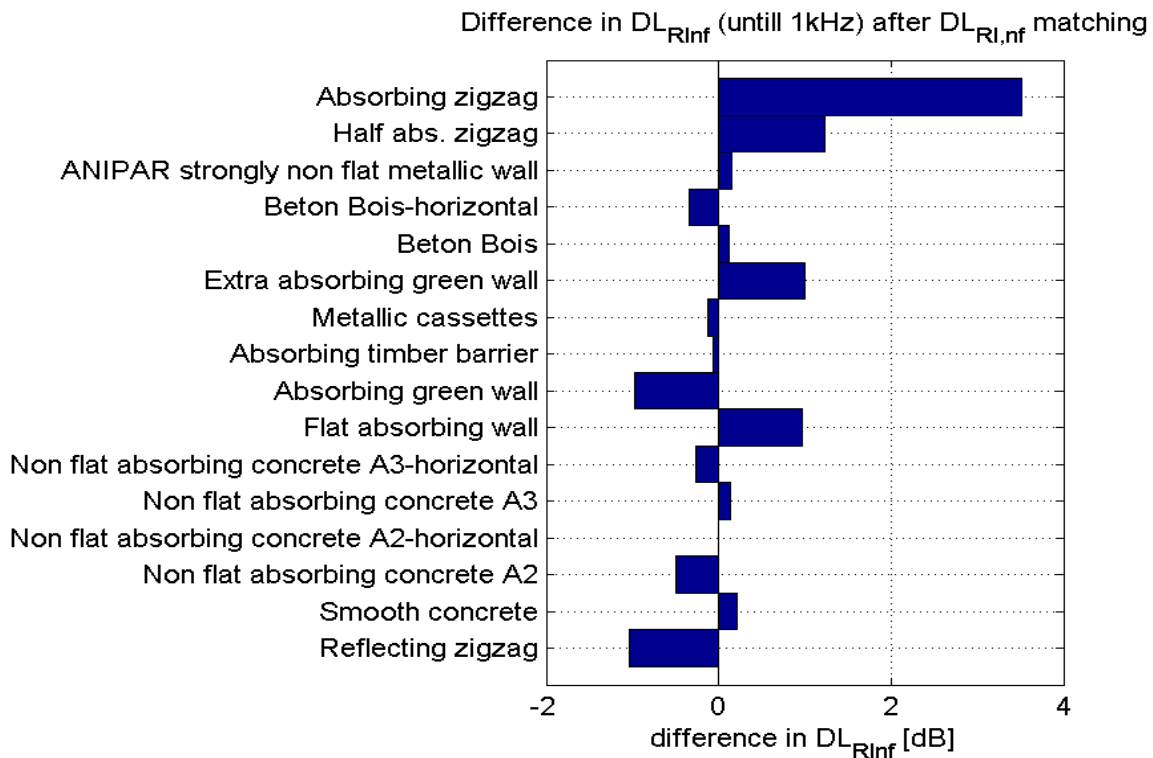
Figure 25 - Difference between fitted and measured $DL_{RI,nf}$ (range < 1kHz)

From the analysed RRT barriers 94% shows a difference between the measured and the fitted $DL_{RI,nf}$ equal to or smaller than 1 dB. The only exception is the absorbing zigzag. Its

relatively high level of absorption is not present in the range of simulated $DL_{RI,nf}$ values for that barrier geometry. The differences between simulated and measured results are of the same order of magnitude (or even smaller) as the differences between the test results of different laboratories (see Figure 21). Specifically the absorbing zig-zag gave a larger spread between the results of different laboratories than the other samples. This may be due to the high degree of absorption: small deviations in the measured absorption coefficients will give large deviations in dB(A), if the absorption coefficients are very low (and the resulting single number rating in dB(A) is high).

The results for each barrier are listed below, giving the material type, flow resistivity and layer thickness of the best fitting simulated case.

From the information in Figure 24 and Table 7 it may be concluded that there seems to be no need to model a barrier with vertical corrugations as a barrier with horizontal corrugations in view of the two-dimensional modelling method that was used for simulations (see section 4.1). The differences between simulated and measured values are comparably small for both types of modelling (horizontal and vertical) for the A2 and A3 porous concrete and the 'beton bois' barrier samples.

Table 7 - **Overview of the shape and material parameters of the best fitting simulated case for the RRT barrier samples**

ANIPAR strongly non flat metallic wall								
	Type	Mat	Θ [deg]	H [m]	B [m]	$DL_{RI,nf}$ till 1kHz [dB]	Flow res.	Layer thickness [m]
Actual	Zigzag	C	90	1	0.36	8	-	-
Fitted	Zigzag	C	90	0.8	0.3	7.9	10	0.15

Flat absorbing wall								
	Type	Mat	Θ [deg]	H [m]	B [m]	$DL_{RI,nf}$ till 1kHz [dB]	Flow res.	Layer thickness [m]
Actual	Inclined	C	90	0	0	3.3	-	-
Fitted	Inclined	B	90	0	0	2.4	20	0.1

Absorbing timber barrier								
	Type	Mat	Θ [deg]	H [m]	B [m]	$DL_{RI,nf}$ till 1kHz [dB]	Flow res.	Layer thickness [m]
Actual	Inclined	C	90	0	0	5.2	-	-
Fitted	Inclined	C	90	0	0	5.3	10	0.1

Non flat absorbing concrete A3								
	Type	Mat	Θ [deg]	H [m]	B [m]	$DL_{RI,nf}$ till 1kHz [dB]	Flow res.	Layer thickness [m]
Actual	Inclined	B	90	0	0	2.5	-	-
Fitted	Inclined	B	90	0	0	2.4	20	0.1

Absorbing green wall								
	Type	Mat	Θ [deg]	H [m]	B [m]	$DL_{RI,nf}$ till 1kHz [dB]	Flow res.	Layer thickness [m]
Actual	Zigzag	A	90	1.06	0.475	3.7	-	-
Fitted	Zigzag	C	90	0.8	0.3	4.7	10	0.1

Extra absorbing green wall								
	Type	Mat	Θ [deg]	H [m]	B [m]	DL$_{RI,nf}$ till 1kHz [dB]	Flow res.	Layer thickness [m]
Actual	Zigzag	B	90	1.06	0.475	6.8	-	-
Fitted	Zigzag	C	90	0.8	0.3	5.8	20	0.15

Non flat absorbing concrete A2								
	Type	Mat	Θ [deg]	H [m]	B [m]	DL$_{RI,nf}$ till 1kHz [dB]	Flow res.	Layer thickness [m]
Actual	Inclined	B	90	0	0	1.5	-	-
Fitted	Inclined	B	90	0	0	2.0	10	0.1

Non flat absorbing concrete A3-horizontal								
	Type	Mat	Θ [deg]	H [m]	B [m]	DL$_{RI,nf}$ till 1kHz [dB]	Flow res.	Layer thickness [m]
Actual	Zigzag	B	90	0.12	0.14	2.5	-	-
Fitted	Zigzag	B	90	0.33	0.1	2.8	20	0.1

Non flat absorbing concrete A2-horizontal								
	Type	Mat	Θ [deg]	H [m]	B [m]	DL$_{RI,nf}$ till 1kHz [dB]	Flow res.	Layer thickness [m]
Actual	Zigzag	B	90	0.09	0.065	1.5	-	-
Fitted	Zigzag	B	90	0.33	0.1	1.5	10	0.15

Smooth concrete								
	Type	Mat	Θ [deg]	H [m]	B [m]	DL$_{RI,nf}$ till 1kHz [dB]	Flow res.	Layer thickness [m]
Actual	Inclined	A	90	0	0	0.1	-	-
Fitted	Inclined	A	90	0	0	-0.2	10000	100

Metallic cassettes								
	Type	Mat	Θ [deg]	H [m]	B [m]	DL$_{RI,nf}$ till 1kHz [dB]	Flow res.	Layer thickness [m]
Actual	Inclined	C	90	0	0	5.5	-	-
Fitted	Inclined	C	90	0	0	5.6	30	0.15

Beton Bois								
	Type	Mat	Θ [deg]	H [m]	B [m]	DL$_{RI,nf}$ till 1kHz [dB]	Flow res.	Layer thickness [m]
Actual	Inclined	B	90	0	0	6.9	-	-
Fitted	Inclined	C	90	0	0	6.8	20	0.15

Reflecting zigzag								
	Type	Mat	Θ [deg]	H [m]	B [m]	DL$_{RI,nf}$ till 1kHz [dB]	Flow res.	Layer thickness [m]
Actual	Zigzag	A	90	0.57	0.57	-0.2	-	-
Fitted	Zigzag	B	90	0.57	0.3	0.8	10	0.05

Absorbing zigzag								
	Type	Mat	Θ [deg]	H [m]	B [m]	DL$_{RI,nf}$ till 1kHz [dB]	Flow res.	Layer thickness [m]
Actual	Zigzag	A	90	0.57	0.57	11.6	-	-
Fitted	Zigzag	C	90	0.57	0.3	8.1	20	0.15

Half abs. zigzag								
	Type	Mat	Θ [deg]	H [m]	B [m]	$DL_{RI,nf}$ till 1kHz [dB]	Flow res.	Layer thickness [m]
Actual	Zigzag	C	90	0.57	0.285	9.3	-	-
Fitted	Zigzag	C	90	0.57	0.3	8.1	20	0.15

Beton Bois - horizontal								
	Type	Mat	Θ [deg]	H [m]	B [m]	$DL_{RI,nf}$ till 1kHz [dB]	Flow res.	Layer thickness [m]
Actual	Zigzag	B	90	0.1	0.08	6.9	-	-
Fitted	Zigzag	C	90	0.33	0.1	7.2	20	0.10

With the material modelling information from the matching procedure the extrapolation to the far field can be performed according to the method described in section 4.3. The far field results of the RRT barrier samples is presented in section 4.3.7.

4.2.3 Input and output of the method

After the development of the matching procedure based on the data from the WP 3 Round Robin test, the method may be considered suitable for general use as a first step of the extrapolation from near field test results to far field performance.

The input for the matching procedure are in the first place the test results of the barrier under consideration, obtained by the renewed CEN/TS 1793-5 method. From the measured RI 1/3-octave spectral values the traffic noise weighted single number value $DL_{RI,nf}$ for the frequency range 100-1kHz is calculated and used as basis for the matching process. The traffic noise weighting values can be found in EN 1793-3 [12].

The second part of the input data are the geometric parameters of the barrier under test. For this purpose the barrier type and, dependent on the barrier type, one or more of the geometric parameters θ, H, B, H/He must be determined. The geometric parameters are respectively the tilt angle, height and depth of the profile and ratio in/outward of the profile.

After matching the test results with the best fitting simulation results the output of the matching procedure is available: the material type, the flow resistivity and the layer thickness of the absorption material. All input and output of the matching procedure are shown in Table 8.

Table 8 - In- and output of the near field matching method

Input	Description
Barrier type	Inclined, saw-tooth, zigzag, panes, steps
ϑ	Angle of inclination (°)
H	Height of profile repetition in [m]
B	Depth of profile in [m]
H/He	Ratio between in and outward part of profile
Output	**Description**
Material type	Rigid (A), porous concrete (B), mineral wool (C)
σ	Flow resistivity in [kPa s m-2]
d	Layer thickness of the absorption material in [m]

4.2.4 Procedure for near field matching

The procedure to extract the material properties of the barrier from the near field test data is established as follows:

1. First the barrier type of the barrier under consideration is determined. When the geometry does not represent one of the barrier types in the data base the barrier falls outside the scope of this study and its far field performance cannot be estimated with this procedure;
2. The geometrical parameters inclination angle θ, height of profile repetition H and profile depth B must be determined.
3. Within the list of the appropriate barrier type a simulated variant is selected, of which the geometrical parameters are in the closest agreement with the parameter of the barrier under consideration. The closest agreement is determined by minimising the sum of squares of the differences for the parameters H, B and θ.
4. From the measured averaged spectral values of RI the $DL_{RI, nf}$ over the frequency range from 100 Hz to 1 kHz is calculated.
5. The measured $DL_{RI,nf}$ value is compared to the thirteen $DL_{RI,nf}$ values for the selected barrier geometry and by minimizing the absolute value of the difference the best fit is determined.
6. The material parameters (flow resistivity and porous layer thickness) of the best fitting variant are presented.

4.3 Extrapolation from effective absorption to far field effects

In this section the design of a set of approximation functions is discussed. These functions can be used to obtain a fast estimate of a barrier's far field value of $DL_{RI\,ff}$. The basis for these functions are the results of the numerical simulations from chapter 2 in which the barrier designs were varied.

4.3.1 Design Approach

The basis for the approximation functions is the large set of numerical simulations as described in section 2.7. In these simulations a noise barrier is modelled and the DL_{RI} for that barrier is calculated at five different receiver heights. Next, the barriers dimensions and material properties are varied, and again the respective $DL_{RI\,ff}$ values are stored. The result is a set of $DL_{RI\,ff}$ values belonging to: one barrier type with one material type, with a range of geometrical variations and a range of variations in material properties.

The far field $DL_{RI\,ff}$ values of the barriers are approximated using simple functions. These functions are the result of fitting polynomials to the far field $DL_{RI\,ff}$ values obtained from the numerical simulations combined with the respective input parameters: the geometry, the material properties of the barrier and the receiver height.

A far field approximation function is made for each combination of barrier type as discussed in section 2.4 and material type as discussed in section 2.3. A full overview of the geometrical properties per barrier type is given in appendix 8.1.

The approximation function itself is a third order polynomial, consisting of a number of terms. Each term consists of a coefficient, variables and exponents belonging to the variables. An example of a third order polynomial, consisting of 10 terms with variables x and y is given in Equation 1. The choice of using a third order function, instead of a higher order, is made in order to keep the fit functions as simple and compact as possible.

$$P(x,y) = C_1 \cdot x^3 \cdot y^0 + C_2 \cdot x^0 \cdot y^3 + C_3 \cdot x^2 \cdot y^1 + C_4 \cdot x^1 \cdot y^2 + C_5 \cdot x^2 \cdot y^0 + C_6 \cdot x^0 \cdot y^2 + C_7 \cdot x^1 \cdot y^1 + C_8 \cdot x^1 \cdot y^0 + C_9 \cdot x^0 \cdot y^1 + C_{10} \cdot x^0 \cdot y^0$$

Equation 1

A different way of notating the polynomial of Equation 1 is shown in Table 9.

Table 9 - Alternate notation of Equation 1

Term	Coefficient	Exponent variable 1	Exponent variable 2
1	C_1	3	0
2	C_2	0	3
3	C_3	2	1
4	C_4	1	2
5	C_5	2	0
6	C_6	0	2
7	C_7	1	1
8	C_8	1	0
9	C_9	0	1
10	C_{10}	0	0

4.3.2 Reduction of the number of terms in a fit

The number of terms in a fit is reduced using an iterative loop. In each loop the least contributing term is identified and removed, after which another fit is made using only the remaining terms. The number of terms versus the accuracy of the function is used to decide the minimum number of terms in the final function.

4.3.3 Avoiding over-fitting

Measures are taken to avoid over-fitting. This is needed in order to properly define the behaviour of the approximation function over the full range that each variable has.

A variable that only has n variations, is modelled using exponents that are limited to an order of n-1. This means that the variable is fitted by a polynomial function that has a lower order compared to the amount of available data points. This approach fully defines the behaviour of the function for values in between the data points.

Example: In case of the porous concrete the simulations only contain two variations for the flow resistivity. The maximum value for the flow resistivity exponent is thus limited to one. This will result in a linear (first order) interpolation in case intermediate flow resistivity values would be used.

4.3.4 Validity range of the approximation function

The approximations functions are fitted to results defined by geometric ranges, ranges in material properties and receiver heights belonging to the results of the numerical simulations. The functions should not be used outside the bounds of these ranges.
For input values that are intermediate to those calculated in the numerical simulations, one should remember that the output values of the approximation function are interpolations. The interpolation order for a variable is dependent of the number of variations in the numerical simulations. The interpolation order is limited by a maximum order of three (see section 4.3.3).

4.3.5 Fit Function Example

As an example the approximation function of an inclined barrier type, with material porous concrete is discussed in more detail.

The inclined barrier type is a flat barrier that can have a given angle with respect to the ground. The geometrical variations that where considered in the numerical simulations are depicted in Figure 26.
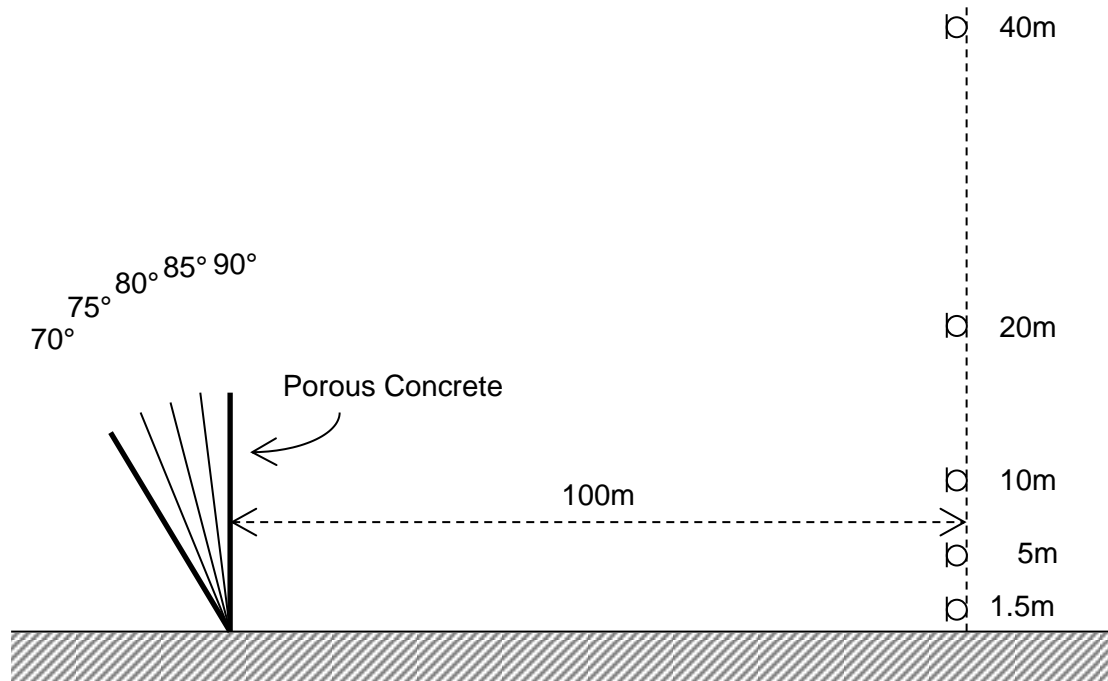
Figure 26 - Variations of the Inclined - Porous Concrete barrier, with receiver locations

The input parameters for the corresponding fit function are:
- The angle of inclination   [degree]
- The receiver height   [m]
- The flow resistivity of the material   [kPa s m-2]
- The thickness of the material   [m]

The resulting approximation function is given by Table 10.

Table 10 - Approximation function for the Inclined - Porous Concrete barrier type

Term number	Coefficient	Exponent Angle [degree]	Exponent microphone height [m]	Exponent material flow resistivity [kPa s m-2]	Exponent material thickness [m]
1	-3,92613222217648E+02	0	0	0	0
2	8,04101745572020E-03	0	2	0	1
3	1,38705416921575E+00	0	1	0	2
4	8,30765381018371E-05	0	0	1	1
5	2,19709651775917E-02	1	1	0	1
6	-2,61554264485773E+00	0	1	0	1
7	4,10062789057933E-04	0	3	0	0
8	-9,82176020167631E+01	0	0	0	1
9	-2,42999645899902E-02	0	2	0	0
10	-2,35254772705490E-02	2	0	0	1
11	3,27561686636256E+00	1	0	0	1
12	8,35376562671896E+00	0	1	0	0
13	1,26831896555825E-03	2	1	0	0
14	-2,03192897425003E-01	1	1	0	0
15	5,91028003685278E-04	3	0	0	0

| 16 | -1,67493816298812E-01 | 2 | 0 | 0 | 0 |
| 17 | 1,46586956881781E+01 | 1 | 0 | 0 | 0 |

Using the approximation function on the input values given in Table 11 gives an estimated $DL_{RI\,ff}$ of 11.65 dB(A) for the receiver at 1.5 m height. This corresponds well to the result of the numerical simulation, which is a $DL_{RI\,ff}$ of 11.35 dB(A).

Table 11 - Example input for the Inclined - Porous Concrete barrier

Variable number	Property	Value	Dimension
1	Angle	80	[Degrees]
2	Microphone height	1.5	[m]
3	flow resistivity	10000	[kPa s m-2]
4	material thickness	0.05	[m]

Figure 27 again shows the match between the numerical simulation and the approximation function, now while varying only the angle from 70 to 90 degrees. The other variables are not varied, and are identical to those shown in Table 11. The approximation function stays within a 1dB error range of the numerical simulations. The figure also shows how the approximation function interpolates in-between the values of the numerical simulations.
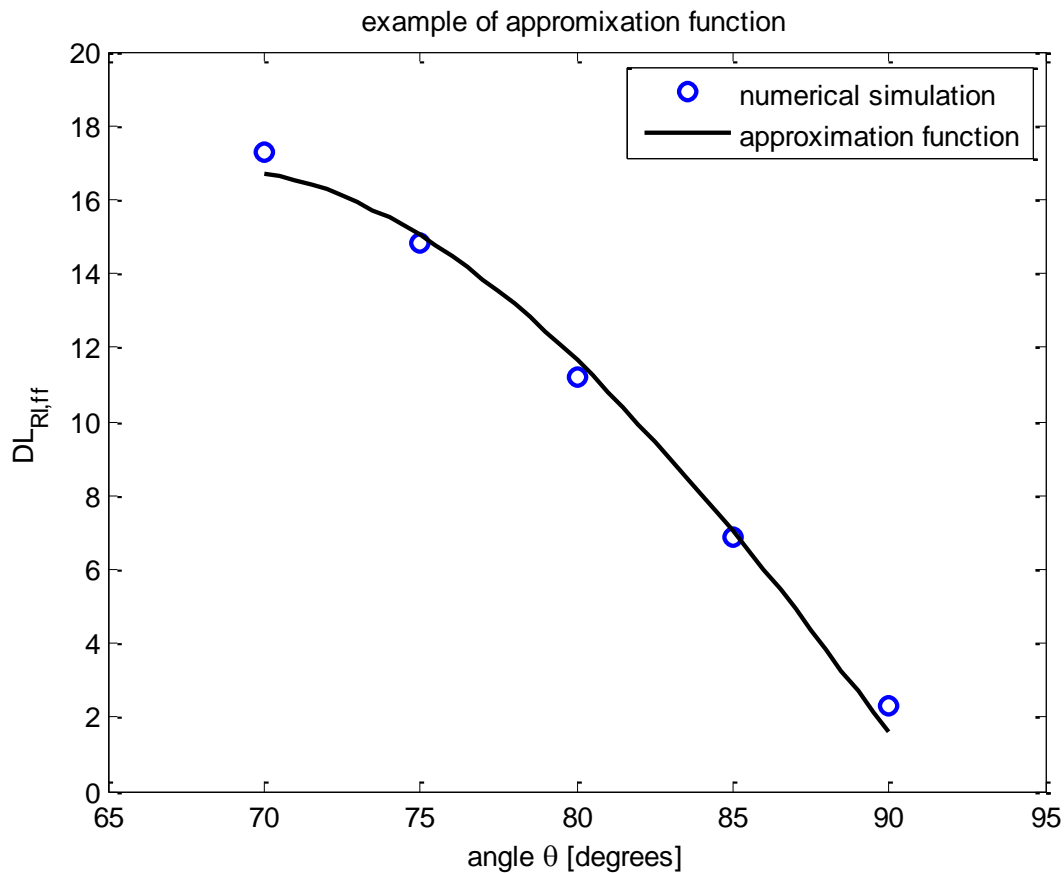
Figure 27 - Example of the match between numerical simulations and approximation function

4.3.6 Performance

Table 12 shows an overview of the far field DL_{RI} approximation functions and their performance. The two left most columns indicate the type of barrier and the type of material used. The third column from the left shows how many terms the fitting function consists of. Next, an overview is given of the number of simulated DL_{RI} values that are approximated within 1 and 2 dB accuracy. As an example: consider the panes type barrier with the material Perforated Cassettes. 893 of the simulated DL_{RI} values are approximated with an error smaller than 2 dB. This corresponds to 99.22% of all simulations for this barrier type and material.

Table 12 - Overview of the performance of the approximation functions

Type	material	Nr Terms	Number of simulated DL_{RI} values at receivers, with absolute error:			% of simulated DL_{RI} values at receivers, with absolute error:	
			<1dB	<2dB	total	<1dB	<2dB
Inclined	Rigid	10	25	25	25	100,00	100,00
	Porous Concrete	17	148	150	150	98,67	100,00
	Perforated Cassettes	25	145	150	150	96,67	100,00
Panes	Rigid	20	127	147	150	84,67	98,00
	Porous Concrete	31	769	882	900	85,44	98,00
	Perforated Cassettes	54	796	893	900	88,44	99,22
Sawtooth	Rigid	18	105	120	120	87,50	100,00
	Porous Concrete	25	656	718	720	91,11	99,72
	Perforated Cassettes	31	707	718	720	98,19	99,72
Steps	Rigid	17	39	45	45	86,67	100,00
	Porous Concrete	33	246	269	270	91,11	99,63
	Perforated Cassettes	23	217	267	270	80,37	98,89
Zigzag	Rigid	10	106	119	120	88,33	99,17
	Porous Concrete	20	600	703	720	83,33	97,64
	Perforated Cassettes	25	605	700	720	84,03	97,22

Table 12 shows that the far field DL_{RI} values of the numerical simulations are approximated well by the approximation function, especially when considering that the approximation function is limited to a third order polynomial. This is also visualised with an example of the fitting results of the zigzag barrier with porous concrete in Figure .

Results of fitting in order of geometric variation   Results of fitting sorted in order of DL
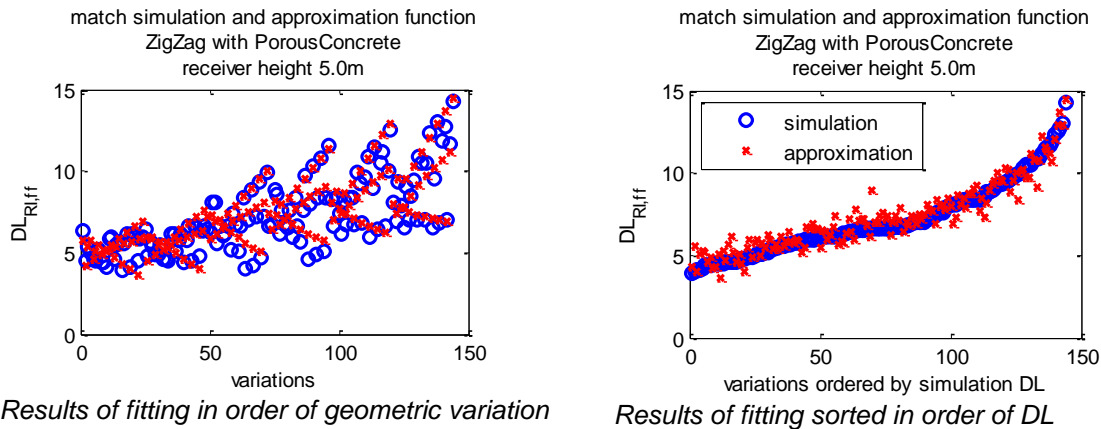
Figure 28 - Example of fitting performance - zigzag with porous concrete

A full listing of fit-functions, their input, input range and performance can be found in appendix 8.5.1 to 8.5.5.

4.3.7 Far field results of Round Robin Test barrier samples

As an example of the results of the engineering extrapolation method the data of the barrier samples from the Round Robin Test of WP 3 were used as input for the engineering method. Both steps of the method, near field matching and extrapolation to the far field, were applied to determine the far field effect of these barriers. The material properties resulting from the matching (tables in section 4.2.2) were used as input for the approximation function. The results are shown in Figure 29. The corresponding near field single number ratings from the reflection tests are given in the table beside the figure.

From these results it can be seen that the far field effect does not always follow closely the near field reflection index values. If the barrier sample has a surface shape with large dimensions in vertical and horizontal sense, the far field effects of this surface design may be substantial and can enhance the reduction of reflections due to the absorption characteristics of the material. In many cases these surface shape effects are also dependent of the receiving height.
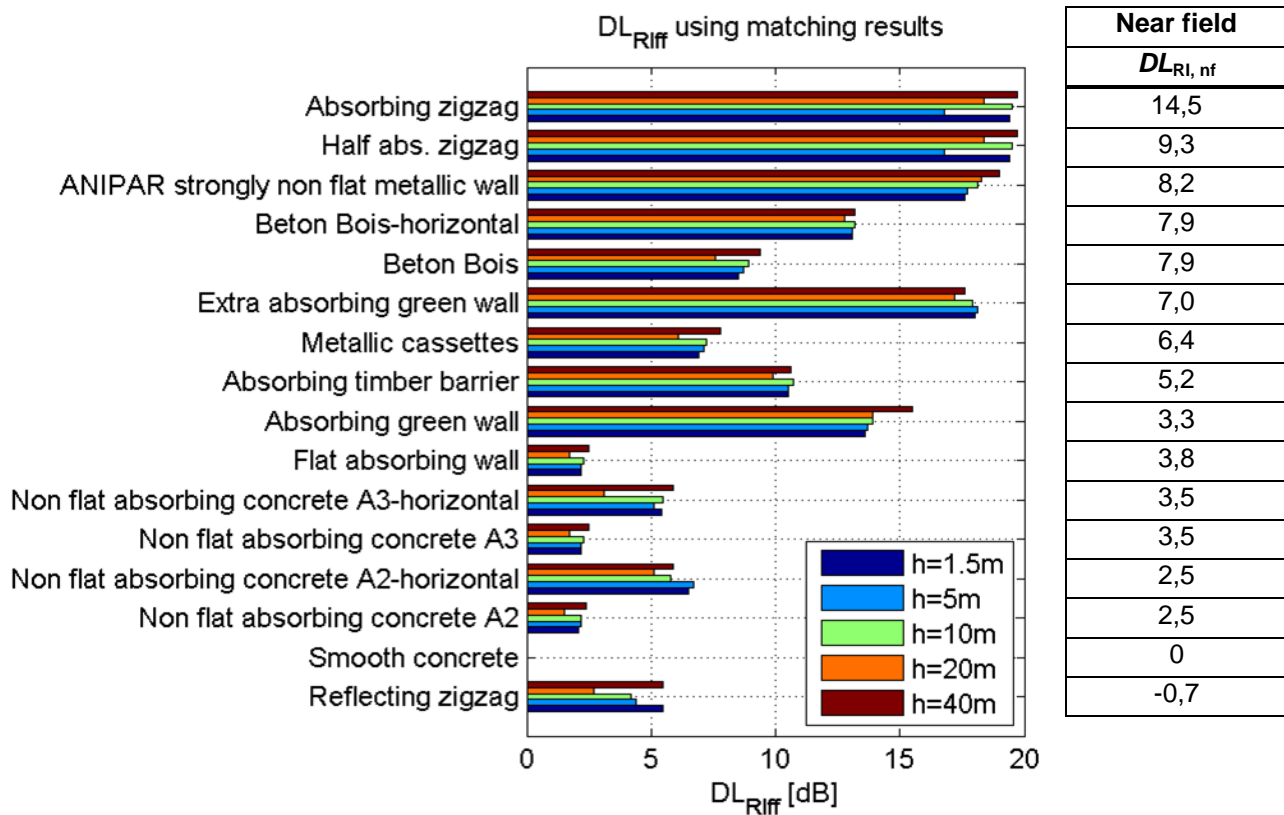
Figure 29 - DL$_{RI\,ff}$ of the RRT barriers

4.4 Résumé of the approximate engineering method

An approximate engineering method has been developed that emulates the results of accurate numerical simulations of the effects in the far field of sound reflections against noise barriers. This engineering method is based on polynomial approximations of the single number rating of the Reflection Index in the far field $DL_{RI\,ff}$. For each combination of geometrical barrier type and type of absorption material a separate polynomial was developed. The input data for the polynomial computation are: geometrical parameters (surface profile height, profile depth, angle of inclination), acoustical material parameters (flow resistivity and layer thickness of the porous absorptive material) and the height of the receiver positions. The distance of the receiver positions to the reflecting barrier is always taken as 100 m.

The accuracy of the polynomial approximation was determined by comparison of results computed with the polynomial with the results of numerical simulations. The differences appear to be less than 1 dB in 88 % of the cases and less than 2 dB in 99 % of the cases.

The geometrical input data for these engineering computations can be acquired from the design (drawings and/or dimensions) of the barrier elements under consideration. The acoustical material parameters can be derived from the test results of a near field reflectivity test of the barrier under consideration. The test has to be carried out according to the revised test method for sound reflectivity developed in WP 3. The acoustical parameters can be obtained from a comparison between the measured test results and the results of numerical simulations of the near field reflected sound field. If a good match between test and

simulation results can be found for a specific barrier design, it may be inferred that the acoustical parameter values used for the near field simulation would also be appropriate as input for the far field approximation.

For the development of the matching method the results of the Round Robin test of the new near field test method from WP 3 were used. Although the near field simulations were executed with a method that simulates the actual measurement process in the time domain a very good correspondence between the frequency characteristics of the measured and the simulated results could not be found for most of the tested barrier samples.

Searching for a good match in all frequency bands between the measured and simulated results did therefore not produce convincing similarities that could be the basis for determination of appropriate values of acoustical parameters.

Based on the outcome of a comparison of several matching methods it was decided to use a method that chooses firstly the variants with the best matching geometrical design from the data base and secondly the best matching near field single number rating $DL_{RI\ nf}$. The search for this second match is not restricted to variants with the same type of absorbing material. By not fixing the type of material a greater variety of single number values is available for comparison and a better match between measured and simulated results can be found.

The selected matching procedure gave deviations between measured and matched simulation results from 0 to 1 dB, with a larger deviation of 3,5 dB for the only variant with a $DL_{RI\ nf}$ value above 10 dB(A). These deviations are of the same order of magnitude as the differences between test results of different laboratories. Therefore the accuracy achieved with the matching procedure is considered satisfactorily accurate.

Also in the second step of the engineering method, the polynomial approximation, similar deviations were found between the results of the approximation and the original simulated results (see section 4.3.6). As both steps have an uncertainty margin of $\pm$ 1 dB the combined uncertainty of the complete method can be estimated as $\pm$ 1,4 dB (=$\sqrt{2}$).

In this assessment of the uncertainty it is assumed that the far field effects simulated with BEM may be considered as the "true" values. In Chapter 5 the results of the validation of these far field simulations will be discussed.

Both components of the engineering method, the near field matching procedure and the polynomial approximation, are implemented in a pre-programmed Excel spreadsheet. This will enable future users to apply the engineering method without additional implementation efforts and to obtain an estimate of the far field reflection effects directly from the near field test results.

The home sheet of the Excel spreadsheet is shown in Figure 30.

Calculation of Far field effects of noise barrier with the test results of CEN/TS 1793-5

1) Fill in RI [-] averaged over the nine microfoons: *1/3 octave frequencies [Hz]*

100	125	160	200	250	315	400	500	630	800	1000	1250	1600	2000	2500	3150	4000	5000
0,87	0,85	0,87	0,94	0,94	0,88	0,86	0,80	0,82	0,64	0,44	0,20	0,33	0,36	0,54	0,50	0,36	0,39

2) DL_{RInf} is calculated: DL_{RInf} till 1kHz = 1,5 dB

DL_{RInf} till 5kHz = 2,6 dB

3) Select barrier category: Sawtooth

4) Determine geometric parameters:
- Theta [deg]   90   Angle of inclination (only **Inclined**)
- H [m]   0,24   Height of profile repetition
- B [m]   0,09   Depth of profile
- He/H [-]   0,55   Ratio in/outward (only **Panes**)

5) Near field matching results:
- Best fitted material is:
- 2,4 DL_{RInf} fitted (till 1kHz)
- Porous concrete   type of material [-]
- 10   Flow resistivity [kPa s m-2]
- 0,05   Layer thickness [m]

6) Far field indicator DL_{Riff}:
- 5,7 $DL_{Riff,LR}$ (Low rise building)
- 3,6 $DL_{Riff,HR}$ (High rise building)

Inclined   Sawtooth   Zigzag   Steps   Panes

TNO innovation for life

QUIESST

Figure 30 - Picture of the home sheet of the pre-programmed spreadsheet for the application of the approximate engineering method

The engineering extrapolation method will also be described in Deliverable D 2.6 of QUIESST in the form of user instructions, intended to be included in a future version of the standard EN 1793-5 as an informative annex. This annex will specify how to process the results obtained with the near field reflection test into an estimate of the reflection contributions to the sound field at a distance of 100 m from the reflecting barrier.

5   Far field validation tests (AIT & CIDAUT)

Validation measurements for the prediction method based on analytical calculations under development in WP2, are described in this section, see also Figure 31.
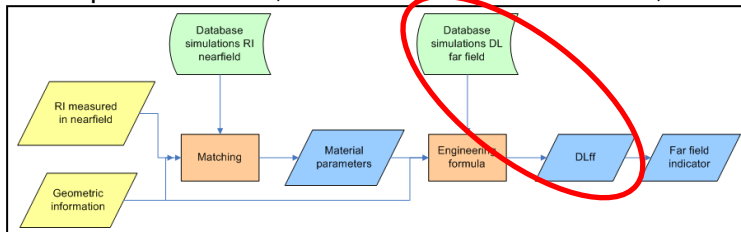
Figure 31 - Overview of approach – step 6

Taking advantage of the NRDs available at CIDAUT facilities in Valladolid (also used in the WP3 for the RRT), different scenarios were implemented, in which a number of samples were characterized in the far field.

First an introduction to the basis of the test method is given. After that the test site and its relevant characteristics with regards to the intended measurement campaign is described. Then test results are shown and analysed.

Details about the used hard and software plus the meteorological conditions can be found in appendix 8.4.

5.1 Measurement methods

Two different approaches were explored experimentally for the RI calculation in the far field. Basically, both methods followed the same set up but used a different noise signal as sound source. Thus, the necessary post processing of measured sound to obtain RI also differs.

5.1.1 Set-up

An (omni-) directional source is placed on the ground at 5m distance and facing the NRD, in order to minimize ground reflections. The sound source is fed with a MLS signal or pink noise depending on the type of post processing method (see section 5.1.2 and 5.1.3). Microphones facing the NRD, are placed at 20m and 30m distance from the barrier at 2 and 4m height. In addition to this test setup with the loudspeaker placed 5 m from the wall and the microphones in 20 respectively 30 m and 2 respectively 4 m heights (configuration I, Figure 32), AIT also used a somewhat smaller test setup with a loudspeaker – noise barrier distance of 4 m, and microphone – noise barrier distances of 10 respectively 20 m and microphone heights of 2 respectively 4 m (configuration I). All information about the hardware used can be found in the appendix 8.4.1.

Measurements of free-field and with a mirror source (representing an infinite rigid barrier) have been carried out using the same geometrical configuration of the loudspeaker and microphones (i.e.: relative distances and orientations). This is visualized in Figure 33 and Figure 34.
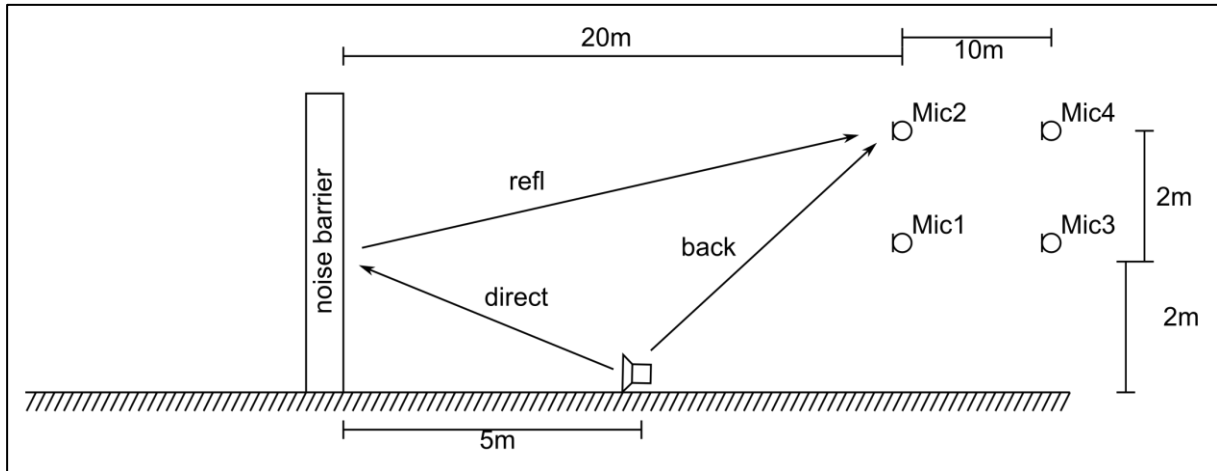
Figure 32 - Test set-up
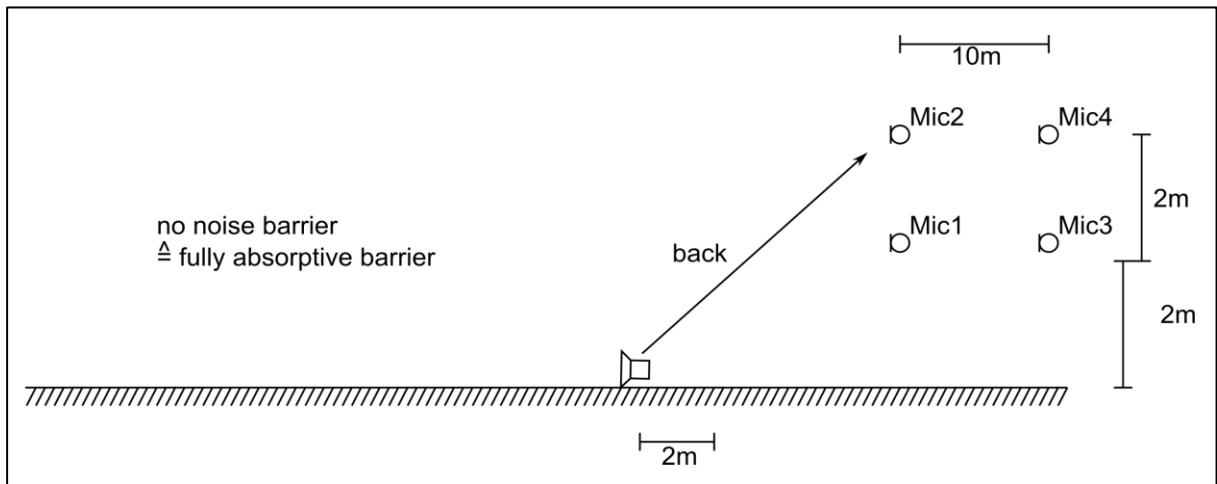
Figure 33 - Free-field measurement to determine the influence of the backwards emitted component
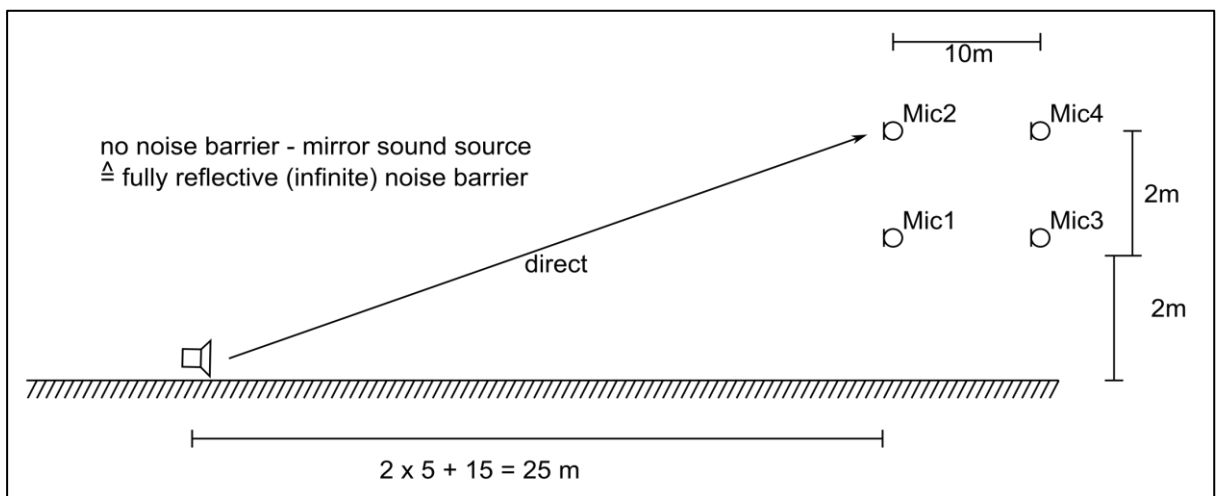
Figure 34 - Measurement to determine the direct component emitted towards the noise barrier according to a mirror sound source model

5.1.2 Method A: Impulse response method

To determine the absorption coefficient of a noise barrier in the far-field, method A uses the impulse response of the transmission path between a loudspeaker and a microphone. In the obtained impulse responses, by windowing in the time-domain, the reflected and the backwards emitted component of the impulse responses can be separated (see Figure 45). The direct component (i.e. incident on the test sample) is determined by a measurement in a setup imitating a mirror sound source (Figure 34). By using this mirror source setup, no propagation correction and no correction due to the directivity of the sound source has to be applied on the different impulse response functions.

Mostly in accordance with CEN/TS 1793-5 and WP3 of the QUIESST project, the sound absorption respectively the reflectivity ρ of the noise barrier can be determined via:

$$\alpha = 1 - \rho = 1 - \frac{\left|F\{h_{reflected}(t)\}\right|^2}{\left|F\{h_{mirror}(t)\}\right|^2}$$

where $h_{reflected}(t)$ and $h_{mirror}(t)$ are the windowed impulse responses and F is the symbol of the Fourier transform.

5.1.3 Method B: Continuous sound signal

The second method makes use of measured sound pressure levels of a continuous sound signal. To obtain the absorption properties of the noise barrier, noise is fed to the sound source over a certain period of time. Here, the measured sound pressure levels consist of the sound emitted by the sound source and reflected by the noise barrier (so called "reflected component") as well as components emitted from the back of the loudspeaker (so called "back component"). Two additional measurements have to be performed to gain enough information to characterize the noise barrier: first, a free-field measurement as shown in Figure 33 has to be done to evaluate the influence of the back component; second, the total sound pressure levels emitted towards the noise barrier ("direct component") have to be determined by the principle of a mirror sound source, as shown in Figure 34

To finally determine the sound absorption α (or the sound reflection factor ρ), the reflected component corrected for the back component is set in proportion to the direct component:

$$\alpha = 1 - \rho = 1 - \frac{p^2_{reflected} - p^2_{back}}{p^2_{mirror}}$$

In order to eliminate the influence of ground absorption, all of these measurements have to be performed on a ground with the same acoustic properties. Also, the use of a highly directive sound source helps to minimise the influence of the back component.

5.2 Test site and barrier samples

The far field validation measurements have been carried out at the CIDAUT test facilities in Valladolid (Spain). The test site (NRD samples) is the same that was used in the Round Robin test campaign within WP3. However, in this occasion samples were covered with acoustic absorptive material to isolate the influence of each barrier from the others. Figure 35 shows the process of NRDs installation and assembly process.

The selected location for the installation of noise barriers is located more than 0.5 km away from the nearest road. The only noise source in the vicinity, apart from the already mentioned road is a small factory placed almost 1 km away. Although the test method is designed to be not affected by background noise, during measurements it was checked that no noticeable undesired background noise was detected. Test facilities are located in a flat area, with no uneven land surface.

Figure 35 - Metallic posts preinstalled before NRD assembly (left) and assembly of NRDs (right)

The test site is prepared for the installation of up to 60m length continuous noise barriers, with a maximum height of 4m. H posts are installed each four meters, allowing for the installation of a great variety of noise reducing samples that can fit within the existing H shaped profile dimensions. The surroundings of the test site and the kind of ground are depicted in Figure 36.

(dimensions in m, not to scale)

Fine aggregate

This area is free of reflective objects. The outside area is vegetation (grass)
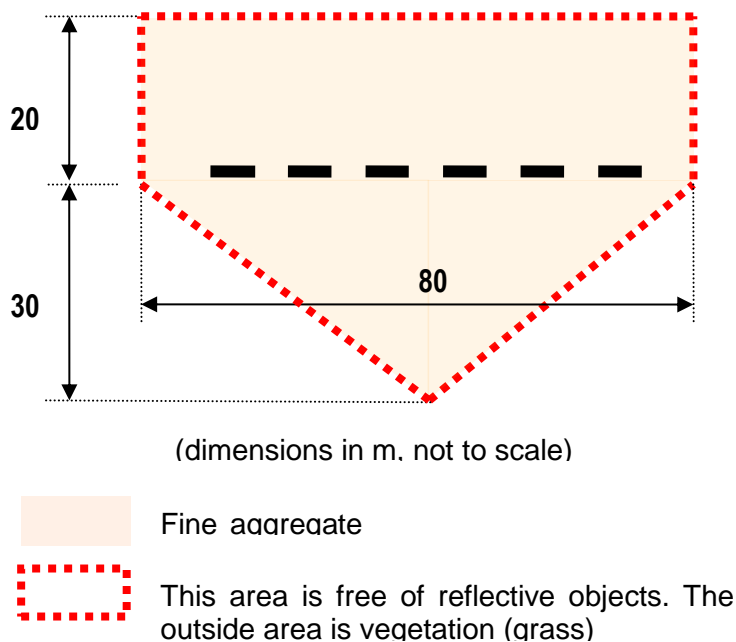
Figure 36 - Test site description (CIDAUT-Valladolid)

The condition of the ground is fine aggregate (sand) as can be seen in the right side of Figure 36 (microphones located at 7m and 20m are within this area) and grass and/or vegetation in the surrounding area (where the 30m distance microphone is located). An overview of the test site and microphones position is given in Figure 37
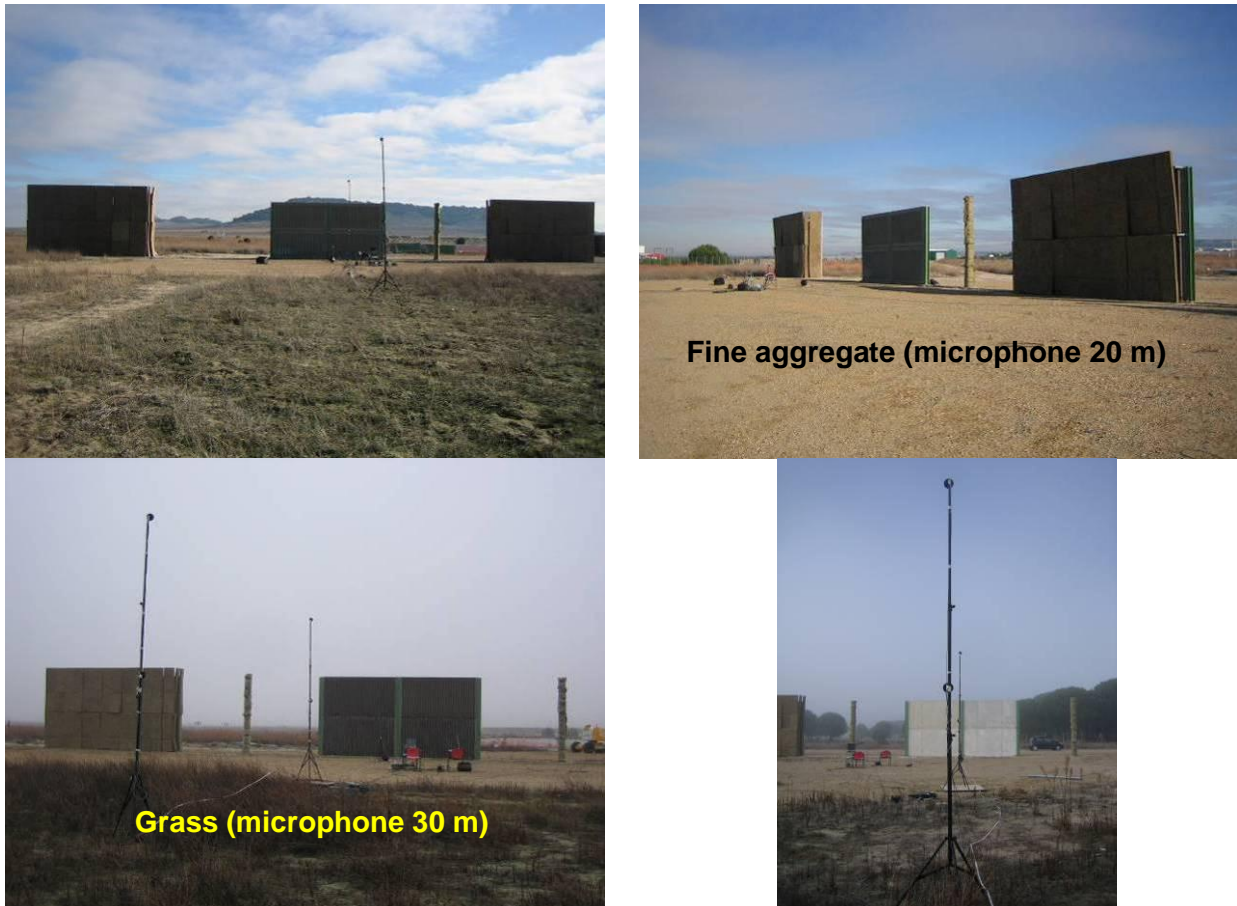
Figure 37 - Microphones and relative distance to NRDs during test

As decided by the consortium, the CIDAUT test site was dedicated to non-flat or absorptive NRD samples. These kind of noise reducing devices are the more challenging ones for the far field test method used for the validation measurements. Although such kind of products are quite rarely manufactured and installed in Spain, three noise barrier manufacturers contributed to the project, providing and installing for free the requested type of samples.
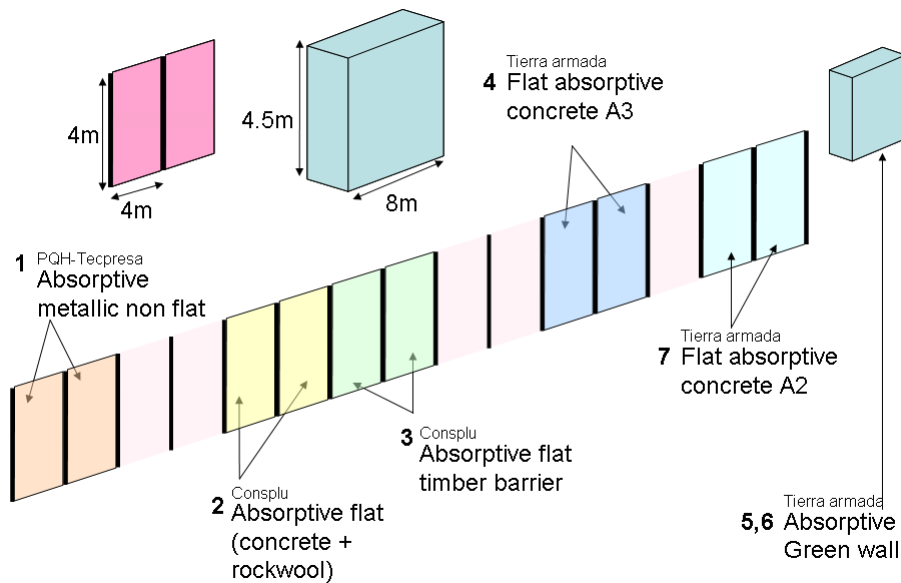
Figure 38 - Sketch of installed samples

Seven different samples were provided (five of them one sided and another one two sided):

- Tierra Armada S.A:
  - Flat absorptive concrete A2 type (#7)
  - Flat absorptive concrete A3 type (#4)
  - Two sided non flat sample:
    - Absorptive green wall (#5)
    - Extra absorptive green wall (#6)
- Consplu S.A:
  - Absorptive flat timber barrier (#2)
  - Absorptive flat (concrete + rockwool) barrier (#3)
- PQH - Tecpresa S.L:
  - Absorptive metallic non flat (#1)
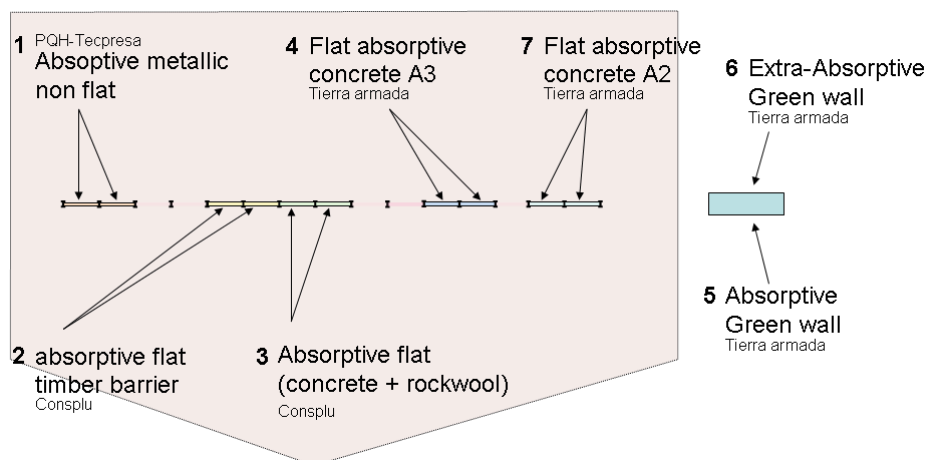
Figure 39 - Description of installed samples, provider and relative location

All samples except the green-wall were 4m height and 4m length, and in order to take into account the influence of metallic posts, they were installed in 8m length (4m+4m). Taking advantage of the available space, some samples were separated by empty spaces, as

depicted in Figure 39. Slightly apart from the already existing infrastructure, a dedicated green wall sample was built, with larger dimensions (4.5m height) and different acoustic properties on each side. More details can be seen in Figure 40.
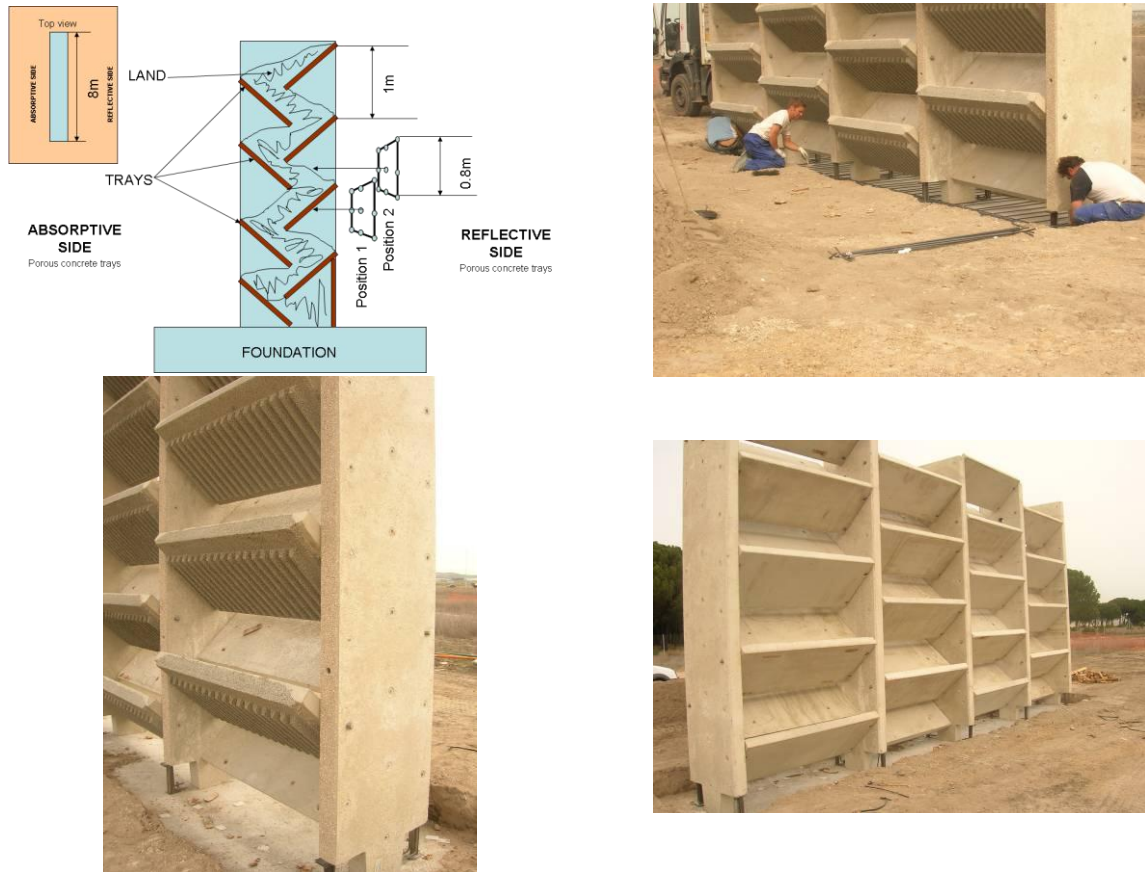
Figure 40 - Green wall sketch (upper left), installation (upper right). Extra absorptive (bottom left) and absorptive (bottom right) sides

Barriers listed below have been addressed in WP2 for the far field validation measurements:
- Barrier 1: Flat absorptive concrete (A2).
- Barrier 2: Non flat absorptive concrete (A3).
- Barrier 3: Flat timber barrier.
- Barrier 4: Flat absorptive (metal+absorptive material+concrete).
- Barrier 5 (reference): Flat rigid barrier.

Three samples (A2, A3 and flat rigid) have been tested by CIDAUT and 5 by AIT. Two samples were excluded from the study (identified in Appendix 8.4.5 by the red cross, those which were strongly not flat). Each barrier has 8m length and 4m height (with a metallic post in the middle), therefore the barrier surface is 32 m2.

Two different measurements were needed for the RI calculation:
- A reference measurement of a perfectly flat and reflective rigid barrier, which was performed thanks to the backside of barrier A3 (number 2 in Figure 39).
- Far field characterisation of absorptive gently non flat noise barriers

In order to reduce unwanted reflections and diffractions, during gently non flat absorptive samples characterisation in the far field, any reflective surface in the vicinity of the tested sample, such as metallic posts and adjacent barrier samples, were covered with absorptive material (hereafter named "acoustic curtain"). The acoustic curtain was specifically designed and manufactured for WP2 measurements, and it was made of 32 panels of 80 mm thickness mineral wool, 1.22m width and 2.44m or 2m height, backed and glued to light rigid panels. Those panels were hanged from a metallic structure specially added to completely cover all samples surfaces. (for more details see **8.4.4**).

Figure 41 - Rock wool panels manufactured to cover NRDs in WP2 measurements
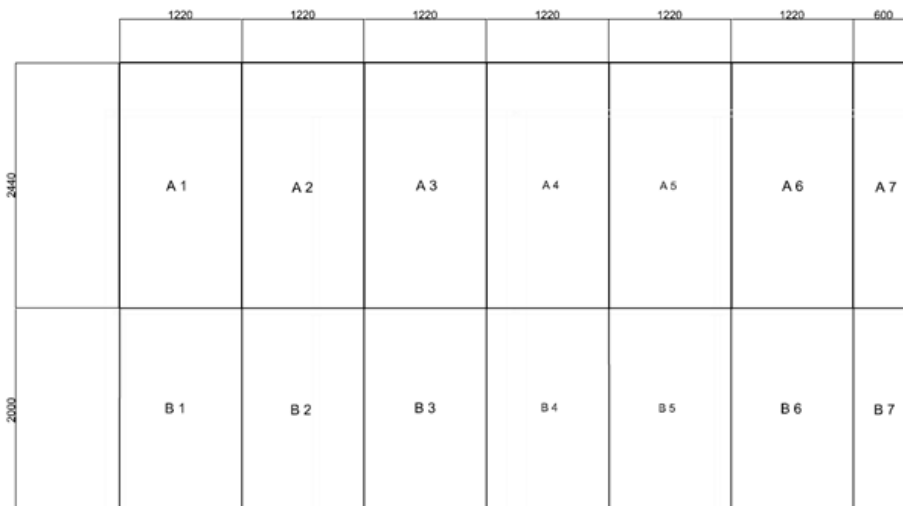
Figure 42 - Acoustic panels size and distribution covering a 4m x 8m noise barrier

After fixing the metallic frame, for each sample characterisation, two operators using a crane assembled and dismantled the acoustic barrier as necessary, to reproduce each test set up. An example of the metallic frame and the acoustic curtain mounted on different noise barriers can be seen in Figure 43.

Figure 43 - Metallic frame (upper left) and acoustic curtain installed. Metallic post covered with acoustically absorptive material (bottom left)

In Appendix 8.4.5 the exact measurement set-up including the placing of the acoustic curtains can be found.

Tested barriers used in the far field validation show differences in geometry and material composition. Figure 44 shows pictures and information of tested barriers (for more details of A2 and A3 geometry see 8.4.6).

Barrier A2		
		Material: Porous concrete **Thickness:**190 mm (teeth valley depth=65 mm)
Barrier A3		
		Material: Porous concrete **Thickness:**265 mm (teeth valley depth=140 mm) NOTE: The porous material was damaged during installation in some areas of the barrier

Flat timber barrier		Material: Timber lames. Thickness: 100 mm
Flat absorptive		**Material:** Perforated metallic panel+absorptive material+concrete **Thickness:** 150 mm
Rigid Barrier		**Material:** smooth concrete **Thickness:**10 mm **NOTE:** A3 backside.

Figure 44 - Detailed description of NRD test samples

5.3 Meteorological conditions

The meteorological conditions at the times of the two separate measurement campaigns of CIDAUT and AIT are listed in appendix 8.4.3.

5.4 Measurement results

According to the test methods described in 5.1, two test campaigns for NRDs far field validation have been carried out by two different laboratories (CIDAUT and AIT). Tests were conducted in two different seasons of the year, so the meteorological conditions experienced by each laboratory were very different. In the following sections a detailed description of test conditions, microphone positions and results obtained by each laboratory is given.

5.4.1 Method A: Impulse response method (CIDAUT)

Recorded impulse response signals consist of a direct component due to the sound from the backside of the loudspeaker, a reflected component coming from the barrier under test and other parasitic components like ground reflection and edge diffractions. The separation of the

different components, have been made by means of temporal windowing in the time domain. The delay between the arrival of direct and reflected component is long enough, therefore the relevant components can be extracted from the overall impulse response by application of the time window (Adrienne length=10 ms) as Figure 45 shows.
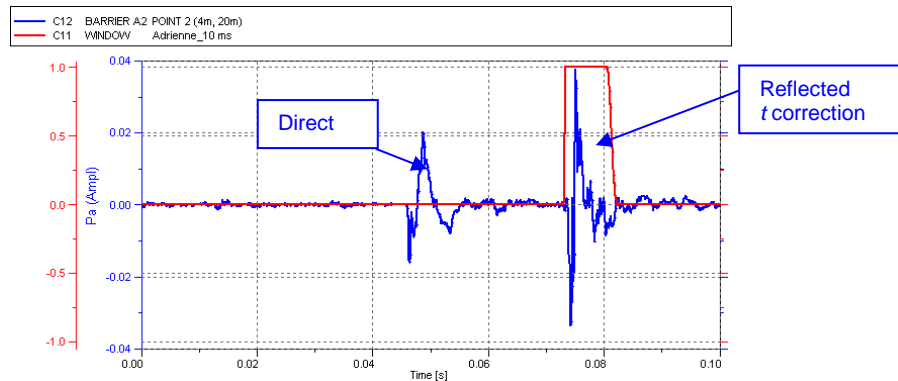
Figure 45 - Method A: example of temporal separation of components for barrier A2, point 2, 4 m height and 20m barrier distance (The Direct component is the backwards emitted sound, directly from the source to the receiving microphones)

From the response impulse like the one shown above, the reflection index in third octave bands in the 100-5kHz range for each microphone (4 positions) is obtained for all three tested barrier samples where the colours represent the different microphone positions:
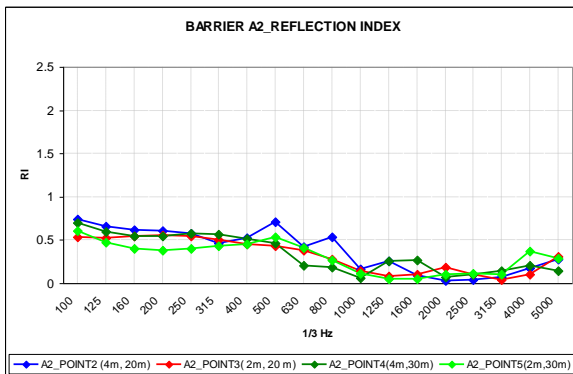
Figure 46 - Method A: Reflection index for barrier A2
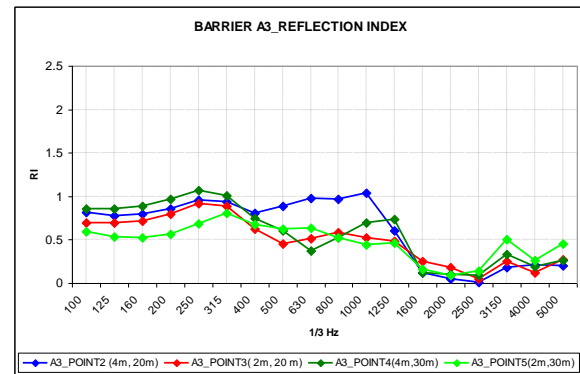
Figure 47 - Method A: Reflection index for barrier A3
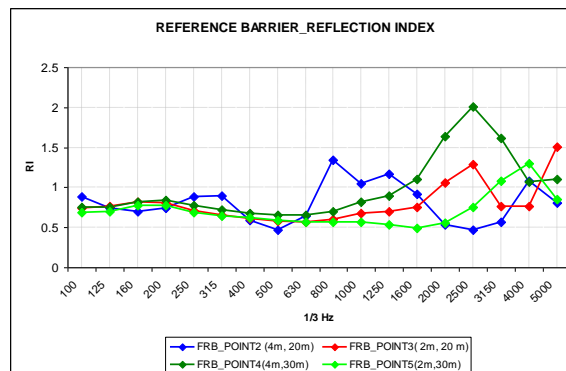
Figure 48 - Method A: Reflection index for reference barrier

The reflectivity of the barrier can also be expressed in the single number rating of sound reflection (DL_{RI}) for each microphone in the 100-5kHz range. The next table summarizes this single number DL_{RI}

	DL_{RI} (100-5000 Hz)
A2_Height=4m,distance=20 m	5
A2_Height=2m,distance=20 m	6
A2_Height=4m, distance=30 m	6
A2_Height=2m, distance=30 m	6
Global_A2	**6**
A3_Height=4m, distance=20 m	2
A3_Height=2m, distance=20 m	3
A3_Height=4m, distance=30 m	3
A3_Height=2m, distance=30 m	3
Global_A3	**3**
FRB_Height=4m, distance=20 m	1
FRB_Height=2m, distance=20 m	1
FRB_Height=4m, distance=30 m	0
FRB_Height=2m, distance=30 m	2
Global_FRB	**1**
Table 13 - Single number rating of sound reflection DLRI (method A)	

Comparison of results different barriers
This section shows the results comparison among the different tested barriers. The Figure 49 shows the comparison of RI values obtained at each microphone position by CIDAUT for A2, A3 and the flat rigid barrier (FRB).
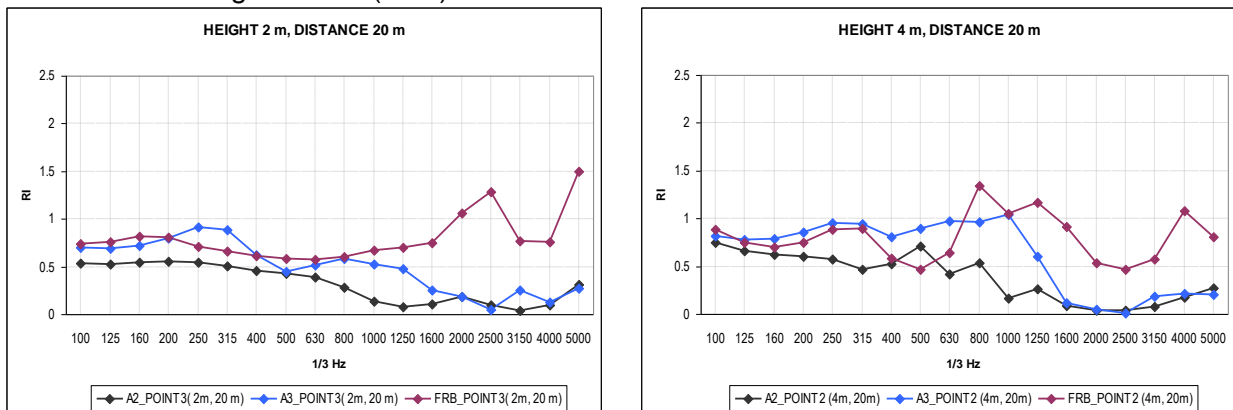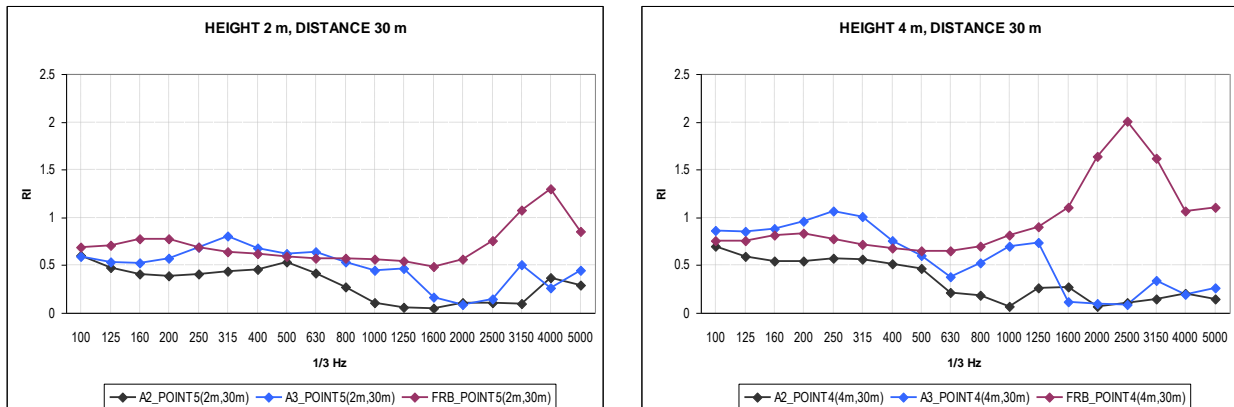
Figure 49 - Method A: Comparison of Reflection Index for each barrier/microphone position. A2 black, A3 blue and FRB purple

In general the rigid barrier shows higher values than the absorbing barriers mainly at high frequencies (over 800-1000 Hz). However, at high frequencies the reflection indexes show a remarkable variability. Reflection index values for the flat rigid barrier should be close to 1 in the whole frequency range, but while at lower frequencies it is, this is not the case at higher frequencies, at which values above 1 are found. Possible reasons for this can be contributions from the own diffractions of the barrier tested, ground effect or the disturbing influence of meteorological conditions.

Barriers A2 and A3 show a similar behaviour in the whole frequency domain where the reflection index is higher at low frequencies and decreases as frequency increase. Remark, that for the low frequencies, barrier A3 (with a thicker layer of absorptive material) shows higher results in the reflection index, while a lower result would be expected. It was noted that some parts of the absorptive material in barrier A3 were damaged during its installation. However, the measurement results of AIT do not show the same tendency.

5.4.2 Method A: Impulse response method (AIT)

The measurements by AIT were performed from 16.04.2012 to 20.04.2012 in Valladolid. During this measurement campaign 5 walls (barrier A2, barrier A3, flat timber, flat absorptive and rigid barrier) where measured. Two different sound sources where used provided by the project partner CIDAUT, one of these a directional speaker ("Celestion"), the other an omnidirectional sound source ("B&K 4296"). In addition to this, three of these walls (barrier A2, barrier A3 and rigid barrier) where measured twice as to obtain an impression of the repeatability of such measurements.

During the measurement period, high wind speeds occurred affecting the measurements and decreasing the data quality. Information about the weather conditions can also be found in the Appendix 8.4.3.

Figure 50 to Figure 54 show an extract of the results of these measurements. All results can be found in appendix 8.4.8. As can be seen from them, an overall trend of the reflectivity can be observed from strong reflectivity in the lower frequencies to good absorption for high frequencies. The performance of the different walls seems to be mainly definable by the frequency where the crossover from reflective to absorptive acoustic behaviour takes place. As the maximum of road traffic noise is in the frequency range about 1 kHz, special focus has to be placed on this region. The crossover frequency occurs in this frequency region for

the test walls A2 and A3, whereas for the flat absorptive and flat timber barriers the transition from reflective to absorptive behaviour takes place at lower frequencies about 400 Hz.

When excluding obvious outliers, also an acceptable repeatability can be seen in the measurements. Also, the results between the different loudspeakers are in reasonable accordance, despite the extremely different directional emission characteristics. Illustration of this can be found in appendix 8.4.8.

Nevertheless, especially the results in the high frequency range have to be scrutinised. As the measurements at the flat rigid barrier show, the meteorological conditions, especially the high wind squalls, have a severe influence on the measured reflectivity in the highest frequency bands. Where a high reflectivity has to be expected for this sample wall, above 3 kHz large deviations between the different microphone positions are seen, clearly indicating the strong influences of the squalls on the measurements despite the large amount of 60 repetitions of the MLS.
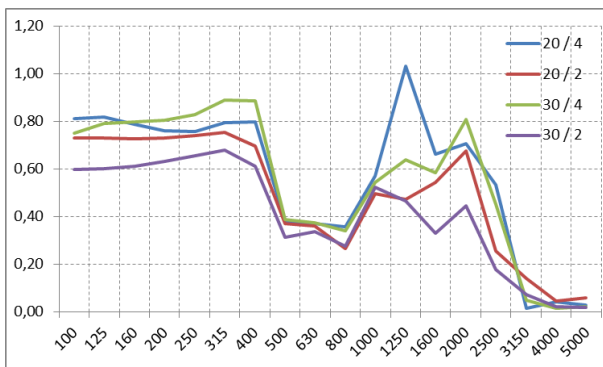
Figure 50 - RI rigid barrier with B&K loudspeaker
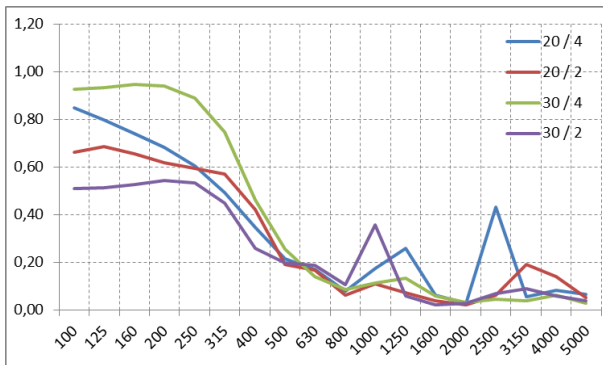
Figure 51 - RI method A flat absorptive barrier with B&K loudspeaker
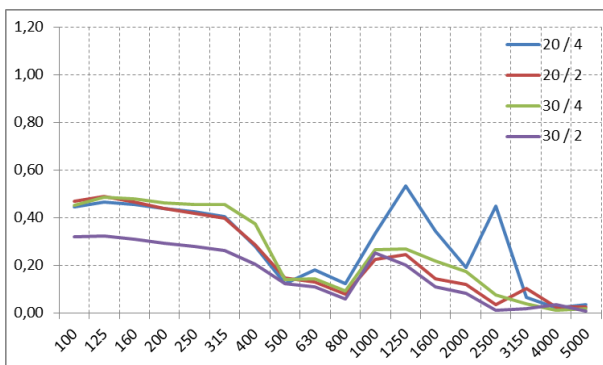
Figure 52 - RI method A flat timber barrier with B&K loudspeaker
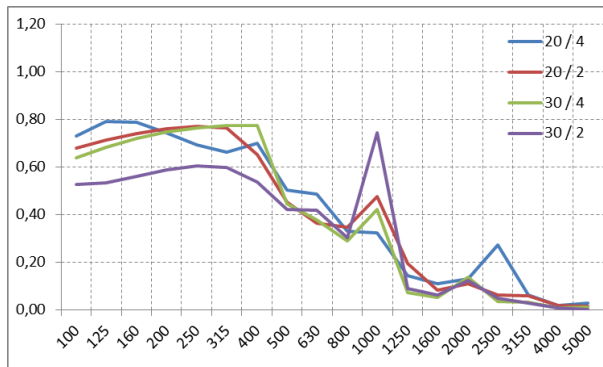
Figure 53 - RI method A barrier A2 with B&K loudspeaker
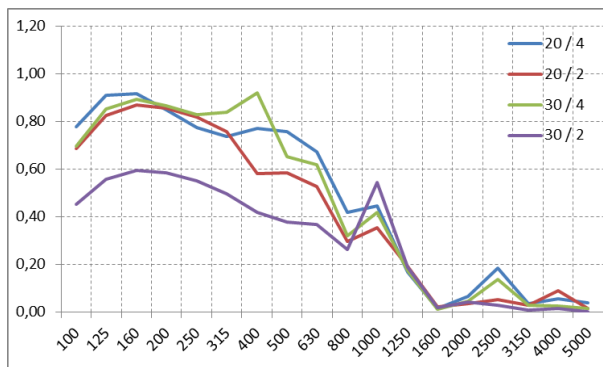
Figure 54 - RI method A barrier A3 with B&K loudspeaker

5.4.3 Method B: Continuous signal (CIDAUT)

Despite the extensive analysis no consistent information or conclusion could be extracted from the measurement with method B.

5.4.4 Method B: Continuous signal (AIT)

The measurements were performed from 16.04.2012 to 20.04.2012 in Valladolid. During this time, 4 walls (A2, A3, flat timber and flat absorptive) where measured. One sound source was used, a directional speaker ("Celestion"). The omnidirectional sound source ("B&K 4296") was excluded from these measurements as the direct component would considerably exceed the desired signal reflected from the barrier under test. One of the walls (A3) was measured twice as to obtain an impression of the repeatability of such measurements.
As mentioned under section 5.4.2, high wind speeds occurred affecting the measurements and decreasing the data quality.

The results of all measurements for configuration I are presented in Figure 55 to Figure 58. All the measurement results including the configuration II and repeatability measurement can be found in appendix 8.4.10. It can easily be seen that, although also showing a trend from reflective to absorptive with rising frequency, the results are much more influenced by the squalls than for method A. The spreading of the reflectivity is much larger, especially in the low frequencies.

Although, when comparing these results with the reflectivity obtained by method A, some parallels can be found for the noise barriers, no definitive conclusions of the effectiveness of the barriers among each other can be drawn.
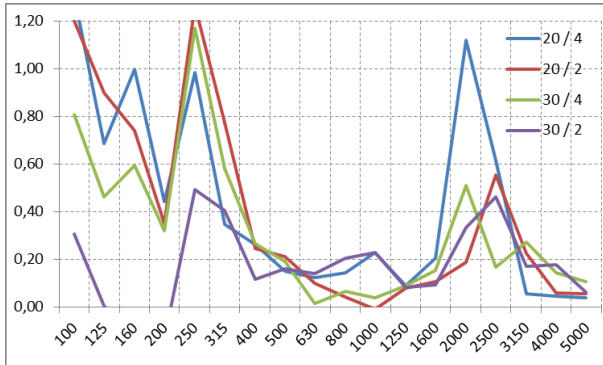
Figure 55 - RI method B flat absorptive barrier
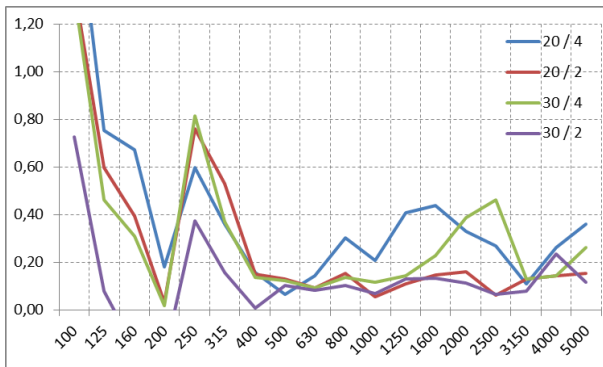
Figure 56 - RI method B Flat Timber barrier
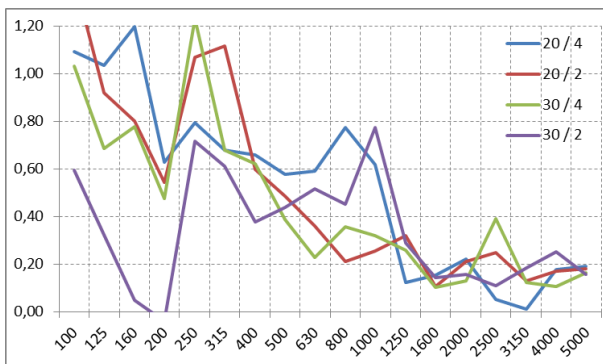
Figure 57 - RI method B A3 barrier, first measurement
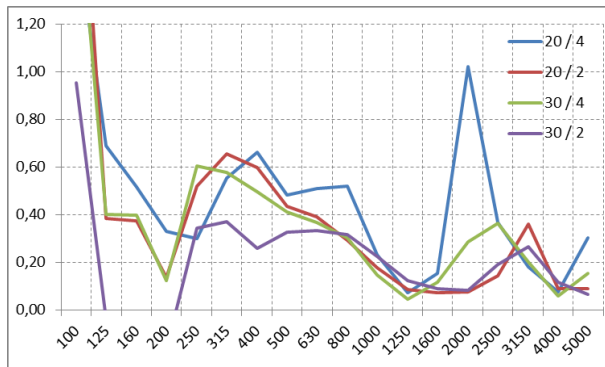
Figure 58 - RI method B A2 barrier

5.5 Conclusions validation measurements

5.5.1 CIDAUT

Method A
The results for Method A obtained by CIDAUT allows to know the absorption tendency (in a qualitative way) for the tested barriers. However, it appears that the results obtained with this method are not very precise. Measured impulse response signals indicate that this method is very sensitive to microphone position and meteorological conditions. Although direct and reflected components can be clearly identified and be separated, corresponding reflection index results might indicate that measured sound signals are influenced by microphone positions, sound propagation conditions (air temperature and wind), and acoustic ground impedance.

Method B
According to results shown in the previous sections, only the flat rigid barrier used as reference provides coherent results suitable for model validation. With the rigid barrier, unexpected values are obtained. Method B is only based on the continuous SPL, which provides much less information than the impulse response, which is based on impulsive direct and reflected components, their arrival times and amplitudes. This fact does not allow identifying the origin of observed discrepancies in the results obtained from both methods. Due to the unreliability of the method B results these will not be used for validation comparisons.

5.5.2 AIT

Method A
When analysing the results obtained with method A, trends for the reflectivity of the noise barriers under test can be found. As high wind speeds and squalls influenced the measurements, the obtained impulse responses had to be improved by an aligning procedure of the single impulse responses, thus producing reasonable outcomes and allowing at least an ordering of the test walls.

Method B
The results acquired with method B are more strongly affected by the meteorological conditions than the results from method A. As the sound pressure levels where measured directly, no opportunity to further improve the measurement results in post-processing was given. The results show large deviations between the results of the different receiving positions and between the different frequency bands, not allowing a reasonable interpretation

of the test walls. Due to the unreliability of the method B results these will not be used for validation comparisons.

5.6 Comparison validation measurement with simulations

BEM simulations were performed for the geometry corresponding to the set-up of the measurements. An omni-directional point source is used and the ground is modelled as rigid, i.e. a mirror source is used to limit the computational times. The source is placed 0.10m above the ground as the centre of the real loudspeaker will also be above ground level. The complex pressures are computed for equally spaced frequencies up to 5kHz.
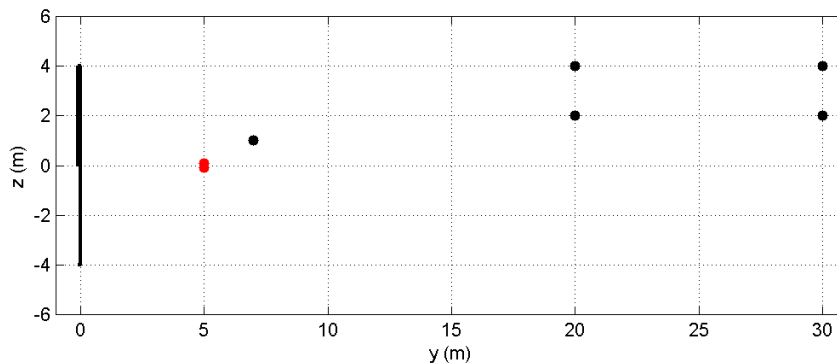
Figure 59 - BEM validation simulation set-up (red dots are source, black dots receivers).

As the absorption coefficient of the barriers sample is not exactly known an engineering guess has to be made for the material. The thickness of the porous layers are derived from the drawings in Appendix 8.4.6.

In Table 14 the best guesses of the flow resistivity used for the validation simulations are listed. Other material parameters like porosity or perforation percentages are defined within the material category. In the table, a figure with the corresponding normal incident absorption coefficients is also shown. For the porous concrete (material B) the frequency with maximum absorption clearly depends on the thickness of the material. Two extra variants of the porous concrete material have been added: barrier A2 with a smaller thickness to simulate a reduced effective absorption, and barrier A3 with the material parameters resulting from the matching procedure described in section 4.2.4.

Table 14 - Best guess of material properties for the barriers A2 and A3

Barrier	Material category	Flow resistivity [kPa s m-2]	Material thickness [m]
A2	B	10	0.07
A2 thin	B	10	0.035
A3	B	10	0.15
A3 matched	B	20	0.10
Rigid	A	-	-

Figure 60 Best guess absorption curves for material on barrier
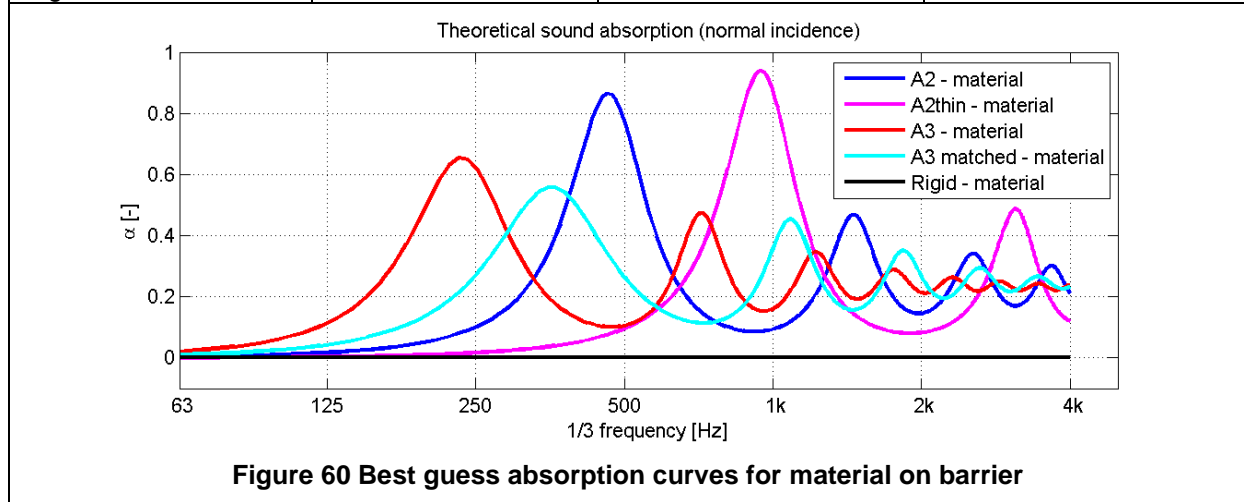
The data from the BEM simulations are postprocessed according to validation measurement method A giving the RI spectra shown in Figure 61.

Figure 61 - RI for all barriers computed with BEM
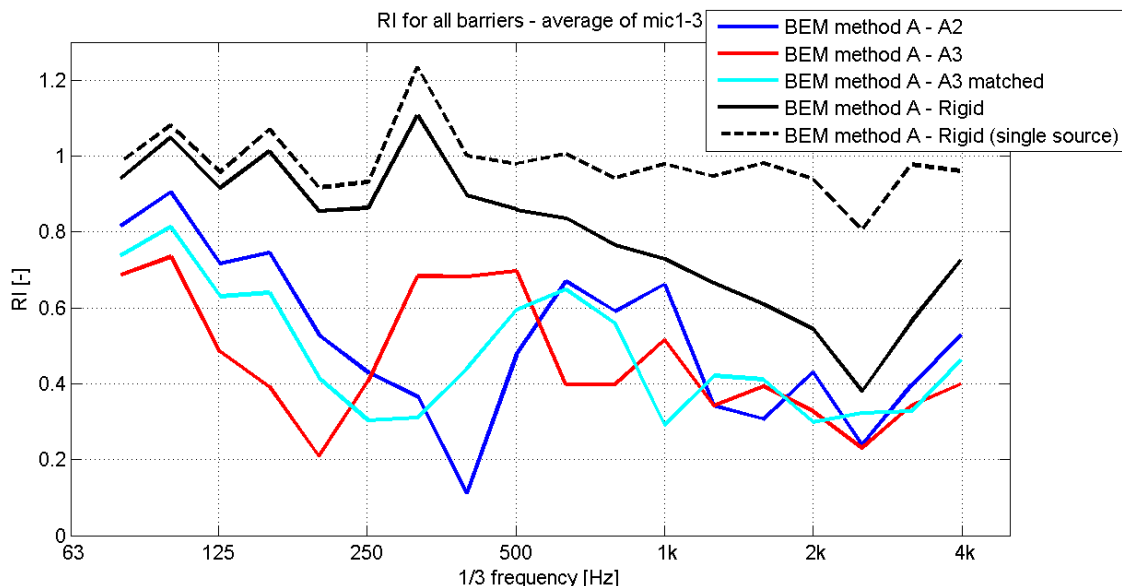
When considering the absorbing barriers A2, A3 and A3-matched, Figure 61 shows that the frequencies for which maximum absorption occurs are also visible for the RI values.

For the flat rigid barrier two numerical simulations were done. One with a source at 0.10m above the ground and with a reflecting surface, and one with the source on the ground (marked as "single source"). For low frequencies both results show RI values around 1.0, as

expected. Due to the edge diffraction from the top of the barrier these values deviate from an exact value of 1.0.

For higher frequencies the RI results for a source slightly (0,10 m) above the surface start to deviate from 1.0. This is due to the interference between the source and the mirror source at –0.10 m.

In the measurement results this effect is assumed to be present too, so the BEM results with a source above the ground are used for the comparison with measurements.

The data is averaged over the microphone positions, as the variation in microphone height and distance to the barrier will result in a variation of the ground interference effect. Instead of all four microphones, the date is averaged over three microphones as the (30,2)m microphone showed an exceptional interference effect. Although still visible, the interference is less pronounced for the measurements as the phase relationship between the direct and the reflected waves is distorted by ground and meteo-effects (see previous figures for AIT and CIDAUT).

The BEM results and the measurements with method A by AIT and CIDAUT are shown in Figure 62. The far field single number rating values ($DL_{RI, ff}$) of the measured and simulated results are given in Figure 63. As the A-weighted traffic noise spectrum is used, values at frequencies around 1000 Hz give the most significant contributions to this single number rating. Therefore, the simulated effects for porous concrete at low frequencies do not have a large influence on the $DL_{RI, ff}$ value.
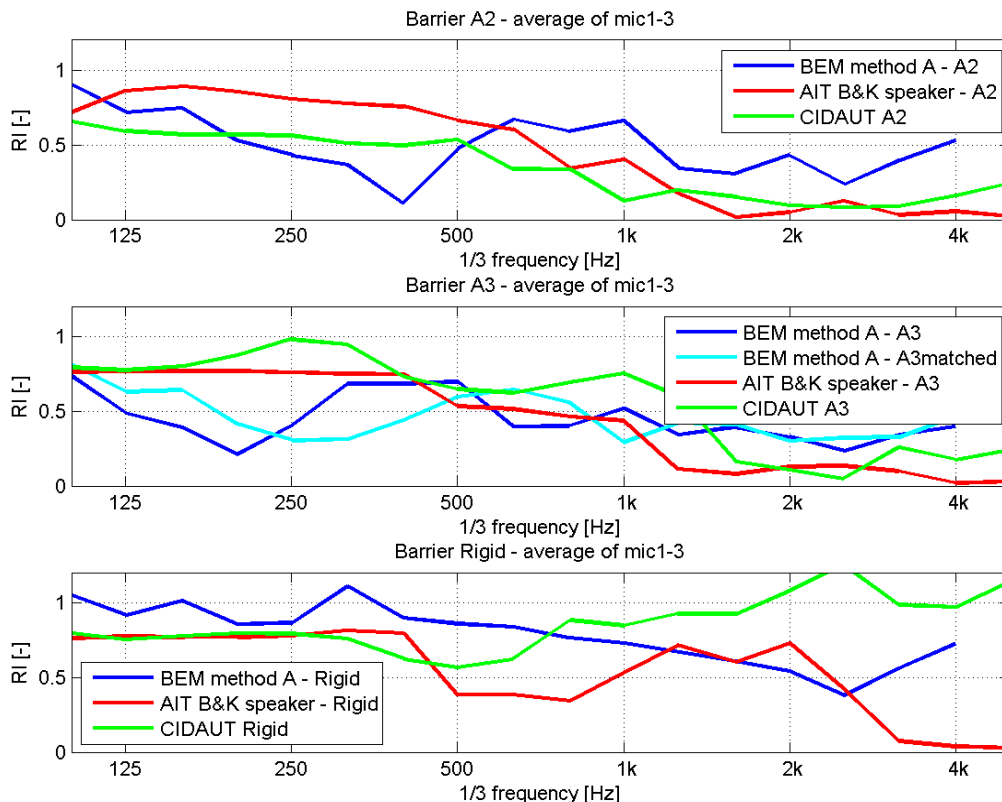
Figure 62 - Comparison of RI values for all barriers measured by AIT and CIDAUT and simulated with BEM – averaged over receiver positions 1 – 3.
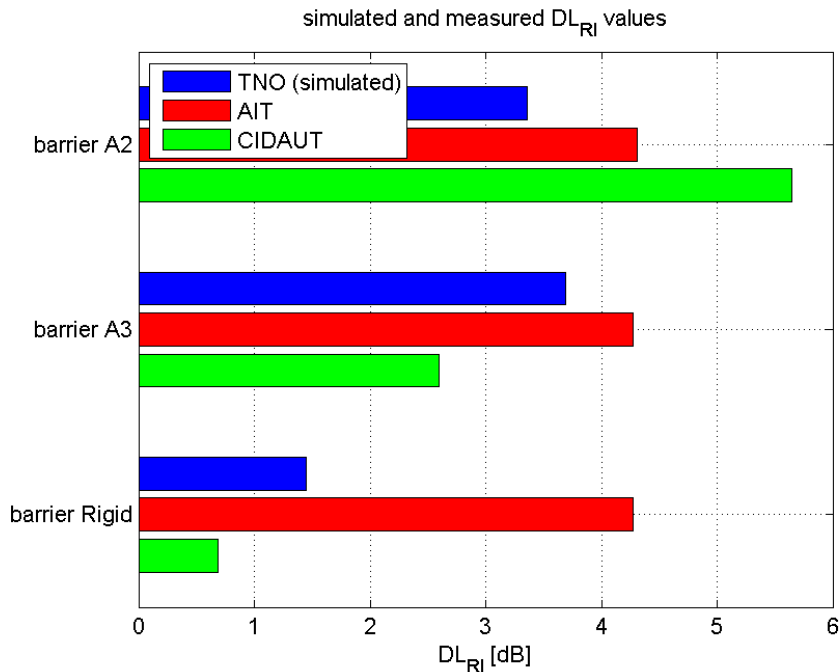
Figure 63 – Far field single number rating results (DL$_{RI, ff}$; computed up to 4 kHz) of simulated and measured barriers.

For the barrier sample A2 the correspondence between the simulated results and the measurements is not so good. In the frequency range from 500 to 3000 Hz the simulated RI results are higher, due to the assumed sound absorbing material behaviour. At lower frequencies (< 500 Hz) the simulated and measured RI values differ considerably. The simulated minimum RI value at 400 Hz does not appear in the measured data. According to the measurement results, the porous concrete material for barrier A2 shows a sound absorption that increases rather smoothly with frequency and seems to behave more like material C "mineral wool in cassette" rather than material B "porous concrete".
As a result the single number value for barrier sample A2 for the simulation (Figure 63) does not agree well with the measurements. The difference between simulation and measurements is 1 dB for the AIT results and more than 2 dB for the CIDAUT results.

For barrier sample A3 a better correspondence is found between 500 and 3000 Hz. But also here, the predicted absorption maximum, resulting in relatively low RI values for frequencies around 200 Hz, is not found in the measurements. Using the input data from the matching procedure does not give a significant improvement. The RI values measured by CIDAUT are over the whole frequency range significantly higher than the values measured by AIT, as was already noted in section 5.4.1.
In this case the single number value of the simulation agrees well with the AIT measurement result, but the difference with the CIDAUT result is rather large.

For the flat rigid reflective barrier the three results show a different behaviour. An RI value of 1.0 is expected, but due to ground and meteorological effect this value is not measured. As noted earlier in this section, the decreasing RI values for higher frequencies is due to the source located at a small height above the ground. The high values for CIDAUT are due to a positive interference at the microphone location (30,4). The low values for AIT between 500 and 1000 Hz cannot be explained, but result in a relatively high single number value of DL_{RI}.

All the above observations for the flat rigid reflective barrier are reflected by the single number values of DL_{RI}. Note that only the CIDAUT result is close to what might be expected at first sight; a DL_{RI} of 0 dB(A), in view of the fully reflective character of the rigid barrier.

5.7 Conclusions

Measuring the reflectivity of noise barriers in the far field has proven to be a challenge. In WP2 a first experimental attempt has been made in which two different measuring methods, applied by two testing laboratories in separate measuring campaigns, have been compared. During the two measurement campaigns the meteorological conditions have been difficult and especially the high wind speed has affected the measurements, as also seen in [10]. Although extensive analyses have been performed on the measurement data, the results for test method A should be considered as indicative for the barrier's reflective properties. Test method B, that applied a continuous sound signal, did not deliver reliable results.

The simulated RI and DL_{RI} results show the same trends as the measurement data. Note that for the simulation the absorptive behaviour of the barrier was estimated. When also considering the other issues (such as meteorological and ground conditions, the use of a mirror source, and a small source height), comparing numerical simulations with real measurements will only enable qualitative conclusions. A quantitative comparison revealed equal deviations between simulation and measurements as between the two measurements among themselves.

Unfortunately the validation measurement results cannot be used as an incontestable proof of the correctness of the BEM far field simulations.

Based on experiences in other studies [6] [13] there is, however, a well-founded confidence in the reliability of the BEM simulation method if it is used for modelling of sound propagation over relatively short distances. Therefore the far field simulation results are considered as reliable data and the engineering extrapolation method based on these results is presented with confidence and the uncertainty values specified in section 4.4 are seen as realistic estimates.

Possible further work may include fine-tuning of the measurement technique under better meteorological conditions to get more robust results. At that moment also measuring more non-flat barrier samples should be considered. Besides that, a better characterisation of the acoustic material on the barrier should be used.

6 Conclusions and recommendations

6.1 Conclusions

6.1.1 Near field simulations

In the earlier stages of QUIESST WP 2 three different simulation methods for the simulation of the near field reflection test on Noise Reducing Devices (NRD's) were tested. The most efficient of these three was chosen to execute a large number of near field simulations. This selected method was the Boundary element method combined with a Fourier transformation to the time domain. It was applied for five different barrier types and three different material types, with systematic variations of geometrical and material parameters. In total 1196 variants of NRD 's were simulated and the results stored in a database.

Next, the numerical results of the near field test data were processed in the time domain in full accordance with the most recent revision of the near field reflection test method developed in WP 3. In order to keep computation times at acceptable values it was necessary to limit the highest simulated frequency to 10 kHz and the frequency resolution to 10 Hz. After Fourier transformation to the time domain this resulted in a time resolution of 0,1 ms, which is much less than the time resolution of the measurements (0,02 ms). This limitation in resolution influenced the shape of the simulated impulse responses and was the cause of deviations between simulated and measured results above 1000 Hz.

Therefore results above 1000 Hz were not used for comparisons between simulated and measured results.

6.1.2 Far field simulations

The BEM simulation method was also used to simulate the contribution of reflected sound to the sound levels in the far field. The same NRD variants were used for a systematic computation series of far field effects, expressed as frequency dependent values of the far field Reflection Index (RI_{ff}) as well as a Single Number rating (DL_{RIff}). The far field Reflection Index has been defined as the ratio between the amount of energy that is reflected by the NRD under test and the energy reflected by a reference NRD.

The computations were carried out for a distance of 100m between the NRD and the receiver, which is believed to be characteristic for many common noise barrier applications. Five receiver heights were chosen, which are supposed to be representative for the majority of practical cases.

All far field simulation results were stored in a database as well.

6.1.3 Far field reflection performance indicator

In order to characterise the performance of NRD's with respect to their reflection behaviour in a simple way the results of the five receiver positions were clustered and averaged. The lowest three positions were used in the definition of the far field Reflection Index Single Number rating for Low-rise buildings ($DL_{RIff,LR}$) and the highest two positions in the definition of the far field Reflection Index Single Number rating for High-rise buildings ($DL_{RIff,HR}$).

6.1.4 Approximate engineering method

The contents of the two databases were used to develop an approximate engineering method for the extrapolation of near field test results to an estimate of the far field reflection effect of a specific NRD design.

It was not possible to find simple algorithms in the form of analytical expressions that would give the far field reflection effects directly as a function of the near field test data.

Therefore a two-step approach was developed:

1. The measurement result of a near field reflection test of the NRD under test is matched to the best fitting simulated variant in the near field database. The matching procedure uses a pre-selection of possible variants based on the NRD type and the geometrical shape parameters. Then the variant with the most similar material performance is selected by comparison of the near field single number ratings based on the range of 1/3-octave frequency bands from 100 – 1000 Hz. The material of the selected variant does not have to be of the same type as the material of the tested sample.

2. The material parameters of the selected variant (type of absorption material, flow resistivity and porous layer thickness) are used as input data for the computation of an estimate of the far field effects of the tested NRD sample. This estimate is computed with a polynomial approximation of the contents of the far field database.

The output of the approximate engineering method are the values of the far field Reflection Index Single Number ratings for Low-rise buildings and for High-rise buildings.

It can be applied for the range of NRD variations that has been included in the databases of simulated results, and covers the majority of NRD's on the European market.

6.1.5 Validation of the methods

The near field simulation method used made it possible to imitate the near field measurement process developed in WP 3 in detail. The final result of the WP3 reflection test method is an average over 9 microphone positions. As a consequence of this it was not possible to do a direct comparison of measured results at one microphone position with simulations results of that same position. Therefore only a comparison of average results of measurements and simulation results in the near field database was possible.

The frequency characteristics of the measured and simulated results showed a good agreement for hard materials and for fibrous absorbing materials, but not so good for porous concrete. The near field Single Number ratings of the most similar variants in the database corresponded reasonably well with the measurements. The deviations were smaller than or equal to 1,5 dB, which is of the same order of magnitude as the spread between the different measurements.

Next, the far field simulations and the far field results of the approximate method were validated with results of the far field validation measurements, that were carried out as a task within WP 2, based on two different methods.

Measuring the reflectivity of noise barriers in the far field has proven to be a challenge.

Due to adverse weather conditions during the validation measurements and due to the sensitivity of the methods for disturbances no quantitative conclusions could be drawn. The method based on impulse response measurements gave indicative results that supported the findings of the simulations in a qualitative sense. The second test method, that applied a continuous sound signal, did not deliver reliable results.

Finally, it could be demonstrated that the results of the approximate engineering method for near field – far field extrapolation were in a satisfactory agreement with the results of the far

field BEM simulations. The overall uncertainty of the approximate method relative to the BEM database is estimated at $\pm$ 1,4 dB.

6.2 Recommendations

It is recommended to include the engineering extrapolation method as an Informative Annex in the future CEN standard that describes the near field reflection test method developed in WP 3.
In order to facilitate the implementation of this recommendation the method is described in a separate Deliverable of WP 2 [14] in the form of a draft Annex to the CEN standard. Also the method has been implemented in a preprogramed Excel spread sheet that can be issued in combination with the proposed Annex.

Furthermore it is recommended to continue the development of a more robust method for the measurement of far field reflection effects of NRD's and to apply this method under favourable weather conditions to provide conclusive evidence that supports the use of the engineering extrapolation method, especially for strongly non-flat NRD's.

7 References

[1]   CEN 1793-1, Road traffic noise reducing devices – Test method for determining the acoustic performance – Part 1: Intrinsic characteristics of sound absorption, CEN, Brussels, September 1997.

[2]   CEN/TS 1793-5, Road traffic noise reducing devices - Test method for determining the acoustic performance - Part5: Intrinsic characteristics - In situ values of sound reflection and airborne souns insulation, CEN, Brussels, March 2003.

[3]   Garai, M., Noise reducing devices acting on aitborne sound propagation - Test method for determining the acoustic performance - Intrinsic characteristics - In situ values of sound reflection under direct sound field conditions, QUIESST Deliverable D 3.3 - ver 4.2, Bologna, 6 April 2012.

[4]   Lutgendorf D., de Roo, F., Numerical near field simulation for the Adrienne sound reflection test method according to EN-1793-5. QUIESST Deliverable D2.1,- version 2.1 - Final 2, TNO, Delft, 23 June 2010

[5]   Defrance, J., State of the art of existing optimisation methods and noise prediction approaches, Quiesst Deliverable D5.1 - version 1.0, CSTB, Grenoble, 29 April 2010.

[6]   Noordhoek, I.M., Salomons, E.M., ed., Sate of the art of modelling, Harmonoise Work Package 2, Report 2.2., TNO, Delft, 19 November 2002.

[7]   Jean, P., Computation of directivities in 2D, 2.5D and 3D, Memo CSTB, Grenoble, 14 June 2011.

[8]   Bérengier, M.C., M.R. Stinson, G.A. Daigle, and J.F. Hamet, Porous road pavements: Acoustical characterization and propagation effects, J. Acoust. Soc. Am. 101, 155-162 (1997).

[9]   Delany, M.E. and E.N. Bazley, Acoustic properties of fibrous absorbent materials, Appl. Acoust. 3, 105-116 (1970).

[10] Reinhard Wehr, Marco Conter, Manfred Haider and Sara gasparoni, Far-Field Measurements of the Acoustic properties of Noise Barriers, Euronoise 2012, Prague,2012

[11] Garai, M., e.a., Deliverable 3.5, QUIESST WP 3, Bologna, October 2012

[12] CEN 1793-3, Road traffic noise reducing devices – Test method for determining the acoustic performance – Part 3: Normalized traffic noise spectrum, CEN, Brussels, September 1997.

[13] Noordhoek, I.M., Van der Toorn, J.D.,Validation of the Harmonoise models, Harmonoise Work Packages 2, 3 and 4, Deliverable D21, TNO, Delft, 24 February 2005.

[14] Roo, F. de, Instructions for processing of near field reflectivity test data and derivation of far field reflectivity indicators, QUIESST Deliverable D2.6, TNO, The Hague, 17 December 2012.

8 Appendix

8.1 Barrier geometries

Zigzag

index	height H m]	depth B [m]	# elements [-]
1	0,80	0,10	5
2	0,80	0,20	5
3	0,80	0,30	5
4	0,67	0,10	6
5	0,67	0,20	6
6	0,67	0,30	6
7	0,57	0,10	7
8	0,57	0,20	7
9	0,57	0,30	7
10	0,50	0,10	8
11	0,50	0,20	8
12	0,50	0,30	8
13	0,44	0,10	9
14	0,44	0,20	9
15	0,44	0,30	9
16	0,40	0,10	10
17	0,40	0,20	10
18	0,40	0,30	10
19	0,36	0,10	11

20	0,36	0,20	11
21	0,36	0,30	11
22	0,33	0,10	12
23	0,33	0,20	12
24	0,33	0,30	12

Inclined
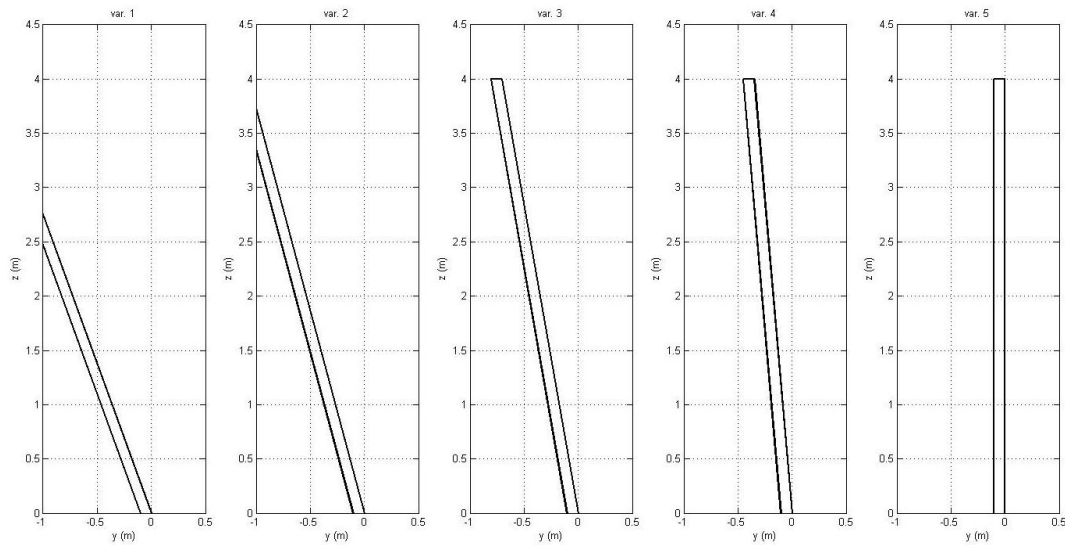
index	Tilt [deg]
1	0,80
2	0,80
3	0,80
4	0,67
5	0,67

Sawtooth

index	height H [m]	depth B [m]	# elements
1	0,80	0,10	5
2	0,80	0,20	5
3	0,80	0,30	5
4	0,67	0,10	6
5	0,67	0,20	6
6	0,67	0,30	6
7	0,57	0,10	7
8	0,57	0,20	7
9	0,57	0,30	7
10	0,50	0,10	8
11	0,50	0,20	8
12	0,50	0,30	8
13	0,44	0,10	9
14	0,44	0,20	9
15	0,44	0,30	9
16	0,40	0,10	10
17	0,40	0,20	10
18	0,40	0,30	10
19	0,36	0,10	11
20	0,36	0,20	11
21	0,36	0,30	11
22	0,33	0,10	12
23	0,33	0,20	12
24	0,33	0,30	12

Panes

	H [m]	B [m]	% outward	Ho [m]	Hi [m]
1	0,10	0,05	50	0,05	0,05
2	0,25	0,05	80	0,20	0,05
3	0,25	0,05	50	0,13	0,13
4	0,25	0,05	20	0,05	0,20
5	0,50	0,05	80	0,40	0,10
6	0,50	0,05	50	0,25	0,25
7	0,50	0,05	20	0,10	0,40
8	1,00	0,05	80	0,80	0,20
9	1,00	0,05	50	0,50	0,50
10	1,00	0,05	20	0,20	0,80
11	0,10	0,10	50	0,05	0,05
12	0,25	0,10	80	0,20	0,05
13	0,25	0,10	50	0,13	0,13
14	0,25	0,10	20	0,05	0,20
15	0,50	0,10	80	0,40	0,10
16	0,50	0,10	50	0,25	0,25
17	0,50	0,10	20	0,10	0,40
18	1,00	0,10	80	0,80	0,20
19	1,00	0,10	50	0,50	0,50
20	1,00	0,10	20	0,20	0,80
21	0,10	0,15	50	0,05	0,05
22	0,25	0,15	80	0,20	0,05
23	0,25	0,15	50	0,13	0,13
24	0,25	0,15	20	0,05	0,20
25	0,50	0,15	80	0,40	0,10
26	0,50	0,15	50	0,25	0,25

27	0,50	0,15	20	0,10	0,40
28	1,00	0,15	80	0,80	0,20
29	1,00	0,15	50	0,50	0,50
30	1,00	0,15	20	0,20	0,80

Steps
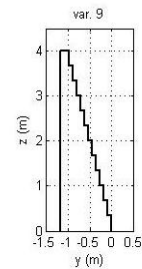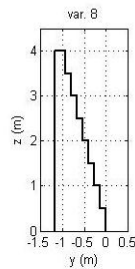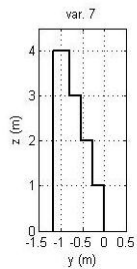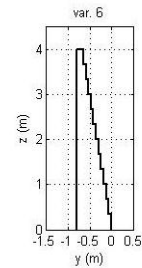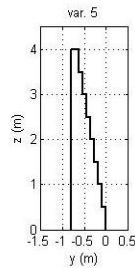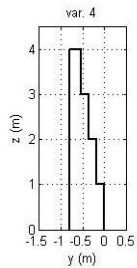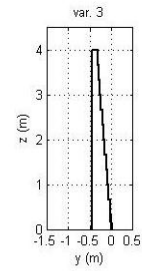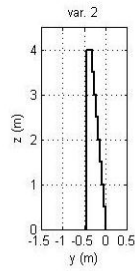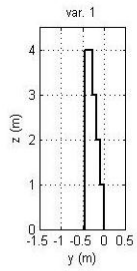
index	# elements	B [m]	H [m]	tilt [deg]
1	4	0,09	1,00	5
2	8	0,04	0,50	5
3	12	0,03	0,33	5
4	4	0,18	1,00	10
5	8	0,09	0,50	10
6	12	0,06	0,33	10
7	4	0,27	1,00	15
8	8	0,13	0,50	15
9	12	0,09	0,33	15

8.2 Results in DLri

8.2.1 Near field

Total DLri of all barrier types and all materials as a function of geometric variation index.
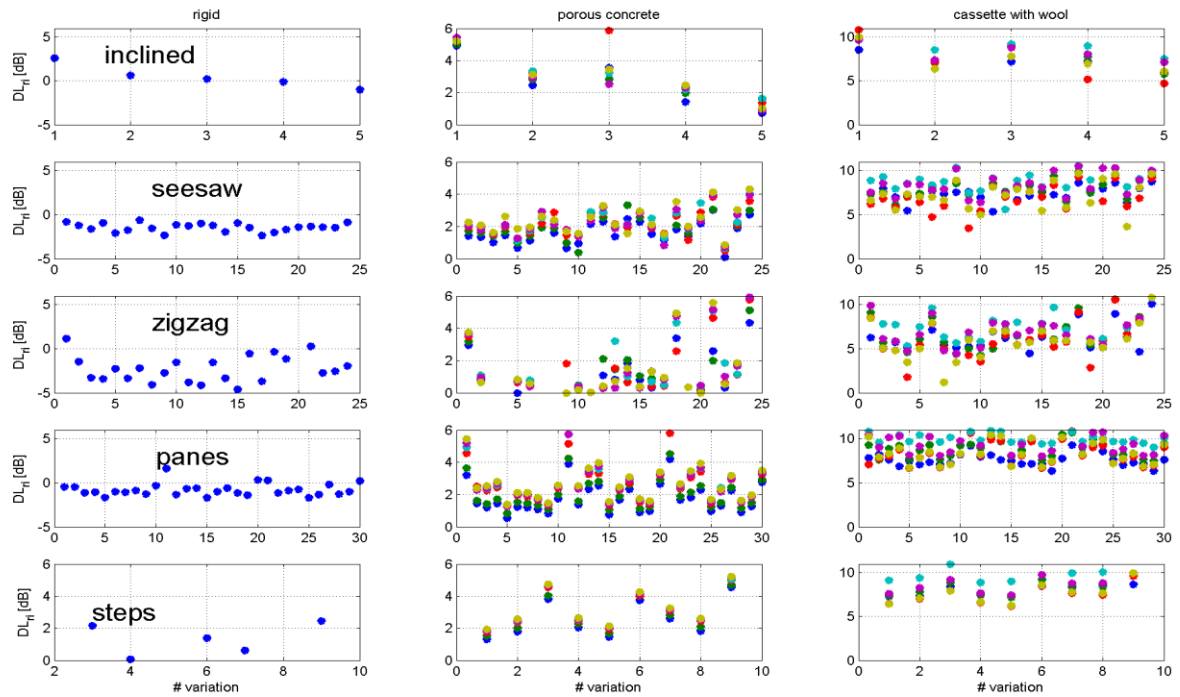
8.2.2 Far field

Receiver 1.5m height.
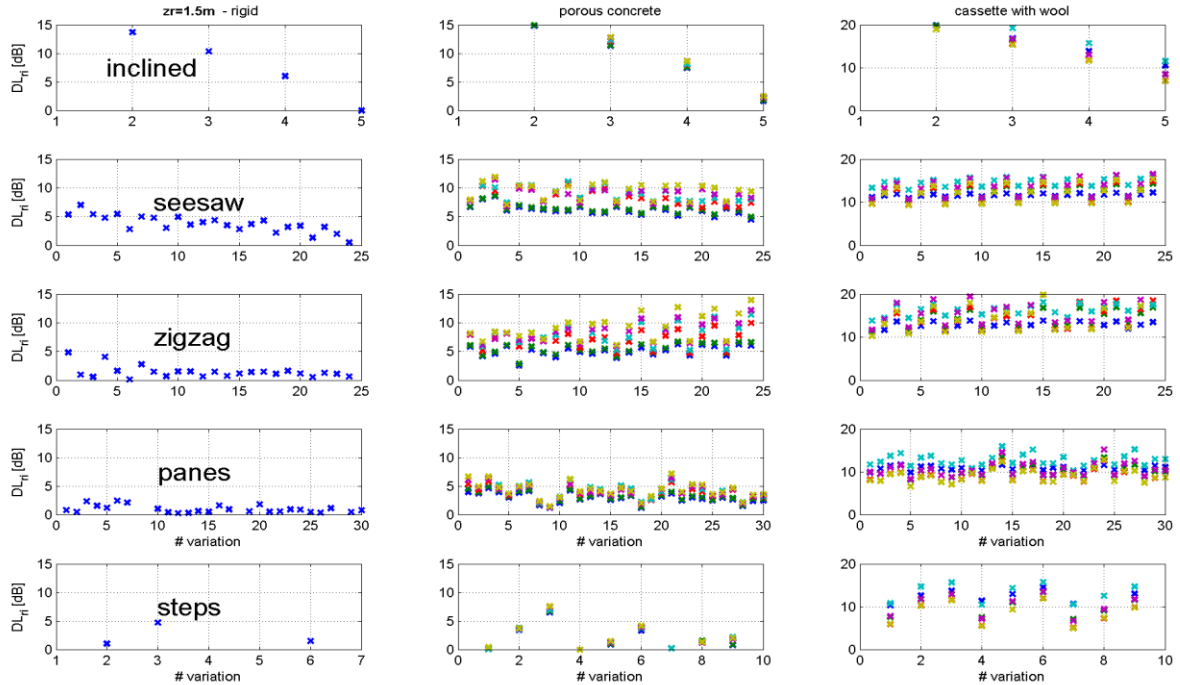
Receiver 5m height.
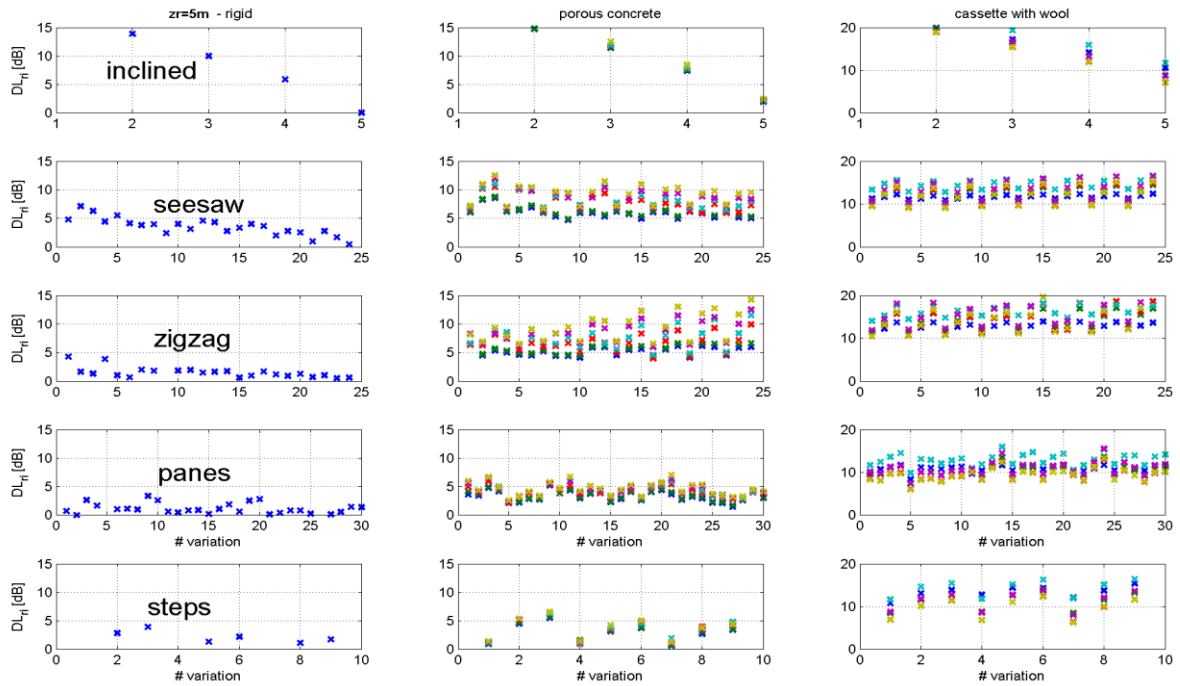
Receiver 10m height
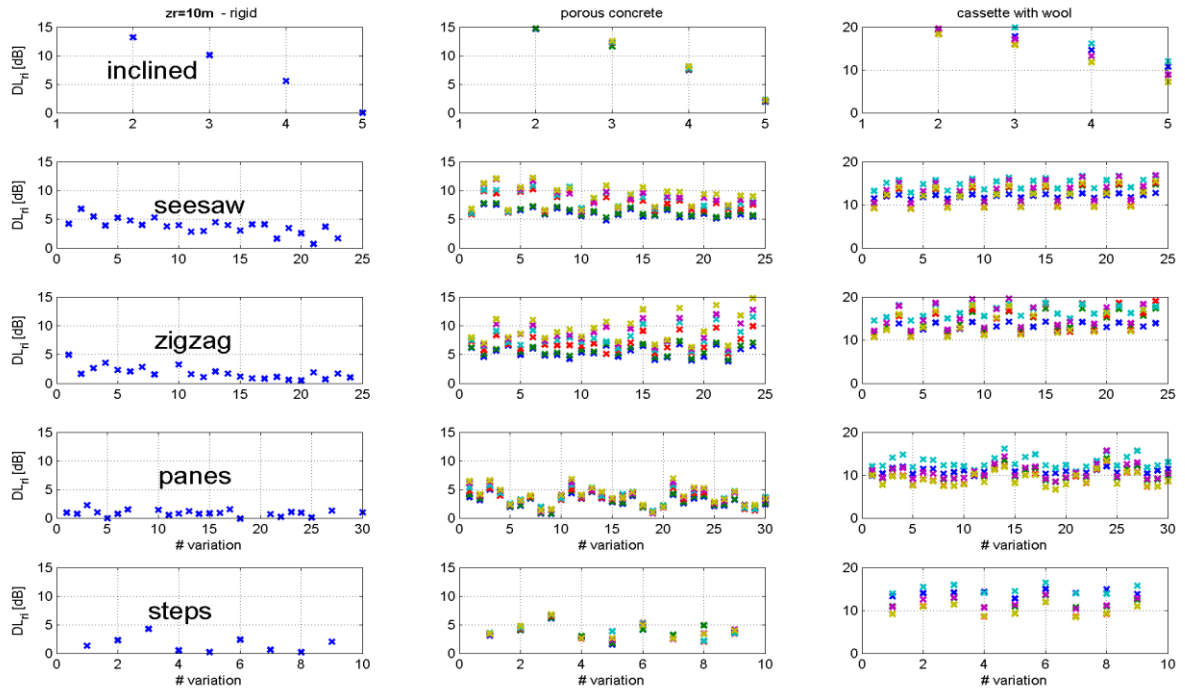
Receiver 20m
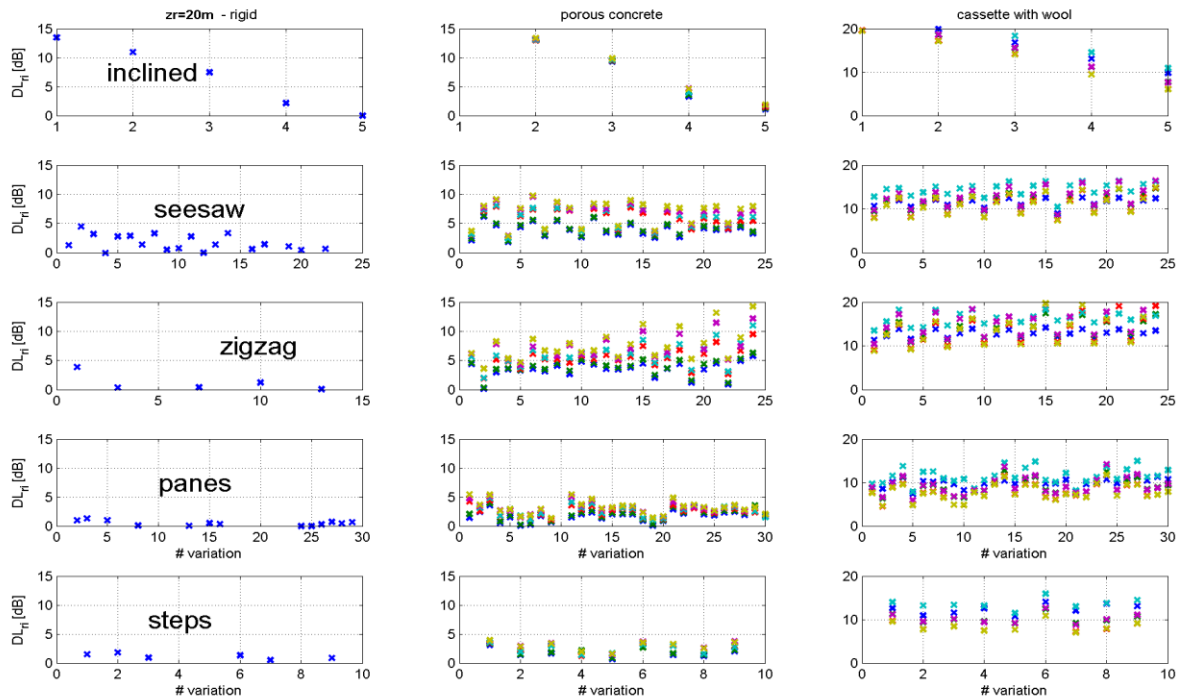
Receiver 40m height
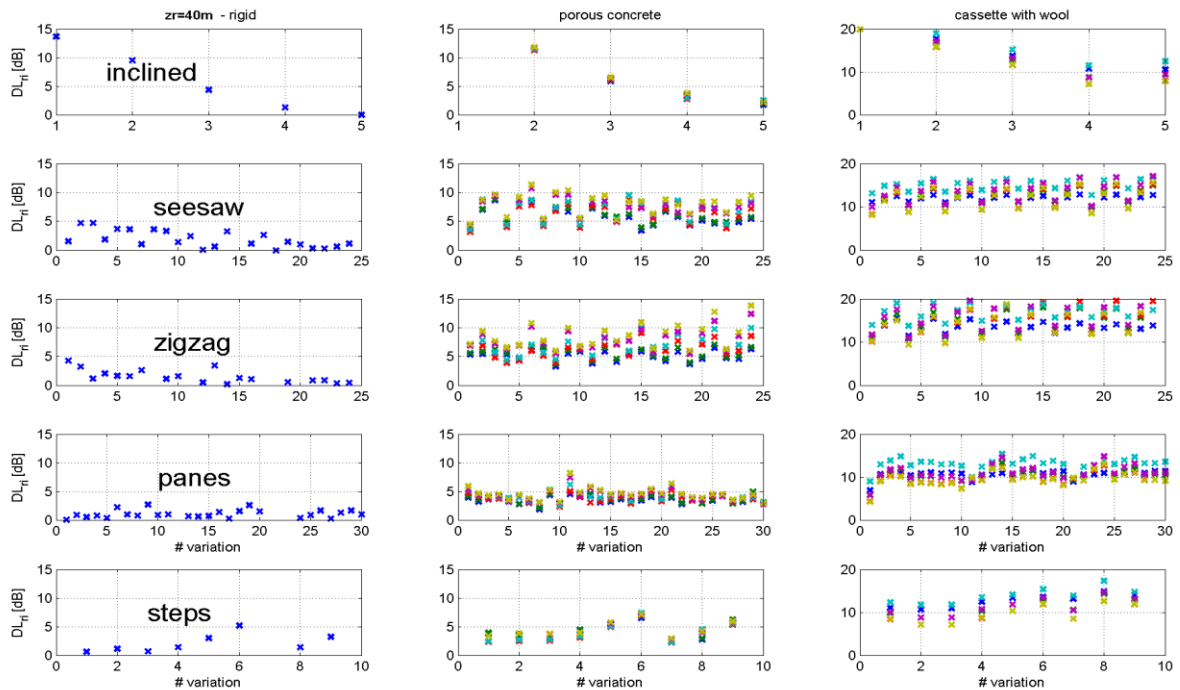
8.3 Separated shape and material effect in the far field

For all barrier type -material combinations the effect of shape and the effect of material, as described in section XXX, is shown in the following figures. The first row contains the results of rigid versions of the barrier type, the second row contains the porous concrete versions and the third row the mineral wool cassettes. The first column shown the total results (material and shape effect), the second column shows the part of the total DL which is caused by material effects and the third column shows the contribution of the shape.

Sawtooth
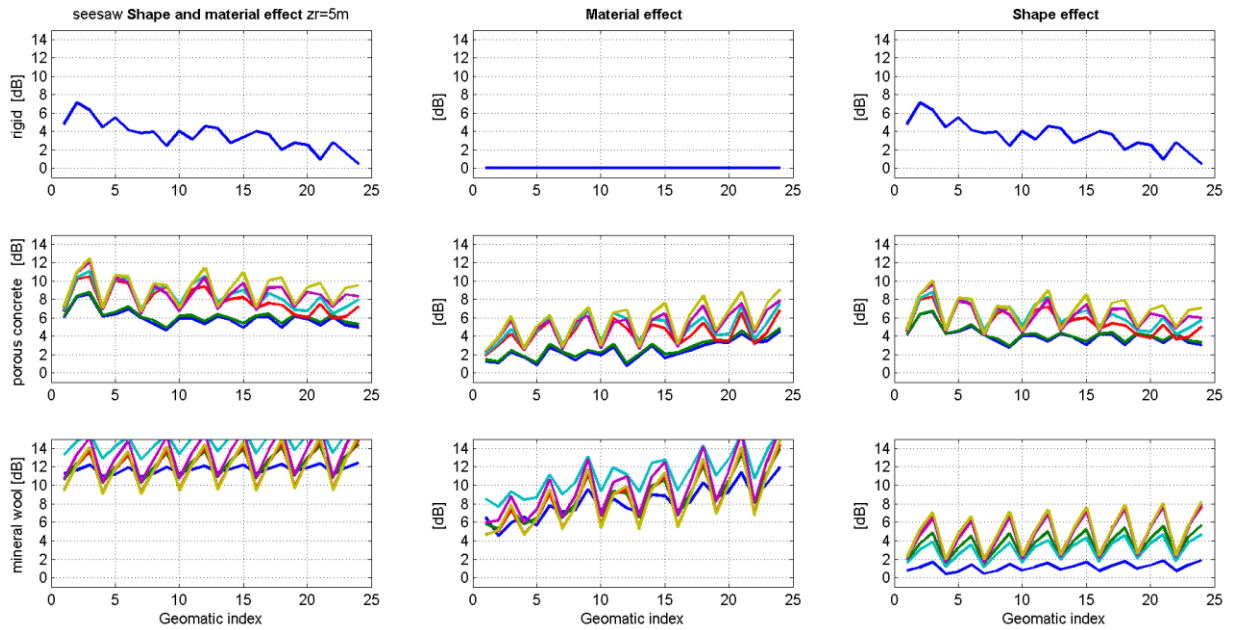
Steps
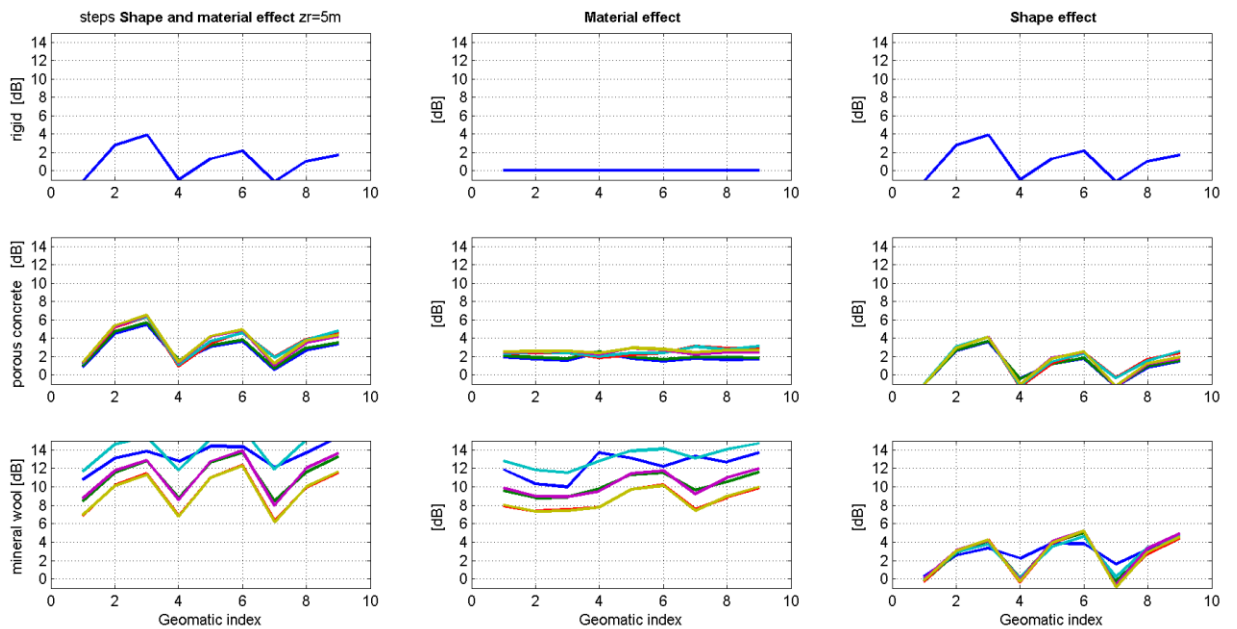
Zigzag
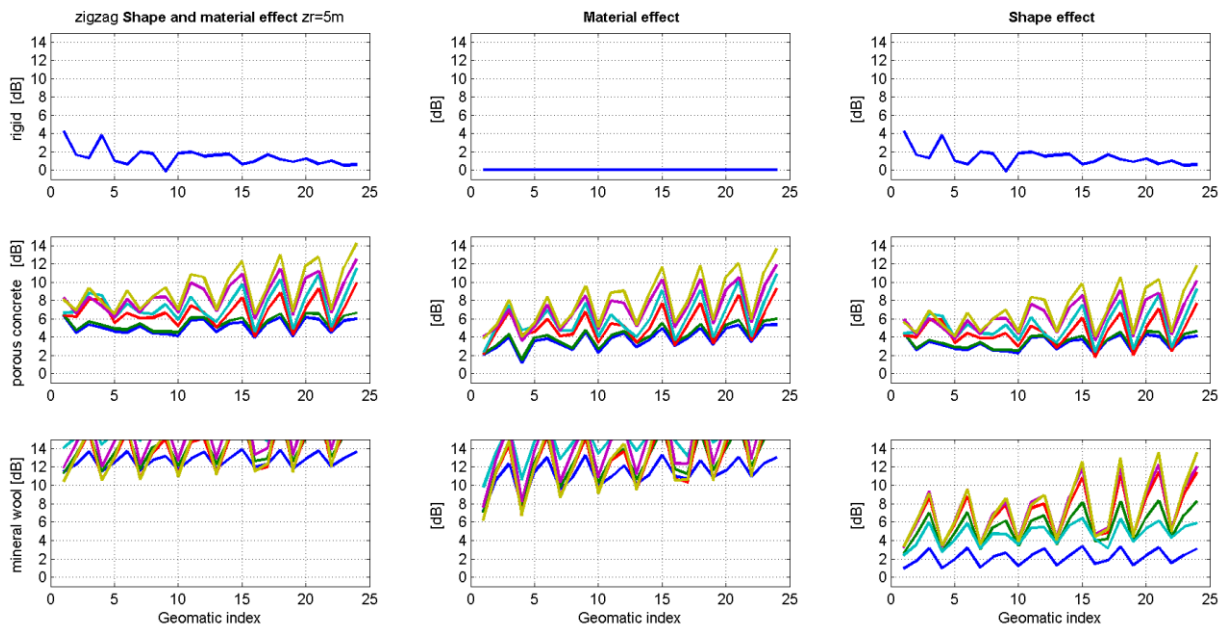
Inclined
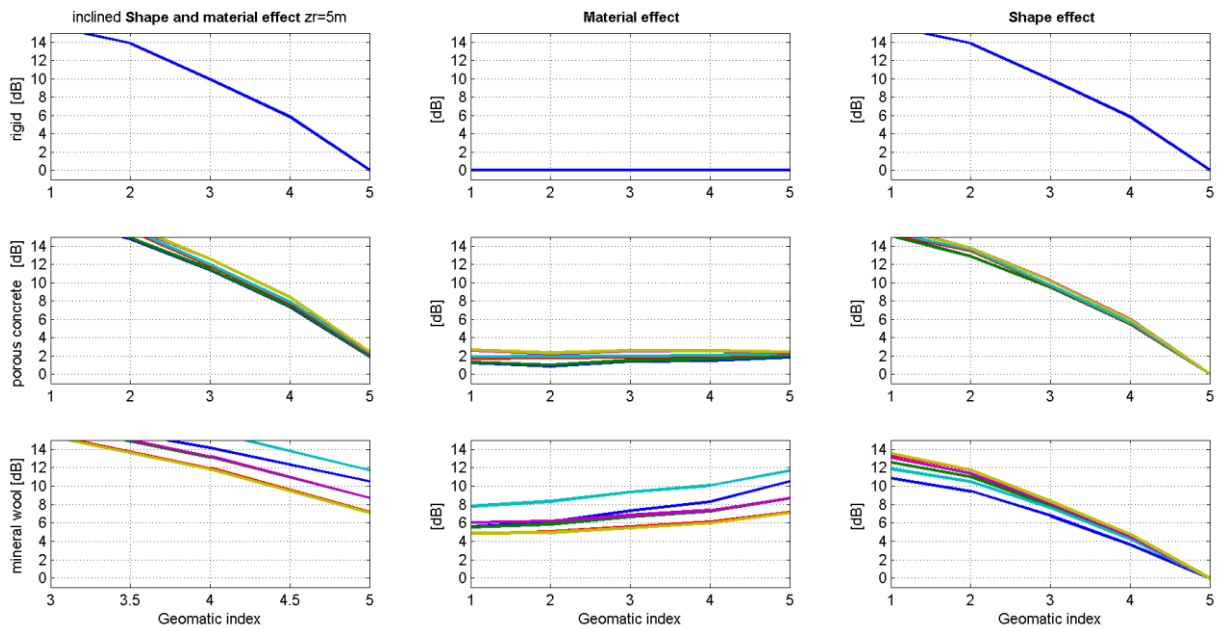
Panes
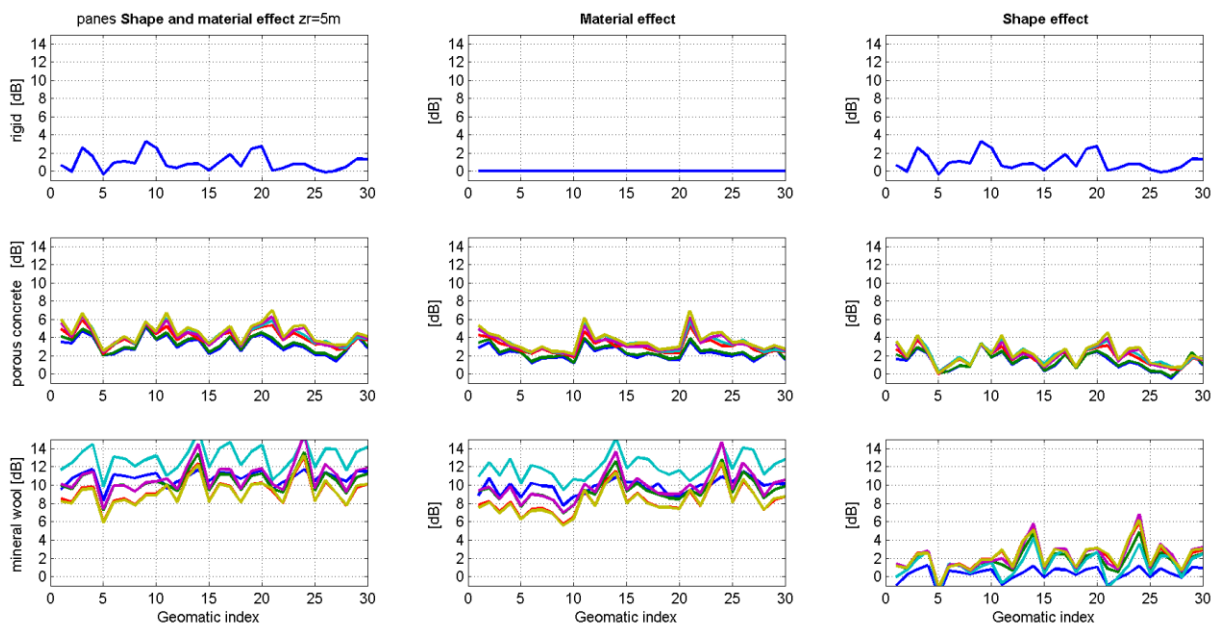
8.4 Details validation measurements

8.4.1 Hard- and software

A list of the used hard- and software used by both laboratories can be found below.

	CIDAUT		AIT	
5 Microphones	Bruel&Kjaer	4190	Bruel&Kjaer	4189
1 Omnidirectional source (Continuous Signal)	Bruel&Kjaer	BK 4296	Bruel&Kjaer	4296
1 Directional source (Impulse response method)	Celestion	QXi012	Celestion	QXi012
1 Power Amplifier	Bruel&Kjaer	BK 2716	IMG Stage Line	STA-320
2 Microphone Conditioning Amplifiers	Bruel&Kjaer	Nexus		
1 Frontend Acquisition	LMS	SCADAS Mobile	Bruel&Kjaer	3560B
1 Microphone calibrator	Bruel&Kjaer	4231	Bruel&Kjaer	4231

Table 15 - Measurement equipment

8.4.2 Measuring settings

	CIDUAT	AIT
Impulsive test		
Sampling rate	51200 Hz	65536 Hz
Nª averages	50	60
Source Signal	MLS	MLS
Recorded Signals	Time Impulse Response	Time Impulse Response
Continuous signal		
Sampling rate	51200	65536
Spectral lines	65536	65536
Resolution	0.39 Hz	1 Hz
Source Signal	Pink Noise	Pink Noise
Time acquisition	60 s	60 s
Nª averages	3	1
Recorded Signals	Time Octave 1/1 and Octave 1/3 Spectrum and Autopower Spectrum	Time 1/3rd octave band spectrum

Table 16 - Measurement settings

8.4.3 Meteorological conditions

The meteorological conditions during both measuring campaigns are listed below.

	CIDAUT	AIT
Barrier A2	Date: 20/12/12 Tª=11.5 ºC Speed wind= 0.5-0.8 m/s HR=61 %	Measurement 1: Date: 17/04/12 Tª = 19.5°C Wind speed: 0-8 m/s Measurement 2: Date: 20/04/12 Tª = 16°C Wind speed: 5-14m/s
Flat rigid barrier	Date: 22/12/12 Tª=7.1 ºC Speed wind= 0.1-0.2 m/s HR%=67 %	Measurement 1: Date: 16/04/12 Tª = 10°C Wind speed: 0-10 m/s Measurement 2: Date: 20/04/12 Tª = 7°C Wind speed: 0-5 m/s
Barrier A3	Date: 23/12/12 Tª=1.4 ºC Speed wind= 0.12-0.2 m/s HR%=89 % Foggy	Measurement 1: Date: 17/04/12 Tª = 8.5°C Wind speed: 0-2 m/s

		Measurement 2: Date: 20/04/12 T^a = 17°C Wind speed: 0-8 m/s
Flat timber barrier		Date: 20/04/12 T^a = 14°C Wind speed: 2-8 m/s
Flat absorptive barrier		Date: 20/04/12 T^a = 8°C Wind speed: 2-6 m/s

Table 17 - Meteorological conditions

8.4.4 Absorptive material data (acoustic curtain).

Material reference	Alpharock-E 225
Nominal density	70 kg/m3
Thickness	80 mm
Absorptive coefficient	 Data for thickness=40 mm according to specifications of manufacturer.
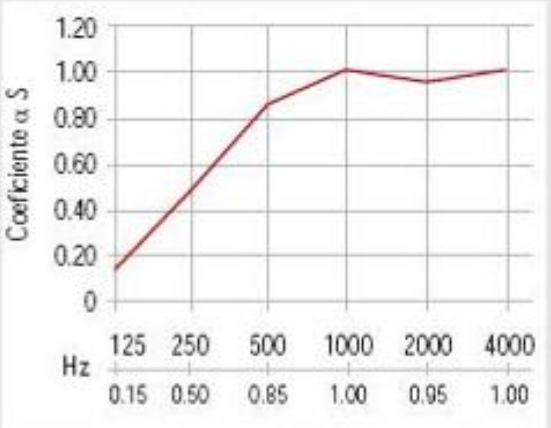
Table 18 - Data of acoustic curtain used as cover layer.

8.4.5 Set-up of each measurement with acoustic curtain

Figure 65 to Figure 68 show the position of each barrier and the distances between them, as well as microphone and loudspeaker relative positions.
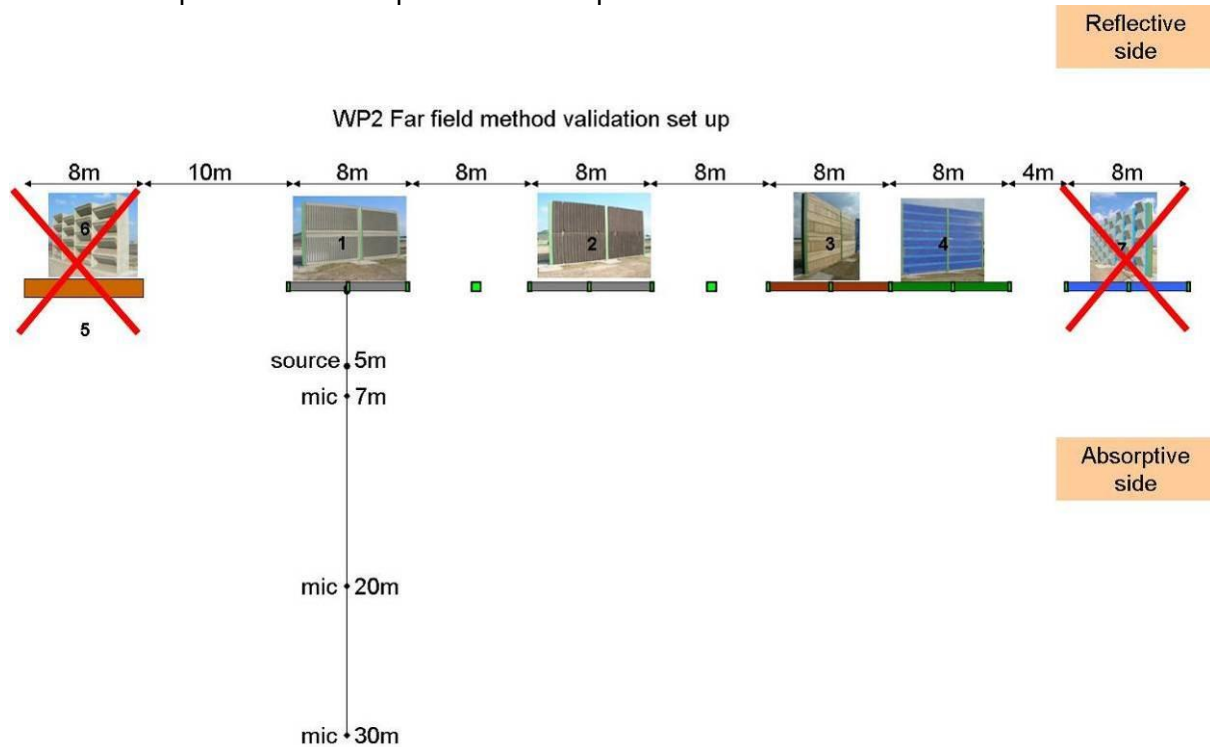
Figure 64 - Far field validation barriers test site set up

Following figures show the test set up used in each sample for its far field characterization (yellow colour around samples represents the acoustic curtain.
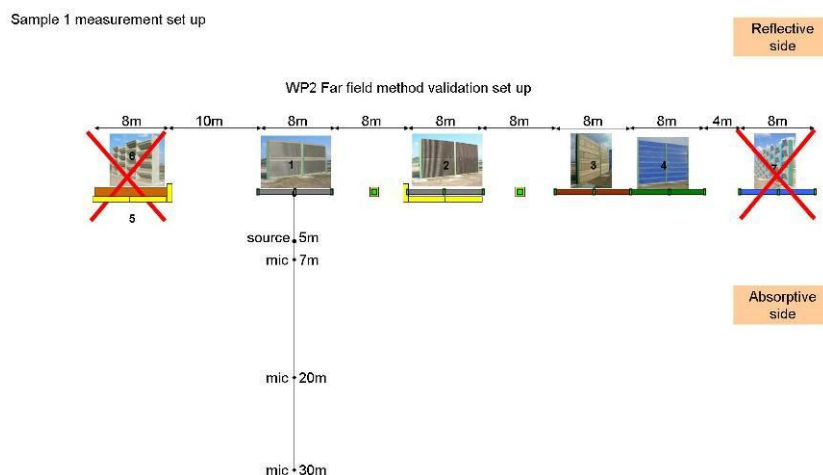
Figure 65 - Barrier 1: Flat absorptive concrete (A2)
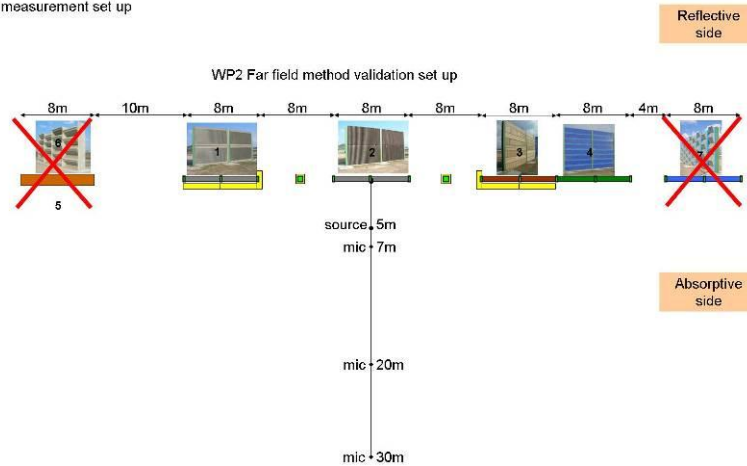
Figure 66 - Barrier 2: Non flat absorptive concrete (A3)
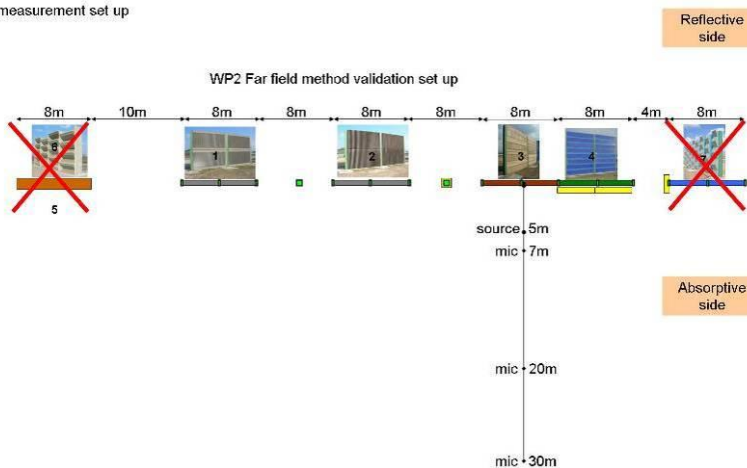
Figure 67 - Barrier 3: Flat timber barrier

NOTE: Due to the adverse weather conditions and lack of time, the A3 barrier was not covered with the acoustic curtain during measurement of the flat timber barrier.
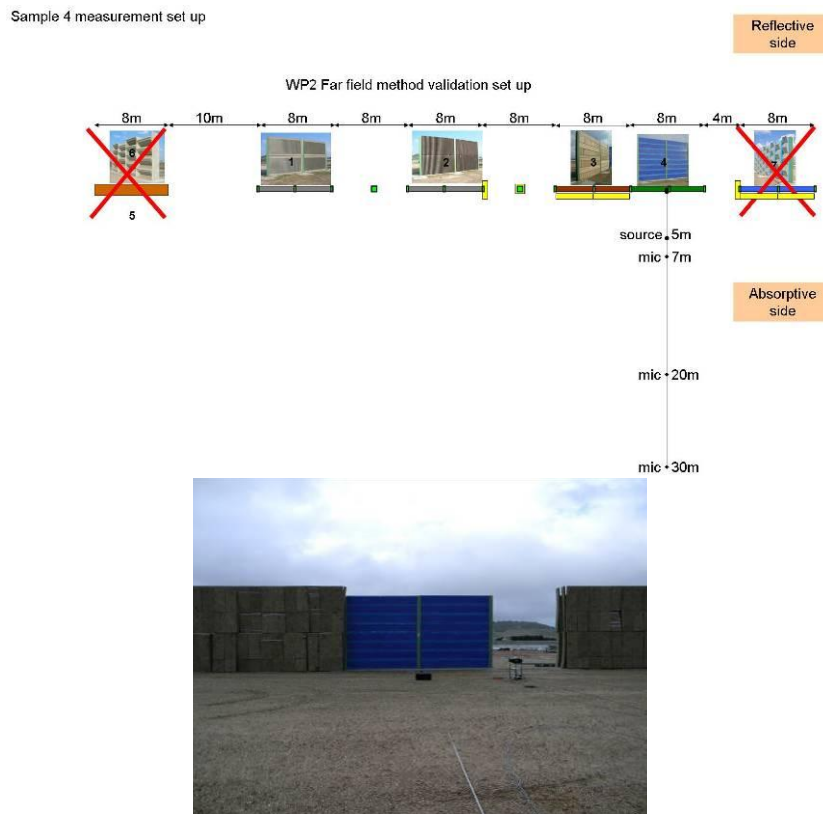
Figure 68 - Barrier 4: Flat absorptive

Taking advantage of the flat a fully reflective backside of concrete NRDs, measurements for the reference sample were carried out on the opposite side

Figure 69 - Reference sample

8.4.6 Barrier samples

Sizes are in mm.

Rigid Barrier

A3 backside.
Smooth concrete.
Thickness=100 mm

Barrier A2
Porous concrete
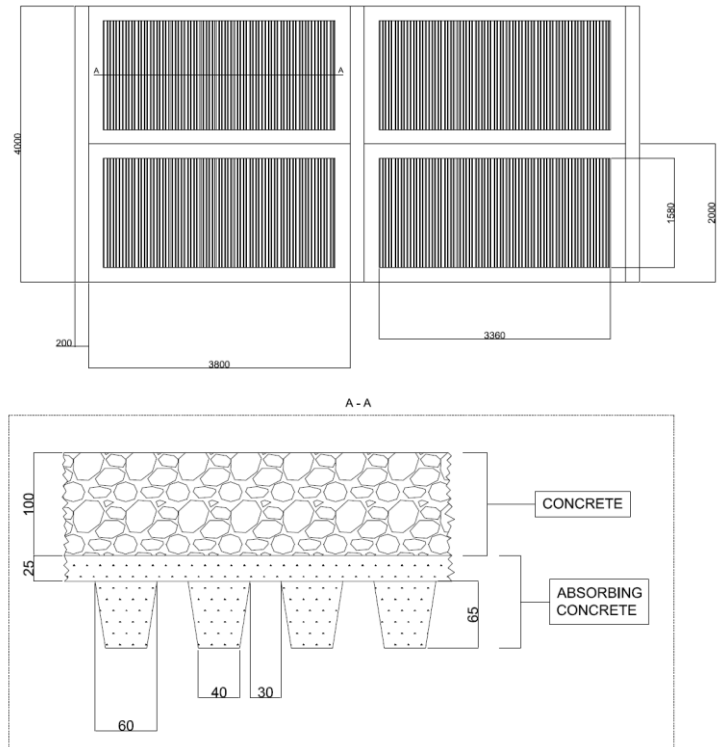
Table 19 - Geometry details absorptive barrier A2.

Barrier A3
Porous concrete
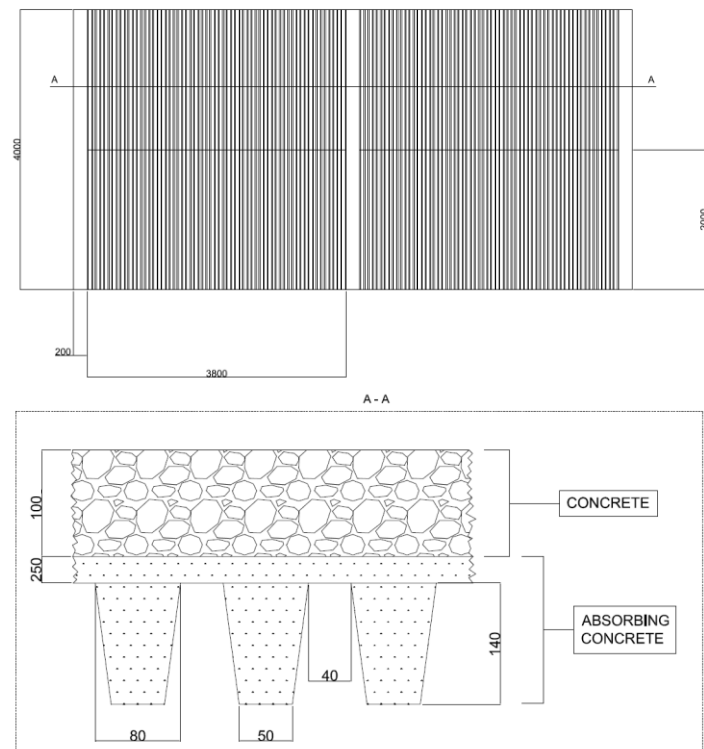
Table 20 - Geometry details absorptive barrier A3.

8.4.7 Details method A - CIDAUT

Recorded impulse response signals consist of a direct component due to the sound propagation towards the backside of the loudspeaker, a reflected component coming from the barrier under test and other parasitic components like ground reflection. The separation of the different components, have been made by means of temporal windowing in time domain. The delay between the arrival of direct and reflected component is long enough, therefore the relevant components can be extracted from the overall impulse response by application of the time window (Adrienne length=10 ms) as Figure 70 shows.
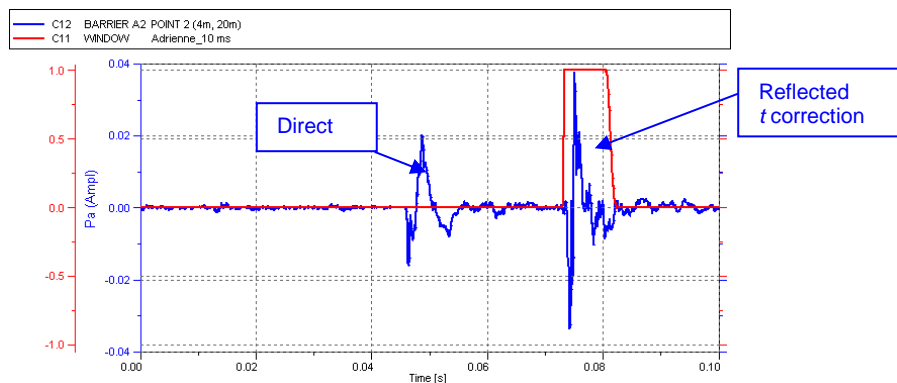
Figure 70 - Method A: Temporal separation of components for barrier A2, point 2, 4 m height and 20m barrier distance

The amplitude of reflected sound waves is attenuated with distance (in manner inversely proportional to the travelled length). In order to compensate this effect, a correction factor "t" is introduced in the numerator and denominator.

The next table shows the summary of the method A (CIDAUT).

Measurements	Impulse response
	• Barriers A2, A3 (gently non flat concrete) and flat rigid barrier.
	• Free field
Results	Reflection index in 1/3, 1/ 1 octave and single number rating for each barrier.
Type of signal	MLS (order 16), 50 averages
Source	Directional source.
Window	Adrienne window Length= 7.9 ms. Used for temporal separation.
RI equation	$$RI_j = \frac{1}{n_j} \sum_{k=1}^{n_j} \frac{\int_{\Delta f_j} \left| F\left[t \cdot h_{r,k}(t) \cdot w_r(t)\right] \right|^2 df}{\int_{\Delta f_j} \left| F\left[t \cdot h_i(t) \cdot w_i(t)\right] \right|^2 df}$$
	F	Fourier transform
	t	time beginning of IR measured
	$h_{r,k}(t)$	reflected component IR
	$w_r(t)$	reflected component time window IR
	$h_i(t)$	direct component IR
	$w_i(t)$	direct component time window free field IR
	n	number of microphones (n=1). IR for each microphone position
	Δf_j	width of j-th one third octave band

Frequency range	100-5000 Hz

Table 21 - Method A Summary

Impulse Response Signal:

In Figure 71, Figure 72 and Figure 73, time response of sound signal measured at each microphone position is shown for each tested NRD. As can be seen there are two main peaks, the first one due to the impulsive signal directly emitted by the sound source, the second peak is coming from the reflection of the NRD. The amplitude of the impulse response measured coming from the reflection on the NRD is already corrected by a t factor, in order to compensate for the amplitude reduction due to propagation.

It can be seen that measured reflected peaks are lower at 30m than at 20m, as it is expected, while there are small differences on the measured signal at same distance but different heights. At first look, we can see that reflected signals are stronger coming from the reference non absorptive NRD, than that of the two absorptive samples.
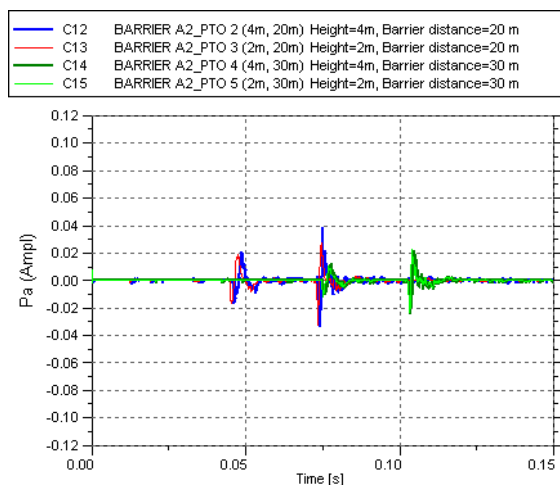
Figure 71 - Method A: Impulse response for barrier A2
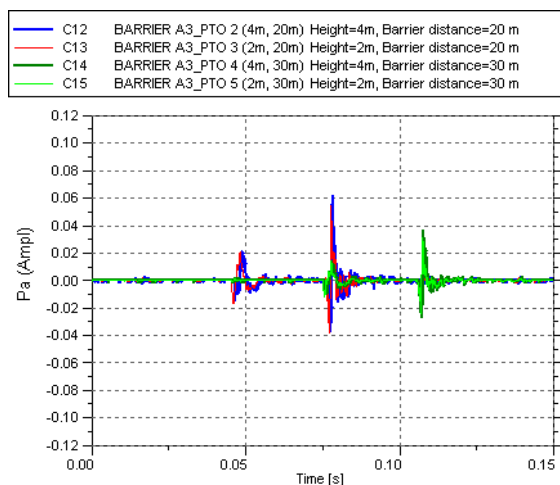
Figure 72 - Method A: Impulse response for barrier A3
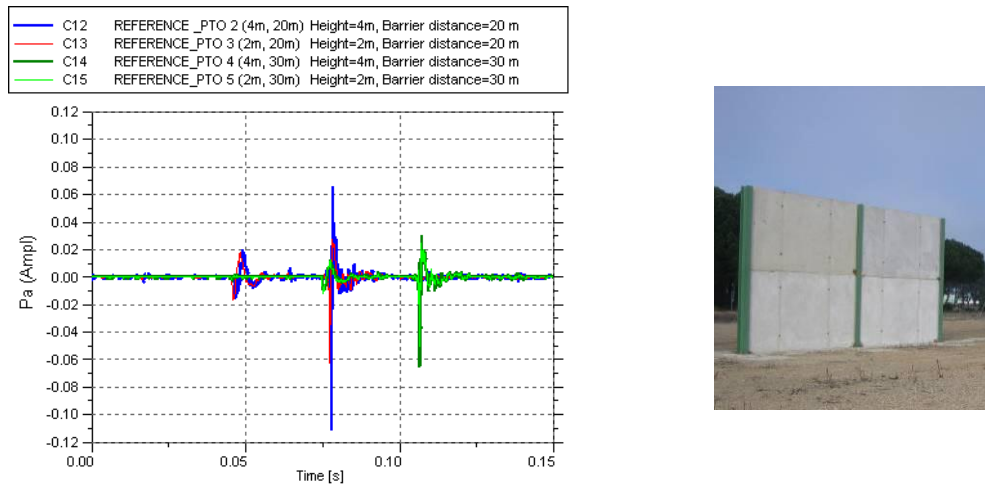
Figure 73 - Method A: Impulse response for reference barrier (flat rigid barrier)

The next table shows the reflected component time arriving (in ms) for each microphone and barrier.

Microphone	Reflected component_t(ms)		
	A2	**A3**	**FRB**
MIC 2(20m,4m)	73.57	76.27	76.02
MIC 3(20m,2m)	72.52	76.02	74.81
MIC 4(30m,4m)	102.87	106.13	104.51
MIC 5(30m,2m)	102.38	105.70	104.12
Table 22 - Reflected component arriving times (method A)			

The reflection of A2 barrier arrives earlier than the rigid and the A3 (see Table 22). Such difference is due to positioning inaccuracy of microphones with respect to each NRD, and a little variation in the sound speed due to temperature and wind speed (temperature gradient in between A2 and A3 tests was about 10 ºC so the sound speed vary about 1.87 %). It is expected to minimize the influence in the results due to this variations with the correction factor "t" introduce in the formula.

8.4.8 Details method A – AIT

To minimise the influence of the wind squalls on the obtained impulse responses (IRs) and to improve the signal to noise ratio, the overall impulse response for each microphone was averaged over 60 periods. In contrast to the normal procedure of averaging over these 60 single impulse responses, due to the by the squalls produced offsets of the IRs, each single impulse response was aligned before the averaging procedure in the time domain to obtain a best fit.

The offset was calculated by convolving the by a cubic spline interpolation upsampled single IRs, the aligning procedure was performed according to the following formula:

$$IR_{align} = iFFT\{FFT[IR_{single}] \cdot e^{2\pi i f \tau}\}$$
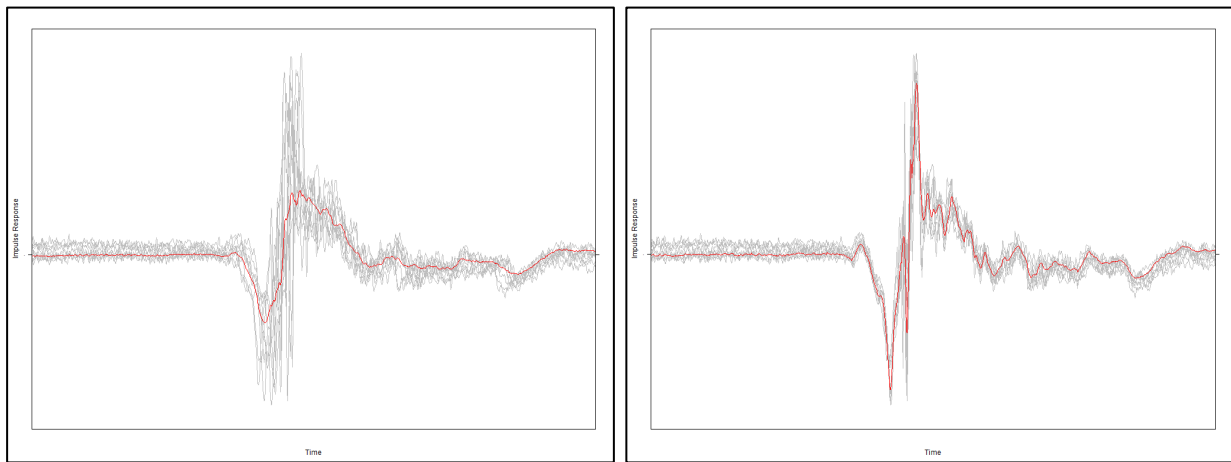
Figure 74 - Uncorrected (left) and by the aligning procedure corrected impulse responses (right) – grey: single impulse responses; red: averaged overall impulse response

The following figures shown the RI result computed with method A from the tested barrier samples, each with two different configurations and two different sources. Also some figures for the purpose of showing repeatability are shown.
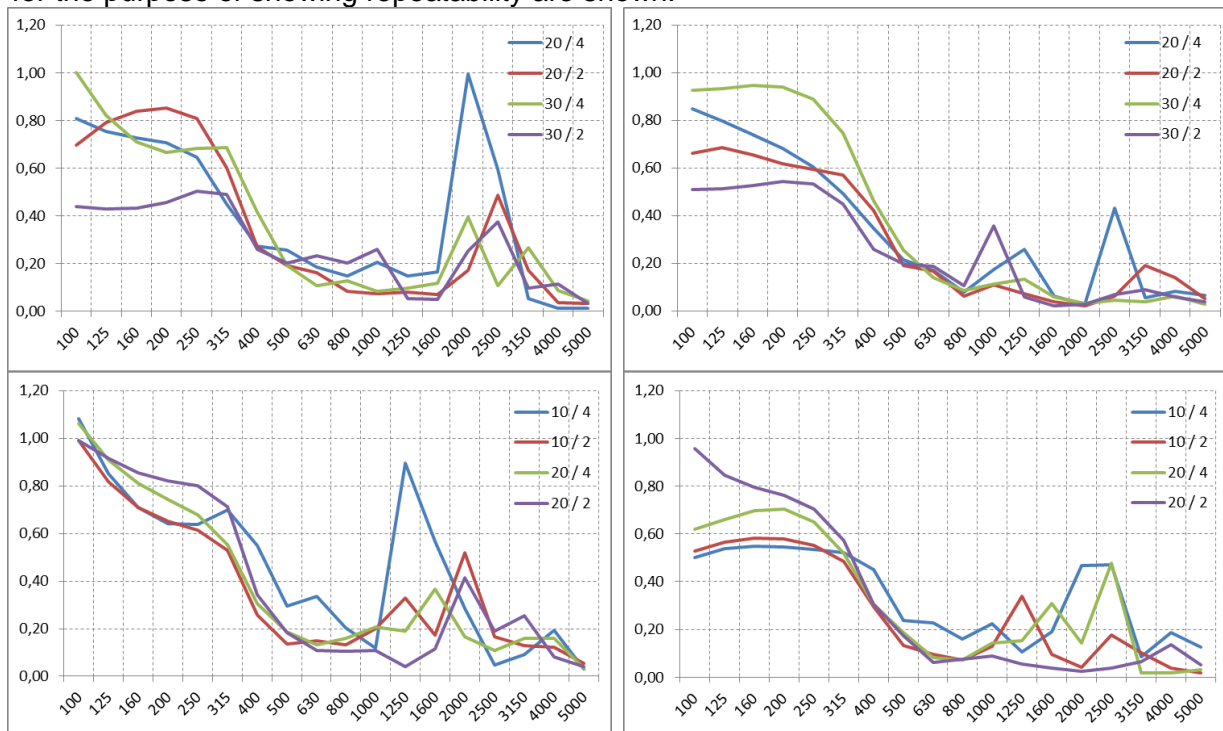
Figure 75 - Reflectivity ρ vs. one-third octave band of the flat absorptive barrier for configuration I (upper row) and configuration II (lower row); left: Celestion; right: B&K 4296
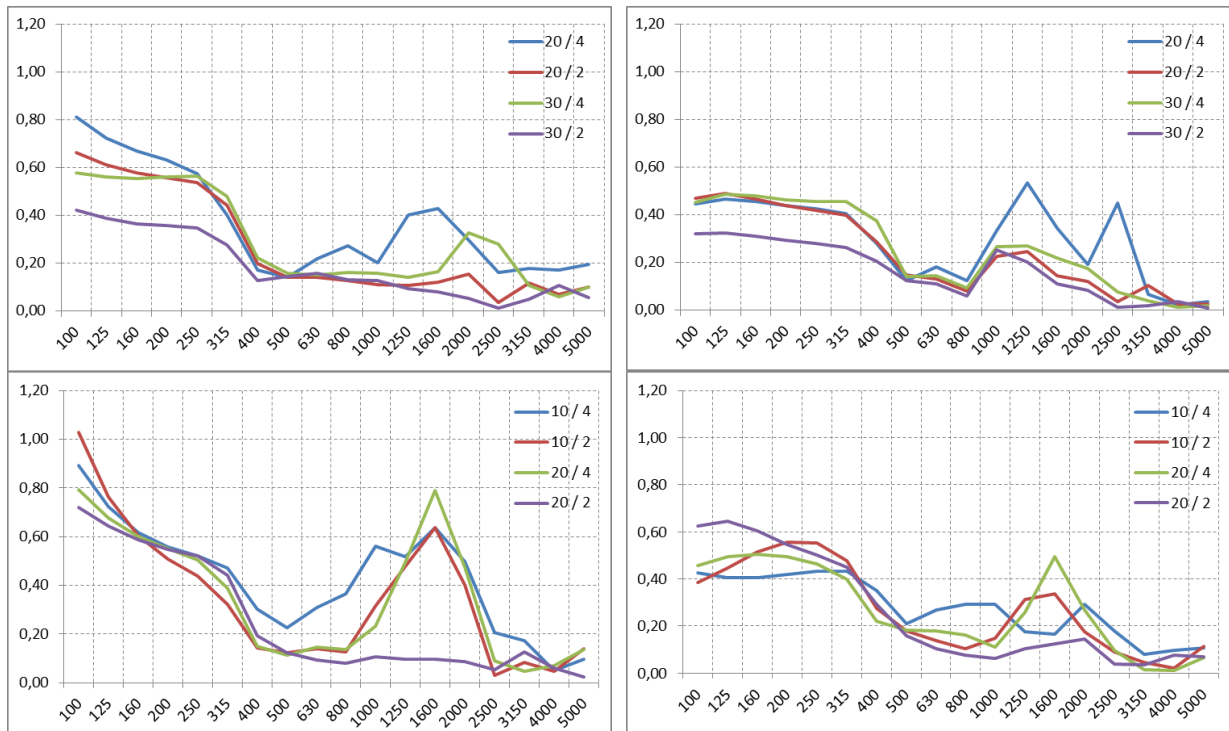
Figure 76 - Reflectivity ρ vs. one-third octave band of the flat timber barrier for configuration I (upper row) and configuration II (lower row); left: Celestion; right: B&K 4296
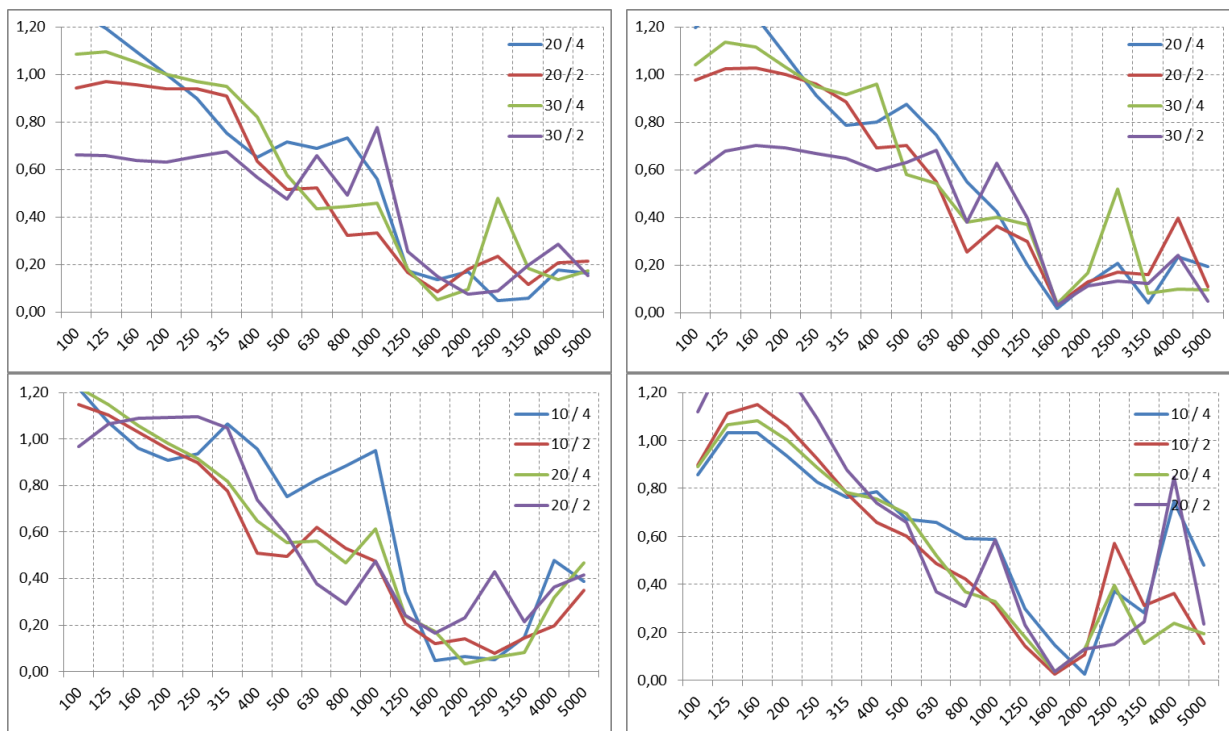
Figure 77 - Reflectivity ρ vs. one-third octave band of barrier A3 for configuration I (upper row) and configuration II (lower row) – measurement No. 1; left: Celestion; right: B&K 4296
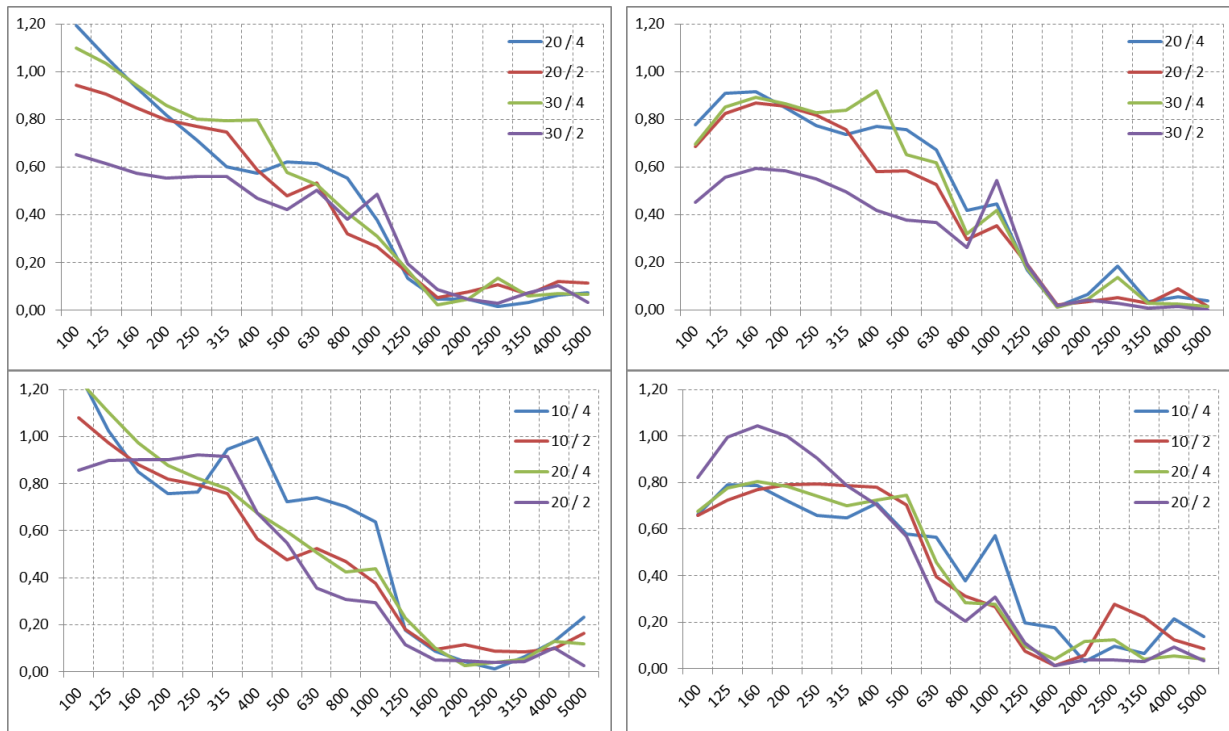
Figure 78 - Reflectivity ρ vs. one-third octave band of barrier A3 for configuration I (upper row) and configuration II (lower row) – measurement No. 2; left: Celestion; right: B&K 4296
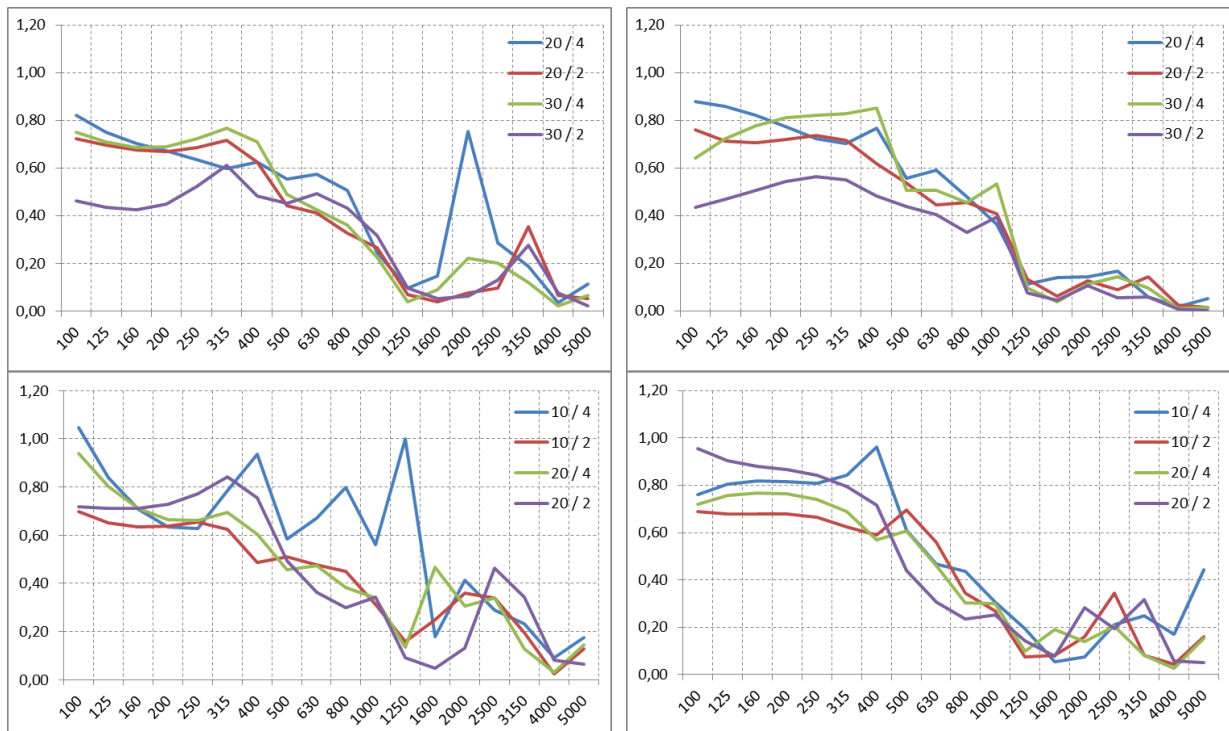
Figure 79 - Reflectivity ρ vs. one-third octave band of barrier A2 for configuration I (upper row) and configuration II (lower row) – measurement No. 1; left: Celestion; right: B&K 4296
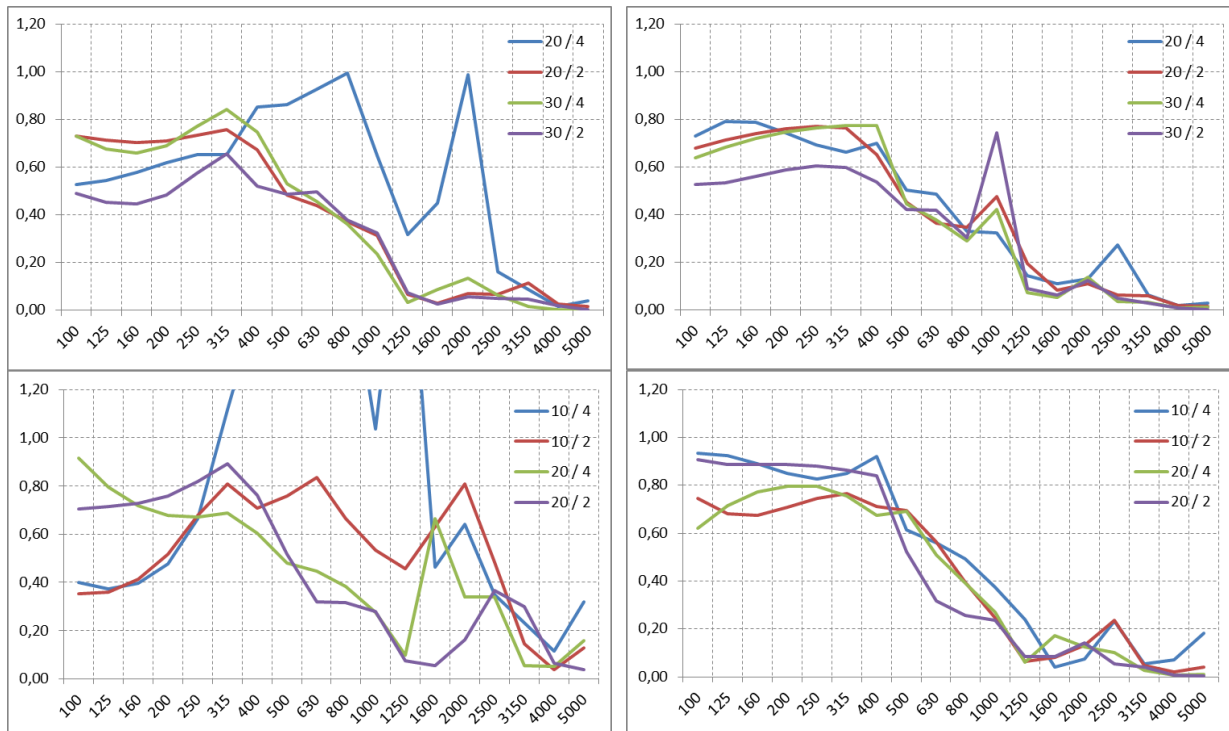
Figure 80 - Reflectivity ρ vs. one-third octave band of barrier A2 for configuration I (upper row) and configuration II (lower row) – measurement No. 2; left: Celestion; right: B&K 4296
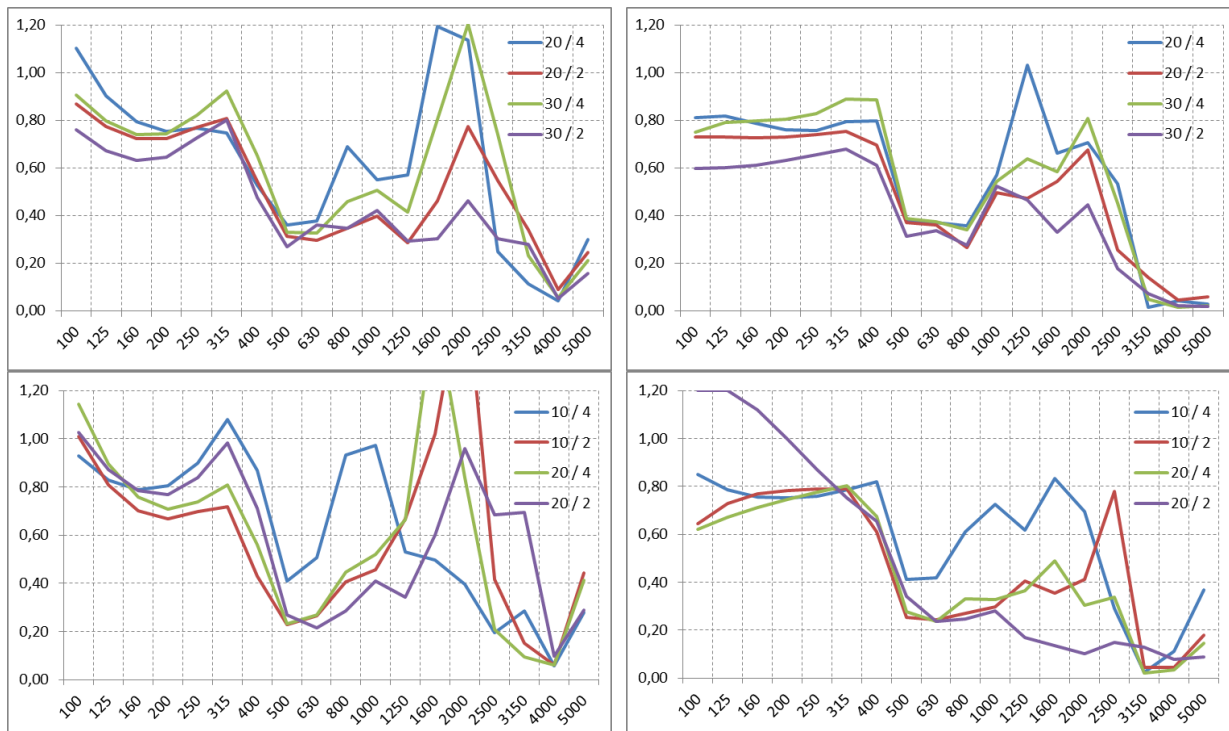
Figure 81 - Reflectivity ρ vs. one-third octave band of the rigid barrier for configuration I (upper row) and configuration II (lower row) – measurement No. 1; left: Celestion; right: B&K 4296
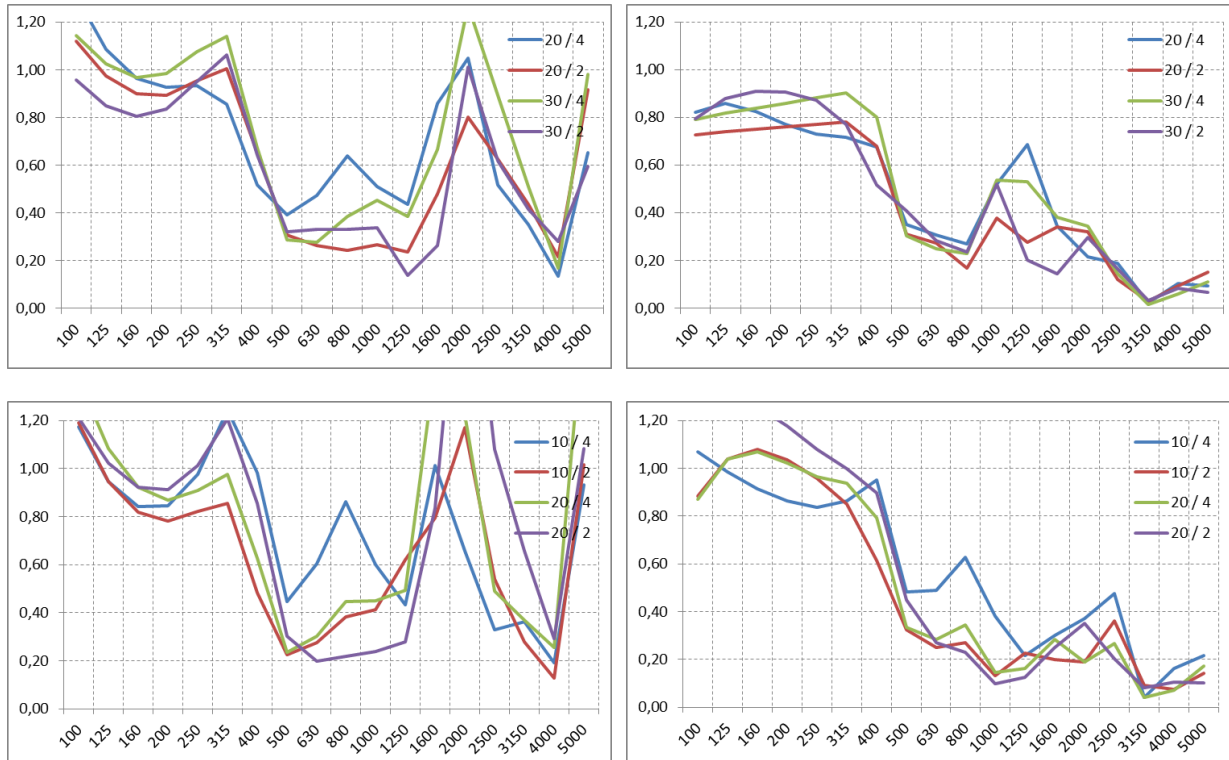
Figure 82 - Reflectivity ρ vs. one-third octave band of the rigid barrier for configuration I (upper row) and configuration II (lower row) – measurement No. 2; left: Celestion; right: B&K 4296

8.4.9 Details method B - CIDAUT

The next table shows a summary of the method B.

Measurements	• Barriers A2, A3. • Flat rigid barrier as reference (smooth concrete). • Simulated rigid flat barrier (mirror position).
Results	SPL at each microphone, Far Field Reflection Index RI$_{ff}$, absorption coefficient, α_{eq}. All data are in 1/3 and 1/1 octave band.
Type of signal	Pink noise
Source	Omnidirectional source.
Formula	$$RI_{ff} = 1 - \alpha_{eq}; \qquad \alpha_{eq} = 1 - \frac{\left(p^2_{measurement} - p^2_{direct}\right)}{\left(p^2_{measurement} - p^2_{direct}\right)_{reference}}$$
Frequency range	100-5000 Hz
Table 23 - Method B Summary	

The figure below shows sound pressure levels for the measurements at the reference microphone (for the three barriers and for the mirror measurement).
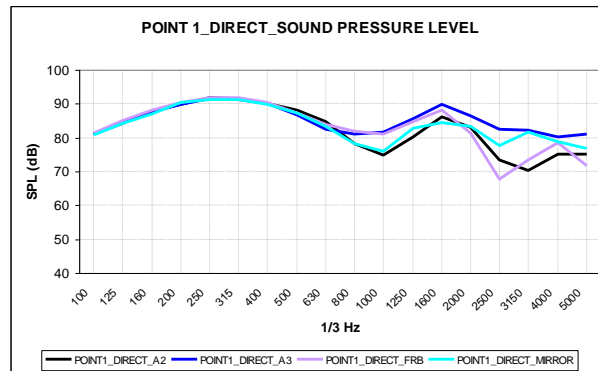
Figure 83 - Comparison SPL at reference position

The SPL at reference position is quite similar for all samples up to 630 Hz, at higher frequencies the SPL presents variations in its amplitude. The SPL is higher between 125 and 500 Hz. Above 630 Hz measured levels at the reference microphone show variations of 5 dB or more.

A similar figure is shown for the microphones at 20 m and 30 m.
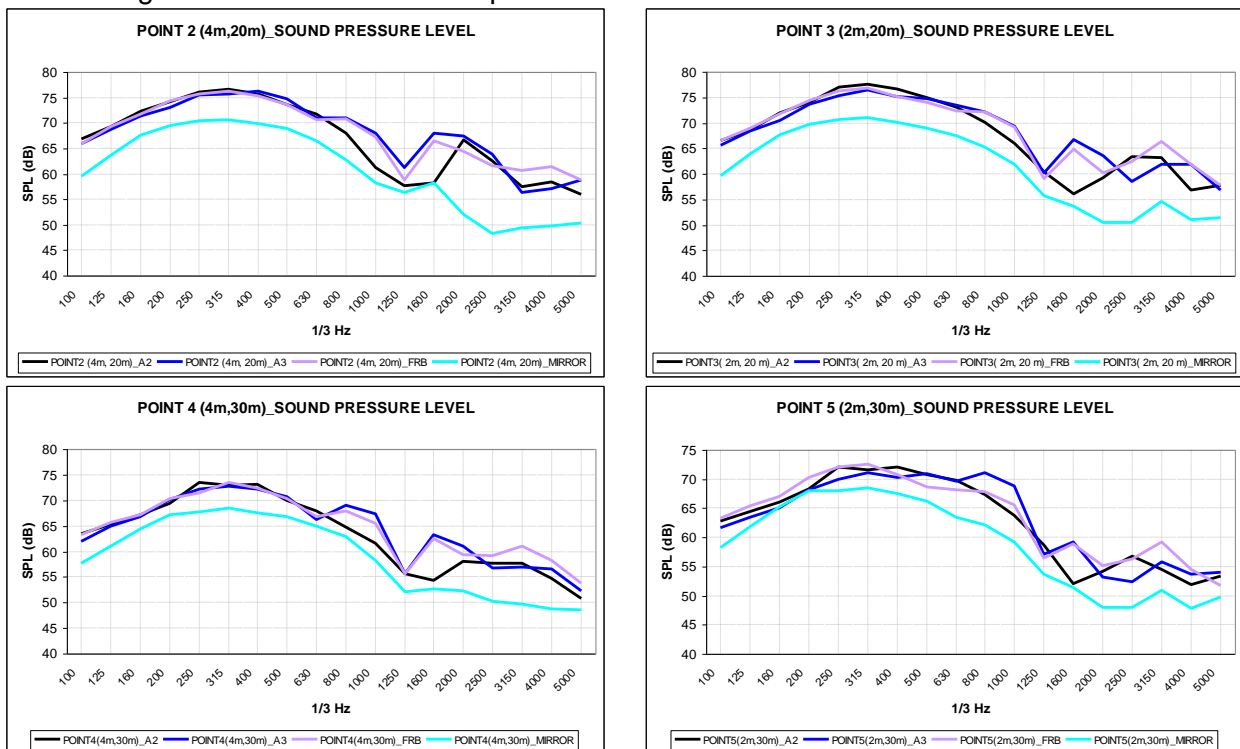
Figure 84 - Comparison SPL for each barrier/microphone position

At 20 m and 30 m the mirror measurements show lower results than the rigid barrier, although the shape of the curve is quite similar to the one measured with the reference wall. This could be explained a cause of the reflection contribution in the mirror measurements is much lower than in the barriers.

Since barriers A2 and A3 are absorptive barriers, the expected values for its SPL must be lower than the SPL measured with the reference barrier (and the mirror method) due to the acoustic energy absorption. Figure 85 and Figure 86 show the relative differences in SPL measured between samples (A2 and A3 barriers) and the two references (flat rigid barrier and simulated barrier with the mirror method).
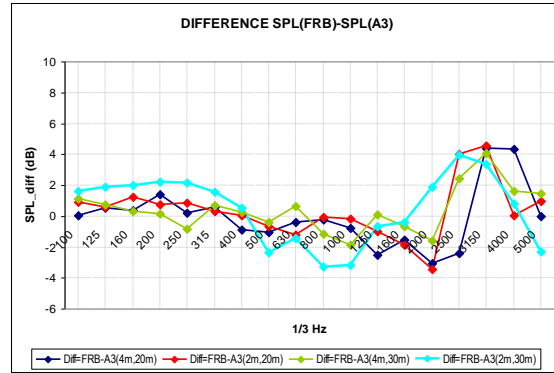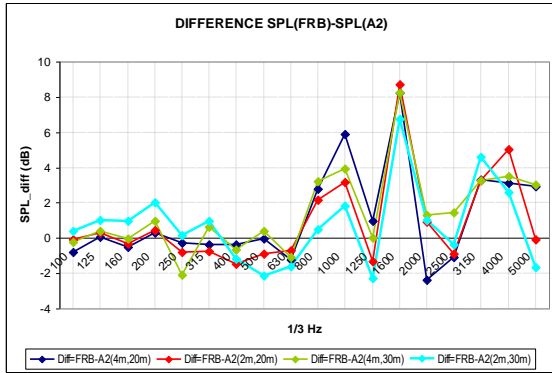
Figure 85 - SPL subtraction, FRB-A2 (left), FRB-A3 (right)
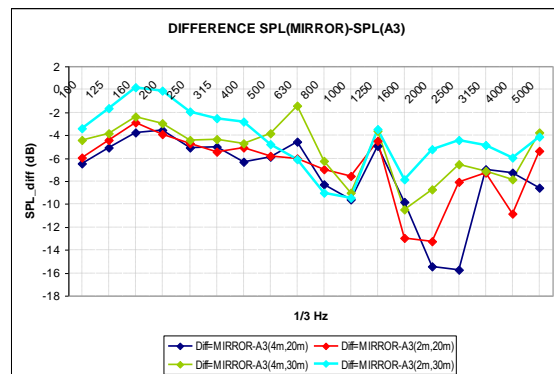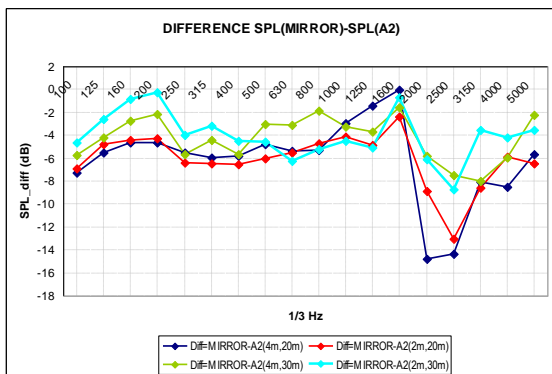
Figure 86 - SPL subtraction, Mirror-A2 (left), Mirror-A3 (right)

Positives values indicate that the measured SPL with reference barriers is higher than the absorptive barriers, as it is expected.

Taking the flat rigid barrier as reference, A2 sample shows a similar behaviour for all microphone positions in the whole frequency range, only the microphone at 2 m height and 30 m distance presents unexpected values in the low frequency, probably due to the acoustic ground absorption (grass). The most significant positive values appear mainly above 800 Hz, although the values are very unsteady changing a lot. For A3 barrier, the higher values for the difference appear above 1500 Hz, and as A2 barrier, microphone at 30 m and 2 m height presents a different behaviour.

With the simulated barrier as reference (mirror configuration), it is not possible to get any conclusion which help to explain the high negative values obtained. It is not a problem with the level emitted by the source, because as Figure 83 showed, the levels at reference position are very similar for all the configurations. In the other hand, the SPL values measured for the simulated barrier configuration are lower than barriers A2 and A3, in some frequencies more than 10 dB which is too much compared with the expected values.

If the same analysis is made for the two references (difference between flat rigid barrier and simulated barrier), it can be seen in Figure 87 that the differences are really high and they cannot be explained only with the energy contained in the reflected component, since the

SPL difference should ideally be constant, regardless measured point location and frequency, which is clearly not the case.
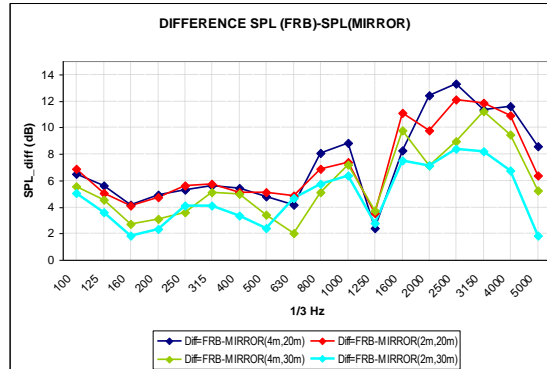
Figure 87 - SPL subtraction, FRB-Mirror

From the above analysis with the simulated rigid barrier as reference, the results indicate that not useful information can be obtained from this test. Therefore, the coefficient absorption obtained from this reference will be not included in this section.

As described in section 5.4.3., the absorption coefficient is calculated for barriers A2 and A3. Figure 88 and Figure 89 show this coefficient (α_{eq}) using the flat rigid barrier as reference.
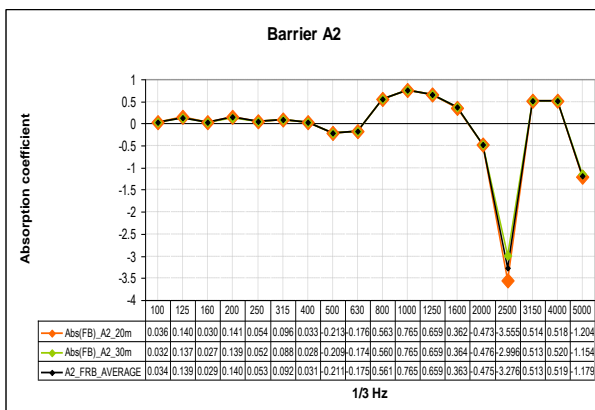
Figure 88 - Absorption coefficient for Barrier A2 (Flat rigid barrier as reference).
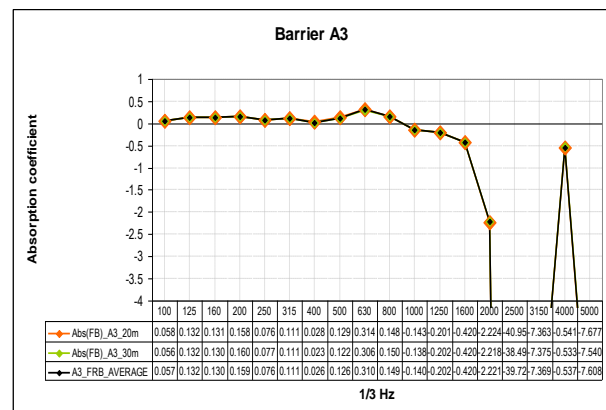
Figure 89 - Absorption coefficient for Barrier A3 (Flat rigid barrier as reference).

For barrier A2, the absorption values are very small at low frequencies (close to zero). For this barrier, acoustic absorption increases in the 800-1600 Hz frequency range, reaching its maximum at 1000 Hz. At higher frequencies a large variability of absorption values can be appreciated.

Barrier A3 shows a similar behavior in the frequency domain as A2 barrier. In this barrier, the absorption values are lower than A2 (it only gets a maximum absorptive coefficient of 0.314 at 630 Hz).

For both barriers, there are not significant differences between the numerical values at each microphone distance (20 and 30 m).

The negatives values for this configuration around 2500 Hz, are due to the level fall of the SPL at reference position for the flat rigid barrier (see **Figure 83**).

8.4.10   Details method B – AIT

In the following figures the RI results computed with method B can be found.
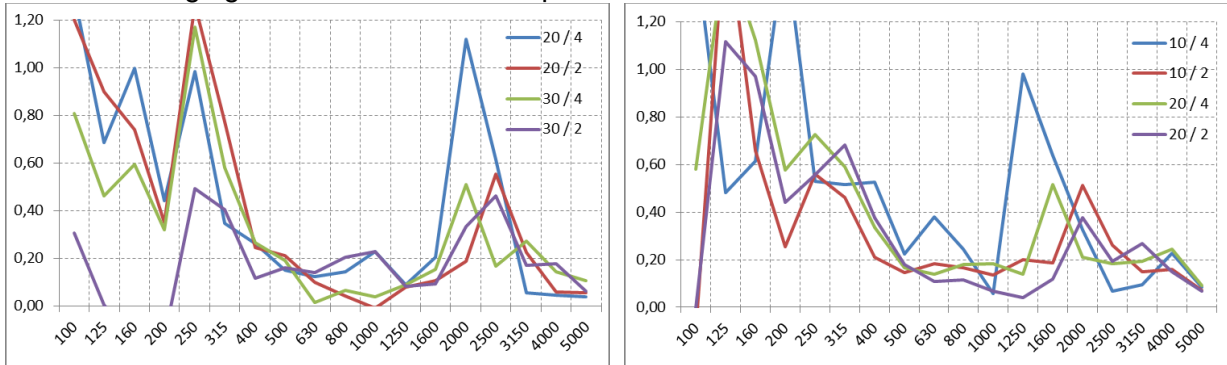
Figure 90 - Reflectivity ρ vs. one-third octave band of the flat absorptive barrier for configuration I (left) and configuration II (right) for loudspeaker Celestion
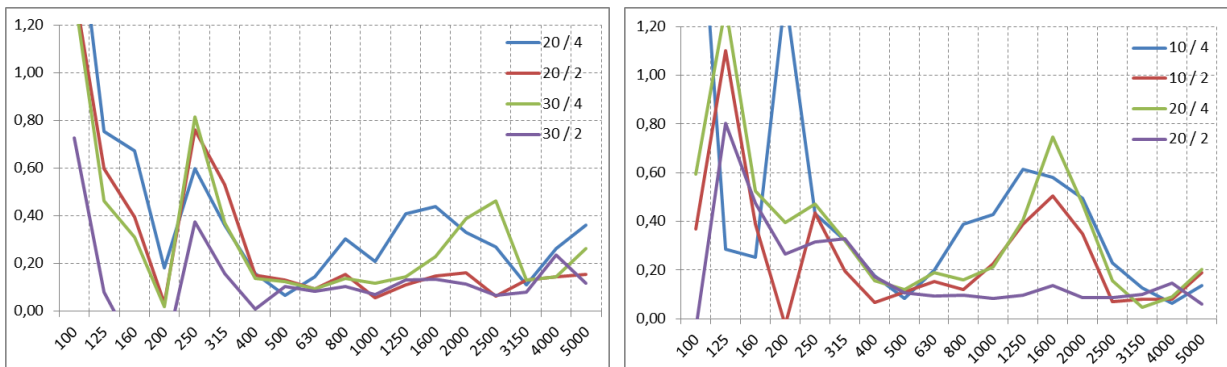
Figure 91 - Reflectivity ρ vs. one-third octave band of the flat timber barrier for configuration I (left) and configuration II (right) for loudspeaker Celestion
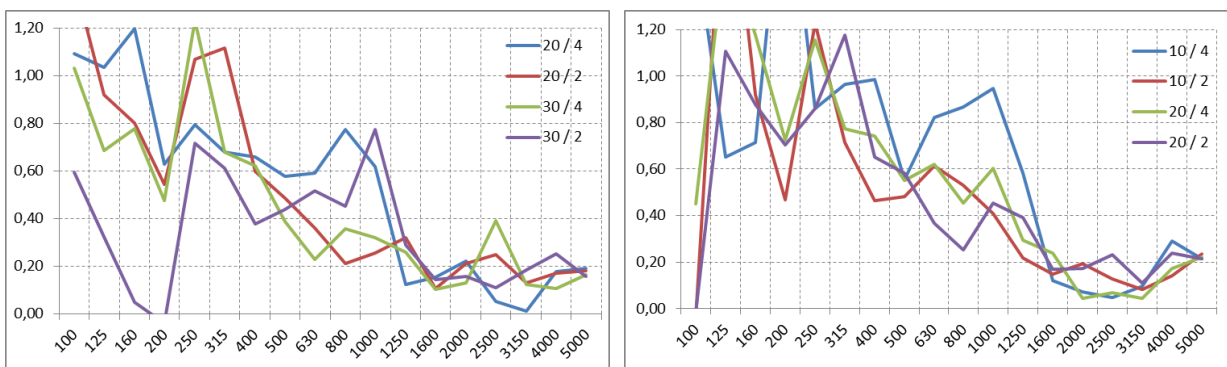
Figure 92 - Reflectivity ρ vs. one-third octave band of barrier A3 for configuration I (left) and configuration II (right) for loudspeaker Celestion – measurement No. 1
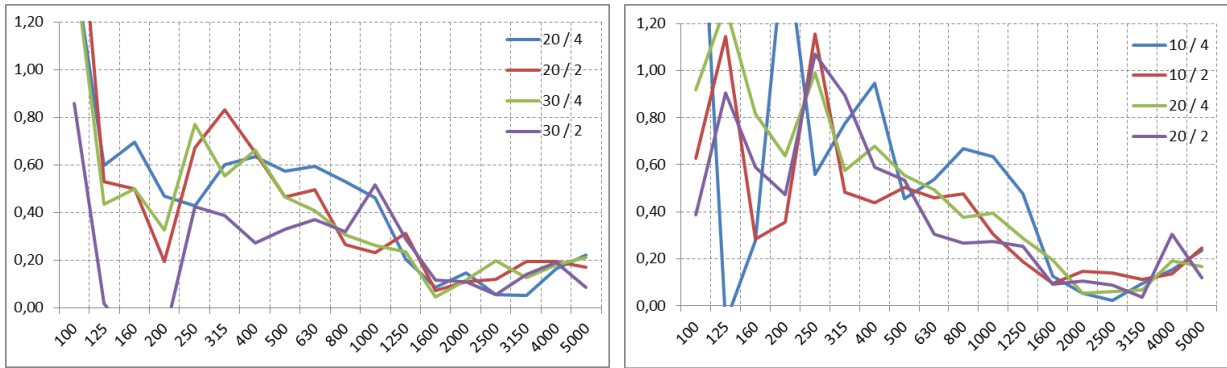
Figure 93 - Reflectivity ρ vs. one-third octave band of barrier A3 for configuration I (left) and configuration II (right) for loudspeaker Celestion – measurement No. 2
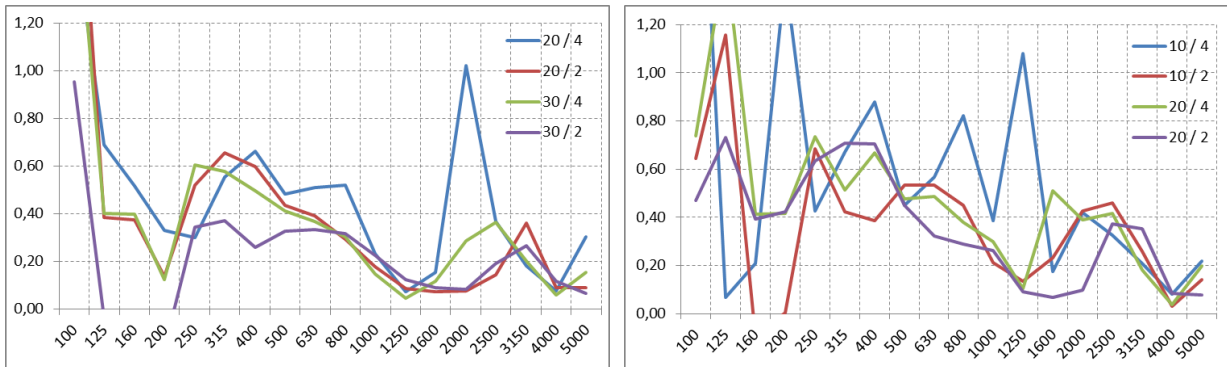
Figure 94 - Reflectivity ρ vs. one-third octave band of barrier A2 for configuration I (left) and configuration II (right) for loudspeaker Celestion

8.5 Details approximation function

8.5.1 Inclined

Input

Variable number	Variable	Dimension
1	Angle (θ)	[degree]
2	Microphone height	[m]
3	Flow resistivity	[kPa s m-2]
4	Material thickness	[m]

Input Range

Geometric variation number	Angle (α) [degree]	
1	70	
2	75	
3	80	
4	85	
5	90	

Microphone height   [1.5, 5, 10, 20, 40]

Rigid
Flow resistivity   [-]
Material thickness   [-]

Porous Concrete
Flow resistivity   [10k, 20k]
Material thickness   [0.05, 0.10, 0.15]

Mineral wool
Flow resistivity   [10k, 20k, 30k]
Material thickness   [0.10, 0.15]

Far Field DL Approximation function
Inclined – Rigid

Term number	Coefficient	Exponent Angle	Exponent Microphone height
1	7,1754105760146500E-04	3	0
2	1,2466542992105500E-03	2	1
3	-2,0024858501076400E-01	2	0

4	-5,9192809942003600E-05	1	2
5	-1,9429533581548400E-01	1	1
6	1,7382029960589100E+01	1	0
7	3,6799844955405900E-04	0	3
8	-1,6105980859736700E-02	0	2
9	7,6676464501245200E+00	0	1
10	-4,6598963896322800E+02	0	0

Far Field DL Approximation function
Inclined - Porous Concrete

Term number	Coefficient	Exponent Angle	Exponent Microphone height	Exponent Flow resistivity	Exponent Material thickness
1	-3,9261322221764800E+02	0	0	0	0
2	8,0410174557202000E-03	0	2	0	1
3	1,3870541692157500E+00	0	1	0	2
4	8,3076538101837100E-05	0	0	1	1
5	2,1970965177591700E-02	1	1	0	1
6	-2,6155426448577300E+00	0	1	0	1
7	4,1006278905793300E-04	0	3	0	0
8	-9,8217602016763100E+01	0	0	0	1
9	-2,4299964589990200E-02	0	2	0	0
10	-2,3525477270549000E-02	2	0	0	1
11	3,2756168663625600E+00	1	0	0	1
12	8,3537656267189600E+00	0	1	0	0
13	1,2683189655582500E-03	2	1	0	0
14	-2,0319289742500300E-01	1	1	0	0
15	5,9102800368527800E-04	3	0	0	0
16	-1,6749381629881200E-01	2	0	0	0
17	1,4658695688178100E+01	1	0	0	0

Far Field DL Approximation function
Inclined - Perforated Cassettes

Term number	Coefficient	Exponent Angle	Exponent Microphone height	Exponent Flow resistivity	Exponent Material thickness
1	-5,5279658894285700E+02	0	0	0	0
2	-1,9379227174769100E-07	2	0	1	0
3	1,8479122615144300E-05	1	0	1	1
4	1,2065615068449500E-07	0	0	2	1
5	2,3203190916961600E-05	1	0	1	0
6	-9,7396112302704800E-06	0	1	1	0
7	-1,2756625349085200E-08	0	0	2	0
8	9,7703332677646000E-08	0	2	1	0
9	6,2137392768033500E-08	1	1	1	0

10	8,5087021169768500E-03	0	2	0	1
11	1,2651073710936700E-02	1	1	0	1
12	-1,4637007114991800E+00	0	1	0	1
13	8,9091475951230100E-05	1	2	0	0
14	2,8041964270818400E-04	0	3	0	0
15	5,8000414802069700E-01	1	0	0	1
16	-9,7176967329662900E-03	2	0	0	1
17	-2,7604585419672900E-02	0	2	0	0
18	1,0702707000791100E+02	0	0	0	1
19	-8,0586537858954000E-03	0	0	1	1
20	1,1798913181158200E-03	2	1	0	0
21	8,3680735131157100E+00	0	1	0	0
22	-1,9523155948483000E-01	1	1	0	0
23	9,2938853210109500E-04	3	0	0	0
24	-2,4231648487313700E-01	2	0	0	0
25	2,0453591553084200E+01	1	0	0	0

Performance

Inclined - Rigid, 10 terms, 2 variables

Receiver (height)	Number of simulations	<1dB	<2dB	%<1dB	%<2dB
All	10	25	25	100,00	100,00
1.5 m	10	5	5	100,00	100,00
5 m	10	5	5	100,00	100,00
10 m	10	5	5	100,00	100,00
20 m	10	5	5	100,00	100,00
40 m	10	5	5	100,00	100,00

Inclined - Porous Concrete, 17 terms, 4 variables

Receiver (height)	Number of simulations	<1dB	<2dB	%<1dB	%<2dB
All	150	148	150	98,67	100,00
1.5 m	30	30	30	100,00	100,00
5 m	30	30	30	100,00	100,00
10 m	30	30	30	100,00	100,00
20 m	30	28	30	93,33	100,00
40 m	30	30	30	100,00	100,00

Inclined - Perforated Cassettes, 25 terms, 4 variables

Receiver (height)	Number of simulations	<1dB	<2dB	%<1dB	%<2dB
All	150	145	150	96,67	100,00
1.5 m	30	30	30	100,00	100,00
5 m	30	30	30	100,00	100,00
10 m	30	30	30	100,00	100,00
20 m	30	30	30	100,00	100,00
40 m	30	25	30	83,33	100,00

8.5.2 Panes

Input

Variable number	Variable	Dimension
1	Height H	[m]
2	Depth B	[m]
3	He/H	[m/m]
4	Microphone height	[m]
5	Flow resistivity	[kPa s m-2]
6	Material thickness	[m]

Input Range

Geometric variation number	H [m]	B [m]	He/H [m/m]	
1	0,1	0,05	0,5	
2	0,25	0,05	0,8	
3	0,25	0,05	0,5	
4	0,25	0,05	0,2	
5	0,5	0,05	0,8	
6	0,5	0,05	0,5	
7	0,5	0,05	0,2	
8	1	0,05	0,8	
9	1	0,05	0,5	
10	1	0,05	0,2	
11	0,1	0,1	0,5	
12	0,25	0,1	0,8	
13	0,25	0,1	0,5	
14	0,25	0,1	0,2	
15	0,5	0,1	0,8	
16	0,5	0,1	0,5	
17	0,5	0,1	0,2	
18	1	0,1	0,8	
19	1	0,1	0,5	
20	1	0,1	0,2	
21	0,1	0,15	0,5	
22	0,25	0,15	0,8	
23	0,25	0,15	0,5	
24	0,25	0,15	0,2	
25	0,5	0,15	0,8	
26	0,5	0,15	0,5	
27	0,5	0,15	0,2	
28	1	0,15	0,8	
29	1	0,15	0,5	
30	1	0,15	0,2	
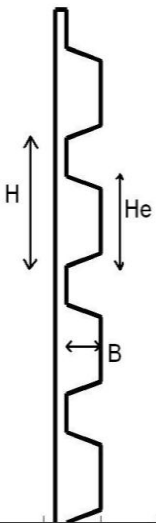
Microphone height   [1.5, 5, 10, 20, 40]

Rigid
Flow resistivity   [-]
Material thickness   [-]

Porous Concrete
Flow resistivity   [10k, 20k]
Material thickness   [0.05, 0.10, 0.15]

Mineral wool

Flow resistivity   [10k, 20k, 30k]
Material thickness   [0.10, 0.15]

Far Field DL Approximation function
Panes - Rigid

Term number	Coefficient	Exponent Height A	Exponent Depth B	Exponent A/C	Exponent Microphone height
1	-2,0335998222760700E-02	0	1	0	2
2	-1,4663680078327600E+02	1	2	0	0
3	9,5870742889422700E+01	0	2	0	0
4	6,0610694202730500E+00	1	0	2	0
5	-5,6424188992484200E-03	0	0	1	2
6	4,3546560445662200E+01	0	1	2	0
7	9,4382499432122400E-01	0	1	0	1
8	3,6280379509457500E+01	1	1	0	0
9	-6,9483281314961200E+00	1	0	1	0
10	-2,3354796736760300E+01	0	1	0	0
11	-4,3325179686347000E+01	0	1	1	0
12	-5,7101998348749900E-03	0	0	0	2
13	2,9697298195960700E-01	0	0	1	1
14	-1,7281076307894900E-01	0	0	0	1
15	2,2244170539680800E-04	0	0	0	3
16	-1,1157553801757700E+01	0	0	2	0
17	8,8429773075292300E+00	0	0	1	0
18	1,2238414820356400E+01	3	0	0	0
19	1,1775930317740000E+01	1	0	0	0
20	-2,2556089095851800E+01	2	0	0	0

Far Field DL Approximation function
Panes - Porous Concrete

Term number	Coefficient	Exponent Height A	Exponent Depth B	Exponent A/C	Exponent Microphone height	Exponent Flow resistivity	Exponent Material thickness
1	3,5065144132718400E+00	0	0	0	0	0	0
2	6,8236931027503900E+01	1	0	0	0	0	2
3	2,5221241570075900E+00	2	0	1	0	0	0
4	3,2934636661870800E+00	1	0	2	0	0	0
5	2,5777254524450400E-03	1	0	0	2	0	0
6	5,1111885124690800E-05	2	0	0	0	1	0
7	-7,6480630364256800E-02	1	0	0	1	0	0
8	-3,3642609991281100E-03	0	0	1	2	0	0
9	4,1639054820738800E+00	0	0	0	1	0	2
10	-8,8880374694055200E-05	1	0	0	0	1	0
11	-4,5754312306869300E+00	0	2	0	1	0	0
12	-2,7458254370564400E+00	0	0	2	0	0	0

13	2,1196303091329400E+01	2	0	0	0	0	1
14	-2,3602635634732300E-02	0	1	0	2	0	0
15	-1,7428736290465300E+02	0	0	1	0	0	2
16	-5,8699670573263000E-03	0	0	0	0	1	2
17	-3,3868645276916700E+01	0	0	2	0	0	1
18	-7,4145892167610200E+00	0	1	0	0	0	0
19	-8,8067509143065500E-01	0	0	0	1	0	1
20	-4,5610148301514100E+00	3	0	0	0	0	0
21	-9,5507436655261400E-02	0	0	0	1	0	0
22	1,5421016538224900E+01	0	0	0	0	0	1
23	2,1082606923437200E-01	0	0	1	1	0	0
24	1,1972724992737200E-03	0	0	0	0	1	1
25	5,8802369943762000E+00	2	0	0	0	0	0
26	-6,9924112726364700E+00	1	0	1	0	0	0
27	-5,0062659149661400E+01	1	0	0	0	0	1
28	2,0666605005582700E+00	0	1	0	1	0	0
29	6,7927721257026000E+01	0	0	1	0	0	1
30	-1,0200768910311600E-02	0	0	0	2	0	0
31	2,7499343466709300E-04	0	0	0	3	0	0

Far Field DL Approximation function
Panes - Perforated Cassettes

Term number	Coefficient	Exponent Height A	Exponent Depth B	Exponent A/C	Exponent Microphone height	Exponent Flow resistivity	Exponent Material thickness
1	-2,0300201985562800E+00	0	0	0	0	0	0
2	-9,4153181660524000E-01	0	1	0	1	0	1
3	4,9121567548537000E-02	1	0	1	1	0	0
4	-6,1902343365949400E-03	0	1	0	2	0	0
5	7,8242396534028300E-02	0	0	2	1	0	0
6	1,3167741531885100E+01	0	1	2	0	0	0
7	1,0924632953450200E+01	0	0	2	0	0	1
8	1,9177765312636000E-03	0	1	0	0	1	1
9	6,4116524131400600E-02	1	0	0	1	0	0
10	2,4815000486163000E-03	1	0	0	2	0	0
11	2,7983051128783100E-03	0	0	1	2	0	0
12	-2,2788806652850000E+00	1	0	1	0	0	0
13	1,1663248040581300E-02	0	0	0	2	0	1
14	5,2403549046320900E-04	1	0	0	0	1	1
15	-7,4612747415585500E-04	0	1	1	0	1	0
16	5,2238595118142900E-01	0	1	0	1	0	0
17	1,3753566089176900E+02	0	2	1	0	0	0
18	-8,3469218022693300E-04	1	1	0	0	1	0
19	-3,6829556110859000E-01	0	0	0	1	0	1

20	-1,4455492050457400E-01	2	0	0	1	0	0
21	-4,4690757087955400E+00	2	0	1	0	0	0
22	-1,9068541855831600E+01	0	1	1	0	0	0
23	-8,2825016066631000E-05	0	0	1	0	1	0
24	3,0134663081378500E+01	1	0	1	0	0	1
25	6,1368336755636900E+00	1	0	2	0	0	0
26	1,5186498268033000E-04	1	0	1	0	1	0
27	-7,4516943126515300E+02	0	2	0	0	0	1
28	-9,4034978016270600E+01	0	2	0	0	0	0
29	1,8987082283018800E+02	1	2	0	0	0	0
30	-1,9030284008294700E+02	0	1	1	0	0	1
31	-2,4373983577419800E-04	0	0	2	0	1	0
32	2,4821624937697800E+01	1	1	0	0	0	0
33	-2,7066417279878500E+01	2	0	0	0	0	1
34	-1,7677390326768700E-01	0	0	1	1	0	0
35	-3,8374852885231200E+01	2	1	0	0	0	0
36	1,9476394475358900E-04	2	0	0	0	1	0
37	-1,6070534198427000E+01	0	1	0	0	0	0
38	-7,0270459995805500E-03	0	2	0	0	1	0
39	-6,5954524218649000E+00	0	0	2	0	0	0
40	2,1957191766443500E-03	0	0	1	0	1	1
41	2,6996551953654200E+02	0	1	0	0	0	1
42	-4,0418196978122200E-04	1	0	0	0	1	0
43	2,7370774923897800E-01	0	0	0	1	0	0
44	-7,2156116285325700E+01	0	0	1	0	0	1
45	2,5129428505064700E-03	0	1	0	0	1	0
46	1,0441149085929000E+01	0	0	1	0	0	0
47	3,7521461311391600E-04	0	0	0	3	0	0
48	2,5032887135531700E-04	0	0	0	0	1	0
49	-3,6491251246223600E-03	0	0	0	0	1	1
50	-2,3043050491038300E-02	0	0	0	2	0	0
51	8,6161081681875100E+01	0	0	0	0	0	1
52	5,0118122282620500E+01	3	0	0	0	0	0
53	3,7436689344373200E+01	1	0	0	0	0	0
54	-7,8560284930737200E+01	2	0	0	0	0	0

Performance

Panes - Rigid, 20 terms, 4 variables

Receiver (height)	Number of simulations	<1dB	<2dB	%<1dB	%<2dB
All	150	127	147	84,67	98,00
1.5 m	30	29	29	96,67	96,67
5 m	30	25	29	83,33	96,67
10 m	30	24	29	80,00	96,67
20 m	30	24	30	80,00	100,00
40 m	30	25	30	83,33	100,00

Panes - Porous Concrete, 31 terms, 6 variables

Receiver (height)	Number of simulations	<1dB	<2dB	%<1dB	%<2dB
All	900	769	882	85,44	98,00
1.5 m	180	163	176	90,56	97,78
5 m	180	140	173	77,78	96,11
10 m	180	147	178	81,67	98,89
20 m	180	154	175	85,56	97,22
40 m	180	165	180	91,67	100,00

Panes - Perforated Cassettes, 54 terms, 6 variables

Receiver (height)	Number of simulations	<1dB	<2dB	%<1dB	%<2dB
All	900	796	893	88,44	99,22
1.5 m	180	172	180	95,56	100,00
5 m	180	157	179	87,22	99,44
10 m	180	164	179	91,11	99,44
20 m	180	143	179	79,44	99,44
40 m	180	160	176	88,89	97,78

8.5.3 Sawtooth

Input

Variable number	Variable	Dimension
1	Height H	[m]
2	Depth B	[m]
3	Microphone height	[m]
4	Flow resistivity	[kPa s m-2]
5	Material thickness	[m]

Input Range

variation	H [m]	B [m]
1	0,80	0,10
2	0,80	0,20
3	0,80	0,30
4	0,67	0,10
5	0,67	0,20
6	0,67	0,30
7	0,57	0,10
8	0,57	0,20
9	0,57	0,30
10	0,50	0,10
11	0,50	0,20
12	0,50	0,30
13	0,44	0,10
14	0,44	0,20
15	0,44	0,30
16	0,40	0,10
17	0,40	0,20
18	0,40	0,30
19	0,36	0,10
20	0,36	0,20
21	0,36	0,30
22	0,33	0,10
23	0,33	0,20
24	0,33	0,30

Microphone height   [1.5, 5, 10, 20, 40]

Rigid
Flow resistivity   [-]
Material thickness   [-]

Porous Concrete
Flow resistivity   [10k, 20k]
Material thickness   [0.05, 0.10, 0.15]

Mineral wool
Flow resistivity   [10k, 20k, 30k]
Material thickness   [0.10, 0.15]

Far Field DL Approximation function

Sawtooth – Rigid

Term number	Coefficient	Exponent Height A	Exponent Depth B	Exponent Microphone height
1	-9,8090809697232200E+00	0	0	0
2	4,1163837068750100E+00	2	1	0
3	1,3069865497923400E-01	2	0	1
4	4,8210647469655100E-01	1	1	1
5	-1,3742732513724800E+02	1	2	0
6	7,5007133636222700E+01	3	0	0
7	-2,1492614597285900E+00	0	2	1
8	7,5148968121040500E-01	0	1	1
9	7,4095649865575500E+01	1	0	0
10	-2,3001599647758100E+01	0	1	0
11	-2,6687481815887900E-02	0	0	2
12	2,2822367746030100E-01	0	0	1
13	8,9520169755036500E-04	1	0	2
14	2,2024817325335600E-03	0	1	2
15	4,8970676856389200E-04	0	0	3
16	-1,3528691962114900E+02	2	0	0
17	8,4235512941613900E+01	1	1	0
18	-3,0571899371843100E-01	1	0	1

Far Field DL Approximation function

Sawtooth - Porous Concrete

Term number	Coefficient	Exponent Height A	Exponent Depth B	Exponent Microphone height	Exponent Flow resistivity	Exponent Material thickness
1	6,9524037552646600E+00	0	0	0	0	0
2	3,6366140720208700E-04	0	0	0	1	1
3	2,0224576213838300E-03	0	1	0	1	1
4	-7,0852180947456000E-04	1	0	0	1	1
5	-9,9691932402790000E-03	0	1	2	0	0
6	-2,1431368852290600E-01	2	0	1	0	0
7	4,5308734981860000E-03	1	0	2	0	0
8	8,3254768503435900E+00	0	0	1	0	2
9	-2,1333477487007400E+00	0	2	1	0	0
10	-1,5407537081925300E+01	0	0	0	0	1
11	1,1910461328794900E-01	0	0	1	0	0
12	-4,9158280213067000E+02	0	2	0	0	1
13	-1,9342351743910000E+00	0	0	1	0	1
14	6,8643531549892400E+01	0	2	0	0	0
15	1,9515699100842600E+01	3	0	0	0	0

16	-1,6360896483120300E+03	0	1	0	0	2
17	-1,7126663210674900E+02	1	2	0	0	0
18	1,4779659675421600E+00	0	1	1	0	0
19	9,2010525440258800E+00	1	0	0	0	0
20	4,3677290563429700E-04	0	0	3	0	0
21	-3,1690908014647300E+01	2	0	0	0	0
22	-2,2312130683130500E-02	0	0	2	0	0
23	1,0349391259774400E+02	1	1	0	0	0
24	6,3605147146938700E+02	0	1	0	0	1
25	-6,8351542868067400E+01	0	1	0	0	0

Far Field DL Approximation function

Sawtooth - Perforated Cassettes

Term number	Coefficient	Exponent Height A	Exponent Depth B	Exponent Microphone height	Exponent Flow resistivity	Exponent Material thickness
1	4,8724235046083000E+00	0	0	0	0	0
2	-4,9113473906018700E-03	0	1	2	0	0
3	-3,4264244860951300E-02	0	0	1	0	0
4	1,3048655269579200E-04	2	0	0	1	0
5	1,2298531345094400E+01	0	2	0	0	0
6	-3,4724515360186600E-04	1	1	0	1	0
7	1,9646396390279500E+01	2	0	0	0	1
8	-1,6168526780344800E-01	2	0	1	0	0
9	-1,0016086409574000E+00	0	2	1	0	0
10	-1,5313066767333300E+02	0	2	0	0	1
11	-9,5047781789338600E-04	0	2	0	1	0
12	1,8742795454412700E+01	2	1	0	0	0
13	-9,2695519425509400E+01	1	1	0	0	1
14	1,5565897287300600E-01	1	0	1	0	0
15	-1,1963153308583800E+01	1	1	0	0	0
16	8,1149850907896100E+00	3	0	0	0	0
17	6,8611163739896900E-01	0	1	1	0	0
18	1,7690210193122100E-03	1	0	0	1	1
19	-4,6550727293909800E-03	0	1	0	1	1
20	1,6645758248933100E-04	0	0	3	0	0
21	-7,7034397740419100E-03	0	0	2	0	0
22	-5,4239365538444400E+01	1	0	0	0	1
23	1,5304325458919600E-04	0	0	0	1	0
24	-3,5649829909418200E-04	1	0	0	1	0
25	-1,5067825311642500E+01	2	0	0	0	0
26	-2,9568831932782100E+01	0	1	0	0	0
27	1,2711423879559900E+01	1	0	0	0	0
28	-3,0334782899177900E-03	0	0	0	1	1

29	1,9172126313583700E-03	0	1	0	1	0
30	3,1671501099454200E+02	0	1	0	0	1
31	6,3628723724265500E+01	0	0	0	0	1

Performance

Sawtooth - Rigid, 18 terms, 3 variables

Receiver (height)	Number of simulations	<1dB	<2dB	%<1dB	%<2dB
All	120	105	120	87,50	100,00
1.5 m	24	22	24	91,67	100,00
5 m	24	19	24	79,17	100,00
10 m	24	23	24	95,83	100,00
20 m	24	21	24	87,50	100,00
40 m	24	20	24	83,33	100,00

Sawtooth - Porous Concrete, 25 terms, 5 variables

Receiver (height)	Number of simulations	<1dB	<2dB	%<1dB	%<2dB
All	720	656	718	91,11	99,72
1.5 m	144	136	144	94,44	100,00
5 m	144	132	143	91,67	99,31
10 m	144	138	144	95,83	100,00
20 m	144	126	144	87,50	100,00
40 m	144	124	143	86,11	99,31

Sawtooth - Perforated Cassettes, 31 terms, 5 variables

Receiver (height)	Number of simulations	<1dB	<2dB	%<1dB	%<2dB
All	720	707	718	98,19	99,72
1.5 m	144	144	144	100,00	100,00
5 m	144	144	144	100,00	100,00
10 m	144	144	144	100,00	100,00
20 m	144	136	142	94,44	98,61
40 m	144	139	144	96,53	100,00

8.5.4 Steps

Input

Variable number	Variable	Dimension
1	Number of steps	[-]
2	Tangent of angle (θ)	[-]
3	Microphone height	[m]
4	Flow resistivity	[kPa s m-2]
5	Material thickness	[m]

Input Range

variation	Nr of steps [-]	Tangent of angle [deg]	
1	4	tan(5°)	
2	8	tan(5°)	
3	12	tan(5°)	
4	4	tan(10°)	
5	8	tan(10°)	
6	12	tan(10°)	
7	4	tan(15°)	
8	8	tan(15°)	
9	12	tan(15°)	
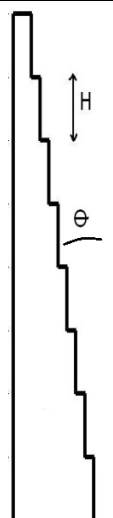
Microphone height   [1.5, 5, 10, 20, 40]

Rigid
Flow resistivity   [-]
Material thickness   [-]

Porous Concrete
Flow resistivity   [10k, 20k]
Material thickness   [0.05, 0.10, 0.15]

Mineral wool
Flow resistivity   [10k, 20k, 30k]
Material thickness   [0.10, 0.15]

Far Field DL Approximation function
Steps - Rigid

Term number	Coefficient	Exponent Number of steps	Exponent tan(α)	Exponent Microphone height
1	-9,2547134240606200E+00	0	0	0
2	-6,2046689076396400E+00	0	2	1
3	-4,5384775339966700E-02	0	0	2

4	1,3221729696442800E-01	1	1	1
5	1,5549415549056700E+00	0	1	1
6	2,2152975562909800E-01	2	1	0
7	1,0379603801912100E+01	1	2	0
8	1,9598804688293600E-04	2	0	1
9	1,9712860289504000E+01	0	1	0
10	9,3843544090055000E-01	0	0	1
11	2,1638856499472900E-04	0	1	2
12	1,0002632893676500E-03	1	0	2
13	1,8582008695079200E+00	1	0	0
14	-9,8666010235367100E+00	1	1	0
15	6,1291740035320900E-04	0	0	3
16	-3,0110806758823300E-02	2	0	0
17	-7,5030973890259900E-02	1	0	1

Far Field DL Approximation function
Steps - Porous Concrete

Term number	Coefficient	Exponent Number of steps	Exponent tan(α)	Exponent Microphone height	Exponent Flow resistivity	Exponent Material thickness
1	6,3311972866940000E-01	0	0	0	0	0
2	6,9500267497413800E-01	0	1	1	0	1
3	2,5589847315360300E-03	2	0	0	0	0
4	-2,9368994158939800E-02	2	0	0	0	1
5	-3,2024732738398300E-04	0	2	0	1	0
6	-3,7062882983338800E-02	2	1	0	0	0
7	1,2278756932582300E-04	0	1	0	1	0
8	-1,2750663231448300E-02	0	0	2	0	1
9	-8,0544232193894700E-03	0	1	2	0	0
10	-4,5601800152321100E+00	1	1	0	0	1
11	1,9139527459095100E+02	0	2	0	0	1
12	6,2475413177821000E-01	1	1	0	0	0
13	9,2648025429099600E-04	2	0	1	0	0
14	-5,5626647046156800E+02	0	1	0	0	2
15	6,5494752089651700E+01	0	1	0	0	1
16	6,5046161069910100E+00	0	0	1	0	2
17	9,9527480269301000E+01	0	0	0	0	2
18	-1,3141778803993500E+01	1	0	0	0	2
19	-9,1327903539481500E-01	0	0	1	0	1
20	-6,4318554365998600E+00	1	2	0	0	0
21	-2,3796851560370300E+01	0	0	0	0	1
22	1,3579618841799200E-01	1	1	1	0	0
23	9,8081952317261200E-04	1	0	2	0	0

24	4,6841630906018300E+00	1	0	0	0	1
25	-7,6044067537709700E+00	0	2	1	0	0
26	6,4004104859527700E-01	1	0	0	0	0
27	1,6416812838380000E+02	0	2	0	0	0
28	2,3255729233326700E+00	0	1	1	0	0
29	6,99116550540910000E-04	0	0	3	0	0
30	-8,7526999533671300E-02	1	0	1	0	0
31	-5,9540617371067900E+01	0	1	0	0	0
32	9,1432468315415100E-01	0	0	1	0	0
33	-4,6357839169823200E-02	0	0	2	0	0

Far Field DL Approximation function

Steps - Perforated Cassettes

Term number	Coefficient	Exponent Number of steps	Exponent tan(α)	Exponent Microphone height	Exponent Flow resistivity	Exponent Material thickness
1	1,0477363721222900E+01	0	0	0	0	0
2	-1,5446301960188600E+00	0	2	1	0	0
3	1,4537013530596800E-02	0	1	2	0	0
4	-6,9248901218438600E-02	2	0	0	0	1
5	-1,6490589535977100E-03	0	1	0	1	1
6	6,5890107506894800E-02	1	1	1	0	0
7	-1,3303533507908900E-01	2	1	0	0	0
8	-6,8464402172084300E-04	0	1	0	1	0
9	1,9303953951148500E-02	2	0	0	0	0
10	-2,2019151411591000E-01	1	0	0	0	0
11	-6,2504686145508000E-05	1	0	0	1	1
12	-1,0806016551597100E-04	0	0	0	1	0
13	7,7538020111013100E-04	1	0	2	0	0
14	8,1904483906038700E-05	1	1	0	1	0
15	3,5498586133376600E+00	1	0	0	0	1
16	1,1856198335994500E+02	0	2	0	0	0
17	-1,8938122409273400E+01	1	2	0	0	0
18	-3,3834522945549300E+01	0	1	0	0	0
19	-5,6164331122837900E-02	1	0	1	0	0
20	6,2104298366527200E-04	0	0	3	0	0
21	7,0276776592524600E+00	1	1	0	0	0
22	9,4564098246982600E-01	0	0	1	0	0
23	-4,5955757445795900E-02	0	0	2	0	0

Performance

Steps - Rigid, 17 terms, 3 variables

Receiver (height)	Number of simulations	<1dB	<2dB	%<1dB	%<2dB
All	45	39	45	86,67	100,00
1.5 m	9	9	9	100,00	100,00
5 m	9	8	9	88,89	100,00
10 m	9	8	9	88,89	100,00
20 m	9	6	9	66,67	100,00
40 m	9	8	9	88,89	100,00

Steps - Porous Concrete, 33 terms, 5 variables

Receiver (height)	Number of simulations	<1dB	<2dB	%<1dB	%<2dB
All	270	246	269	91,11	99,63
1.5 m	54	52	54	96,30	100,00
5 m	54	49	54	90,74	100,00
10 m	54	46	53	85,19	98,15
20 m	54	46	54	85,19	100,00
40 m	54	53	54	98,15	100,00

Steps - Perforated Cassettes, 23 terms, 5 variables

Receiver (height)	Number of simulations	<1dB	<2dB	%<1dB	%<2dB
All	270	217	267	80,37	98,89
1.5 m	54	47	54	87,04	100,00
5 m	54	39	54	72,22	100,00
10 m	54	44	54	81,48	100,00
20 m	54	40	51	74,07	94,44
40 m	54	47	54	87,04	100,00

8.5.5 ZigZag

Input

Variable number	Variable	Dimension
1	Height H	[m]
2	Depth B	[m]
3	Microphone height	[m]
4	Flow resistivity	[kPa s m-2]
5	Material thickness	[m]

Input Range

variation	H [m]	B [m]
1	0,80	0,10
2	0,80	0,20
3	0,80	0,30
4	0,67	0,10
5	0,67	0,20
6	0,67	0,30
7	0,57	0,10
8	0,57	0,20
9	0,57	0,30
10	0,50	0,10
11	0,50	0,20
12	0,50	0,30
13	0,44	0,10
14	0,44	0,20
15	0,44	0,30
16	0,40	0,10
17	0,40	0,20
18	0,40	0,30
19	0,36	0,10
20	0,36	0,20
21	0,36	0,30
22	0,33	0,10
23	0,33	0,20
24	0,33	0,30

Microphone height   [1.5, 5, 10, 20, 40]

Rigid
Flow resistivity   [-]
Material thickness   [-]

Porous Concrete
Flow resistivity   [10k, 20k]
Material thickness   [0.05, 0.10, 0.15]

Mineral wool
Flow resistivity   [10k, 20k, 30k]
Material thickness   [0.10, 0.15]

Far Field DL Approximation function
ZigZag - Rigid

Term number	Coefficient	Exponent Height A	Exponent Depth B	Exponent Microphone height
1	-6,4728038983416700E+00	0	0	0
2	9,9490496312039700E+00	0	1	0
3	1,2655371738650400E+02	1	2	0
4	3,0625720355200700E-01	0	0	1
5	2,7410325295614400E+01	3	0	0
6	-8,2844688525668200E+01	1	1	0
7	5,7872276124014600E-04	0	0	3
8	-4,4024545373061100E+01	2	0	0
9	-3,0682889174356900E-02	0	0	2
10	3,6550164101481300E+01	1	0	0

Far Field DL Approximation function
ZigZag - Porous Concrete

Term number	Coefficient	Exponent Height A	Exponent Depth B	Exponent Microphone height	Exponent Flow resistivity	Exponent Material thickness
1	-1,6270618806668700E+01	0	0	0	0	0
2	-5,5172764579607400E-07	0	0	0	1	1
3	3,0489068648694100E-03	0	1	0	1	1
4	2,1616563883109900E+00	0	2	1	0	0
5	-2,5505862558014200E+02	1	1	0	0	1
6	-9,0028103821337300E-01	0	1	1	0	0
7	1,0486882595099700E+02	2	0	0	0	1
8	3,0316577742032100E+01	0	0	0	0	1
9	2,2308229742299900E+02	0	1	0	0	1
10	3,1060138870167100E-01	0	0	1	0	0
11	-1,0447433717938600E+02	1	0	0	0	1
12	4,3283803875537100E-04	0	0	3	0	0
13	1,5868190658392100E+02	2	1	0	0	0
14	-1,9666327572741000E+02	0	2	0	0	0
15	-3,3954652413466400E+01	2	0	0	0	0
16	4,0370856418376300E+02	1	2	0	0	0
17	-2,3100517703981400E-02	0	0	2	0	0
18	1,3731280936690500E+02	0	1	0	0	0
19	5,8255859282201300E+01	1	0	0	0	0
20	-3,6664854357355500E+02	1	1	0	0	0

Far Field DL Approximation function
ZigZag - Perforated Cassettes

Term number	Coefficient	Exponent Height A	Exponent Depth B	Exponent Microphone height	Exponent Flow resistivity	Exponent Material thickness
1	-2,3080412694761900E+00	0	0	0	0	0
2	-1,7211439862492400E-02	1	0	1	0	0
3	1,7121049755445600E+01	2	1	0	0	0
4	4,5713645478279400E+01	1	2	0	0	0
5	-1,6708079403818800E+00	0	2	1	0	0
6	1,3188619351779200E-04	0	0	3	0	0
7	3,7569799426971100E-03	0	1	0	1	1
8	-1,5220399816115200E+02	1	1	0	0	1
9	6,5115866726899000E+01	2	0	0	0	1
10	8,1519964691284000E-01	0	1	1	0	0
11	2,6890804708878000E+01	1	1	0	0	0
12	-6,7632375652586800E-03	0	0	2	0	0
13	1,7195942478664700E+01	3	0	0	0	0
14	1,4847836866991600E+02	0	1	0	0	1
15	9,0032465013796600E-04	2	0	0	1	0
16	-8,2644810178999200E+01	1	0	0	0	1
17	-2,5680375415870800E-03	1	1	0	1	0
18	-3,5958843753919600E+01	0	1	0	0	0
19	1,9410958523064000E-03	0	1	0	1	0
20	4,1196841365318400E-04	0	0	0	1	0
21	-7,9240463947880400E-04	1	0	0	1	0
22	-3,9583374321961500E-03	0	0	0	1	1
23	1,1269220575681100E+02	0	0	0	0	1
24	-5,1411477881759400E+01	2	0	0	0	0
25	3,5834262844710400E+01	1	0	0	0	0

Performance

ZigZag - Rigid, 10 terms, 3 variables

Receiver (height)	Number of simulations	<1dB	<2dB	%<1dB	%<2dB
All	120	106	119	88,33	99,17
1.5 m	24	24	24	100,00	100,00
5 m	24	23	24	95,83	100,00
10 m	24	21	24	87,50	100,00
20 m	24	18	23	75,00	95,83
40 m	24	20	24	83,33	100,00

ZigZag - Porous Concrete, 20 terms, 5 variables

Receiver (height)	Number of simulations	<1dB	<2dB	%<1dB	%<2dB
All	720	600	703	83,33	97,64
1.5 m	144	126	144	87,50	100,00
5 m	144	126	143	87,50	99,31
10 m	144	124	142	86,11	98,61
20 m	144	118	140	81,94	97,22
40 m	144	106	134	73,61	93,06

ZigZag - Perforated Cassettes, 25 terms, 5 variables

Receiver (height)	Number of simulations	<1dB	<2dB	%<1dB	%<2dB
All	720	605	700	84,03	97,22
1.5 m	144	119	138	82,64	95,83
5 m	144	121	138	84,03	95,83
10 m	144	124	139	86,11	96,53
20 m	144	120	141	83,33	97,92
40 m	144	121	144	84,03	100,00